OPERATION PLUMBBOB.

Investigation of Effects of Nuclear Detonations on Electromagnetic Wave Propagation and Nuclear Radiation Detector Design

Project 2.7.

May 1962

Nevada Test Site.
May-Oct [redacted] 57

T. D. H[redacted]

NOTICE

This is an extract of **WT-1416, Operation PLUMBBOB, Project 2.7,** which remains classified **SECRET/ RESTRICTED DATA** as of this date.

15 DNA001-79-C-0454

Extract version prepared for:
Director
DEFENSE NUCLEAR AGENCY
Washington, D. C. 20305

11

1 Sep [redacted] 80

Approved for public release; distribution unlimited.

Unclassified

SECURITY CLASSIFICATION OF THIS PAGE (When Data Entered)

REPORT DOCUMENTATION PAGE	READ INSTRUCTIONS BEFORE COMPLETING FORM
1. REPORT NUMBER: WT-1416 (EX)	2. GOVT ACCESSION NO.: AD-A995 057
3. RECIPIENT'S CATALOG NUMBER:	
4. TITLE (and Subtitle): Operation PLUMBBOB, Investigation of Effects of Nuclear Detonations on Electromagnetic Wave Propagation and Nuclear Radiation Detector Design, Project 2.7	5. TYPE OF REPORT & PERIOD COVERED:
	6. PERFORMING ORG. REPORT NUMBER: WT-1416 (EX)
7. AUTHOR(s): T. D. Hanscome et al	8. CONTRACT OR GRANT NUMBER(s):
9. PERFORMING ORGANIZATION NAME AND ADDRESS: Headquarters Field Command, Defense Atomic Support Agency, Sandia Base, Albuquerque, New Mexico	10. PROGRAM ELEMENT, PROJECT, TASK AREA & WORK UNIT NUMBERS:
11. CONTROLLING OFFICE NAME AND ADDRESS:	12. REPORT DATE: May, 1962
	13. NUMBER OF PAGES: 97
14. MONITORING AGENCY NAME & ADDRESS (if different from Controlling Office):	15. SECURITY CLASS. (of this report): UNCLASSIFIED
	15a. DECLASSIFICATION/DOWNGRADING SCHEDULE:

16. DISTRIBUTION STATEMENT (of this Report)

Approved for public release; unlimited distribution.

17. DISTRIBUTION STATEMENT (of the abstract entered in Block 20, if different from Report)

18. SUPPLEMENTARY NOTES

This report has had the classified information removed and has been republished in unclassified form for public release. This work was performed by the General Electric Company-TEMPO under contract DNA001-79-C-0455 with the close cooperation of the Classification Management Division of the Defense Nuclear Agency.

19. KEY WORDS (Continue on reverse side if necessary and identify by block number)

Operation PLUMBBOB
Nuclear Effects
Radiation Detection Techniques
Electromagnetic Wave Propagation

20. ABSTRACT (Continue on reverse side if necessary and identify by block number)

DD FORM 1 JAN 73 1473 EDITION OF 1 NOV 65 IS OBSOLETE

Unclassified

SECURITY CLASSIFICATION OF THIS PAGE (When Data Entered)

ABSTRACT

The objectives were to: (1) proof test (at Nevada Test Site altitudes) telemetry and nuclear radiation detection techniques intended for use in measurements of effects of high-altitude nuclear detonations, (2) study radio wave propagation in the vicinity of nuclear detonations, (3) study the effects of the electromagnetic (EM) signal produced by the detonation on the equipment used, and (4) compare the calculated and measured attenuations.

Transmitters in the frequency range 160 to 9850 Mc were located in shielded bunkers to transmit radially outward from ground zero, such that the transmission path went through the fireball, and such that the signal reflected from the fireball could be received. Receivers were installed in Building 400, about 12 miles from the various ground zeros. Scintillation detectors were installed at some of the stations closer to ground zero, as were instruments to monitor the effects on the transmitters of the EM signal generated by the detonation.

For frequencies near 10,000 Mc, radial path attenuations greater than 50 db but probably less than 75 db and lasting about 5 μsec were observed for transmitters at about 1,300 yards from a 10.3-kt device (Wilson). For a radial path and a 71-kt device (Hood), the attenuations were greater than 75 db and lasted about 15 μsec for a transmitter at 1,600 yards from ground zero. In both of these measurements, the signal strength recovered to its preshot value in less than about 30 μsec.

Transmission at 160, 960, and 9750 Mc through the fireball was interrupted as long as the fireball intersected the path between transmitter and receiver but was restored as soon as the fireball moved out of the direct path. Extensive diffraction and multiple-path phenomena were observed.

An upper limit of 0.09 was established for the reflection coefficient of the Shot Priscilla fireball at 9750 Mc.

Gamma ray measurements were obtained at 1,600 yards from Shots Hood and Owens. The detectors performed satisfactorily and were not affected by the EM signal from the detonation.

Serious effects due to the EM signal from the detonation were noted in a bunker 1,270 yards from Hood and in the receiving station about 15 miles from ground zero. The effects in the bunker were apparently due to penetration of the copper shield by the EM signal. Those in the receiving station were apparently due to the large voltage excursions induced on the powerline system.

From Shot Diablo, the maximum intensities of the components of the EM signal that fell in the pass bands of the receivers were found to be 25 μv/m at 160 Mc and 40 μv/m at 960 Mc; no signal was observed at 9850 Mc (minimum detectable signal was 50 μv/m). From Shots Kepler and Owens, the peak intensities of the EM signals at Building 400 were found to be – 10 and – 45 v/m, respectively.

A Monte Carlo calculation of the electron energy distribution has been made; preliminary results of this calculation have been used, with the measured gamma rays, to calculate the radio wave attenuation. The calculated and measured values do not agree over the entire time of attenuation. It is apparent that there are other factors that must be taken into account before a satisfactory calculation of the expected attenuation can be made.

Pgs. 1 thru 4 Deleted

FOREWORD

This report presents the final results of one of the 46 projects comprising the military-effect programs of Operation Plumbbob, which included 24 test detonations at the Nevada Test Site in 1957.

For overall Plumbbob military-effects information, the reader is referred to the "Summary Report of the Director, DOD Test Group (Programs 1-9)," ITR-1445, which includes: (1) a description of each detonation, including yield, zero-point location and environment, type of device, ambient atmospheric conditions, etc.; (2) a discussion of project results; (3) a summary of the objectives and results of each project; and (4) a listing of project reports for the military-effect programs.

PREFACE

The experimental work reported here was done at the Nevada Test Site during the spring and summer of 1957.

Project 2.7 was conceived and carried out through the joint efforts of many people. During the intervening 3 years, several of them have left the Naval Research Laboratory, and are no longer in Metropolitan Washington.

The data interpretation and analysis, and the theoretical work in this report have been carried out by three members of the original group— P. A. Caldwell, S. G. Gorbics, and C. A. Pearse. Several other members of the original group have been consulted, during the preparation of this report, concerning details of their portions of the original work. Similarly, the sections they contributed to the Interim Test Report have been drawn on in the preparation of this report.

CONTENTS

Chapter 1

INTRODUCTION

In the initial concept, the objective was to proof test equipment and techniques for neutron and gamma ray measurements during high-altitude detonations planned for Operation Hardtack. In the early planning stages, since it was planned to telemeter the results of these measurements to a ground station, it became necessary to determine whether or not prompt telemetering of the data was feasible. There was no completely adequate theory and very little experimental data available for use in calculating the expected magnitude and duration of the attenuation of radio signals to be expected in the vicinity of a high-altitude nuclear detonation. Because of this lack of information, the objectives were augmented to provide information on electromagnetic (EM) wave attenuation. It was felt that this information would also prove useful in future radar and guidance studies.

For this reason, Project 2.7 was subdivided into two major efforts: Project 2.7.1, the proof test of techniques and equipment for use in the measurements planned for the high-altitude detonations during Operation Hardtack, and Project 2.7.2, the measurement of the radio wave attenuation in the vicinity of a nuclear detonation. The two projects have not been separated in this report, since most of the experiments had applications to both phases of the problem. In Chapter 5, the extent to which each of the objectives was met is summarized separately.

1.1 OBJECTIVES

The specific objectives can be summarized as follows:

(1) To measure radio wave attenuation as a function of range by placing four X-band transmitters on a radial line from ground zero to the receivers, located at distances such that the calculated peak attenuation would cover the range between 20 and 50 db. This measurement was intended to check the radial dependence of attenuation as calculated in Section A.2.

(2) To measure radio wave attenuation as a function of frequency for three radio links operating on frequencies of about 160, 960, and 10,000 Mc. Ranges and positions were so chosen that the calculated peak attenuation would be approximately 40 db. The results of this measurement were to be used in evaluating the calculation of the dependence of attenuation on radio frequency, as outlined in Section A.1.

(3) To measure the attenuation at a single frequency with a time resolution of 0.01 μsec. This data, with gamma ray data of similar resolution, would allow a determination of an upper limit for the mean lifetime of free electrons that would be smaller than the current upper limit.

(4) To measure the gamma ray flux as a function of time with a time resolution of about 0.01 μsec. This measurement fulfilled several functions, since these results were necessary for the interpretation of the attenuation measurements, including the high-resolution experiment, and provided a proof test of the techniques for measuring high-intensity gamma ray fields.

(5) To transmit measured neutron and gamma ray flux on a microwave (X-band) telemetry link, to look for systemic effects. This objective was not carried out directly, since the radiation measurements were made in Objective 4 and the telemetry link was examined as a part of Objectives 1 and 2.

(6) To observe at the receiver station the duration and magnitude of the EM effect at 160, 960, and 10,000 Mc.

(7) To monitor equipment performance in the bunkers, to determine the effects of the EM effect on the measuring equipment.

(8) To measure radio wave attenuation through the fireball as a function of time at several different frequencies.

(9) To measure radio wave reflection by the fireball as a function of time at several different frequencies.

1.2 BACKGROUND

The attenuation of EM waves in the vicinity of a nuclear detonation depends essentially on three factors: (1) the instantaneous electron production rate, (2) the rate of removal of free electrons, and (3) the complex conductivity. The first of these factors, the electron production rate, is dependent upon the gamma ray production rate and has been measured by various investigators (References 1 and 2). The uncertainty in the available data relating to the rate of removal of free electrons and to the calculation of the complex conductivity, which depends on the collision frequency, prompted an emergency project during Operation Redwing (Reference 3).

The objective of the Redwing project was to make a measurement of attenuation versus time with 1-μsec resolution over radial paths for which the attenuation was to be kept within the dynamic range of readily available equipment (25 db). If it is assumed that the gamma ray intensity from a nuclear device scales directly as the yield (Reference 2), it is possible to deduce that the mean lifetime of free electrons at sea level is about 6.6×10^{-8} second. Using the laboratory measurements pertaining to the attachment of slow electrons in oxygen (Reference 4), an electron mean lifetime of 1.7×10^{-8} second can be calculated. If 1.7×10^{-8} second is assumed to be the more nearly correct value, the disparity between these two values indicates that scaling of the gamma ray intensity directly would generally be inappropriate. A plot of the experimental results for Shot Osage along with the calculated attenuation is shown in Figure 1.1. The shape of this attenuation curve is independent of the electron mean lifetime, but the magnitude depends directly on the mean lifetime and the gamma ray intensity.

It appeared to be desirable to make measurements of gamma ray intensities and EM wave attenuation simultaneously. This would reduce the uncertainty (due to the inaccuracy of scaling the gamma ray intensities with weapon yield) in estimates of the mean lifetime of free electrons and the complex conductivity. More reliable values of these parameters were necessary, to estimate more accurately the duration of radio blackout in the vicinity of a high-altitude nuclear detonation. This information was of considerable importance in determining whether it would be necessary to delay the transmission of data from the instrumentation pods of Projects 2.6 (then being contemplated) and 2.7 at Operation Hardtack. To accomplish the above objectives, Operation Plumbbob Project 2.7 was initiated.

1.3 ELECTROMAGNETIC WAVE ATTENUATION IN THE VICINITY OF A NUCLEAR EXPLOSION

In Section A.1, a general expression for the attenuation of EM waves in an ionized medium has been derived (Equation A.17). This expression shows that attenuation depends primarily on two factors: (1) the instantaneous electron density $N_e(z,t)$ and (2) the real part of the complex conductivity. At Nevada Test Site (NTS) altitudes, (air particle densities of the order of $10^{19}/cm^3$) the electron density is assumed to satisfy the following differential equation:

$$\frac{dN_e}{dt} = Q_e(t) - \alpha_e N_e N_+ - \beta N_e N_{O_2} - K N_e (N_{O_2})^2 \qquad (1.1)$$

Where: $Q_e(t)$ = the rate of production of secondary electrons ($E \approx 20$ ev)

α_e = the electron ion recombination coefficient

β = the two-body dissociative attachment coefficient of oxygen

K = the three-body electron attachment coefficient of oxygen

N_e = number density of electrons

N_+ = number density of positive ions

N_{O_2} = number density of oxygen molecules

For a typical electron density, $N_e = 10^9$, and letting $\alpha_e \approx 10^{-6}$ (Reference 5),

$$\alpha_e N_e N_+ = 10^{12}/\text{sec}$$

assuming $N_e \approx N_+$. The second removal term, using $\beta = 3 \times 10^{-11}$ (Reference 4), has a value

$$\beta N_e N_{O_2} = 1.6 \times 10^{17}/\text{sec}$$

and the final term, with $K \approx 5 \times 10^{-30}$ (Reference 4), yields

$$K N_e (N_{O_2})^2 = 1.4 \times 10^{17}/\text{sec}$$

Upon comparing the relative magnitudes of these items, it can be seen that the electron-ion recombination term is negligible with respect to the attachment terms, so it is possible to write Equation 1.1 as,

$$\frac{dN_e}{dt} = Q_e(t) - N_e [\beta N_{O_2} + K (N_{O_2})^2] \tag{1.2}$$

Since the two attachment coefficients β and K are functions of energy, it seems reasonable to replace them by average values obtained by "averaging" β and K over the electron energy distribution function. The electron energy distribution may be considered quasi-constant, subject only to the condition that the fractional change in $Q_e(t)$ is small enough in a time of order τ. Since this condition is met in the present case (with the exception of the α phase, i.e., the initial rise in gamma ray production), the expression in brackets of Equation 1.2 will be replaced with $1/\tau$, where τ will be called the mean electron lifetime. Equation 1.1 finally becomes

$$\frac{dN_e(t)}{dt} = Q_e(t) - \frac{N_e(t)}{\tau} \tag{1.3}$$

To calculate a value for τ, it is necessary to examine the mechanism by which electrons are produced, moderated, and captured. The gamma ray energy spectrum from the device contains photons with energies up to 5 Mev (Reference 2). These photons undergo collisions with the oxygen and nitrogen molecules in the atmosphere and produce electrons whose average energies are of the order of half the original photon energy. Each of these high-energy electrons then produces, approximately 25,000 secondary electrons through ionizing collisions, losing on the average 34 ev per collision. About 14 ev of this is the energy of ionization, with the remaining 20 ev going into kinetic energy of the secondary electrons. These secondary electrons are then moderated through elastic and inelastic collisions until their energy is low enough (essentially thermal) for them to be captured. Although inelastic collisions account for only about 1 percent of the total number of collisions, the overall energy loss is largely due to

this process, because the average energy loss due to a single elastic collision is only about 1/100,000 of the average energy loss that results from an inelastic collision.

A Monte Carlo program was developed for an LGP-30 Royal McBee computer, to calculate an electron velocity distribution function together with a mean electron lifetime appropriate to the present problem. Steady-state conditions were assumed to prevail so that the numbers of secondary electrons being born and removed per unit of time were taken to be equal. The number of electrons being born per unit time in the i^{th} energy interval, ΔE_i, was determined by the secondary energy distribution function for electrons as measured in Reference 6. The "path" of a given electron is followed in detail, starting with an energy E_i (located in the ΔE_i energy interval) and ending with its being captured. As is usual in Monte Carlo programs, the distance between successive collisions, whether the collision is to be with oxygen or nitrogen molecules, whether the collision is to be elastic or inelastic, and the amount of energy lost in inelastic collisions are all determined by means of drawing random numbers, which are then compared to the appropriate relative cross sections. The program computes and stores the amount of time that each electron spends in any given energy interval during the process of being moderated. The total time that each electron has lived is also recorded. From this information a mean electron lifetime, and an energy or velocity distribution histogram can be calculated.

The accuracy of such a calculation depends directly upon the various collision cross sections, as well as upon other factors. For the purposes of this program, the various electron cross sections used were taken from References 4, 7, 8, 9, and 10.

In Equation 1.3, $N_e(t)$ referred only to a specific point in space. In the present case, it is necessary to include also a spatial coordinate, obtaining

$$\frac{dN_e(z,t)}{dt} = Q_e(z,t) - \frac{N_e(z,t)}{\tau} \tag{1.4}$$

since the electron production function Q_e is a function of both position and time.

If it is assumed that

$$Q_e(z,t) = Q_e(z)\, Q_e(t)$$

then the standard solution of Equation 1.4 will be

$$N_e(z,t) = Q_e(z) \int_0^t Q_e(t')\, e^{(t'-t)/\tau}\, dt' \tag{1.5}$$

Examination of the integrand of Equation 1.5 reveals that it has a sharp spike at $t' \approx t$, provided that $\tau \ll t$. If $Q_e(t')$ is nearly constant, over a time span of order τ, then it may be removed from the integral, and setting $t' = t$ gives

$$N_e(z,t) \approx Q_e(z)\, Q_e(t) \int_0^t e^{+(t'-t)/\tau}\, dt'$$

$$= Q_e(z)\, Q_e(t)\, \tau \left[1 - e^{-t/\tau}\right]$$

$$N_e(z,t) \approx Q_e(z)\, Q_e(t)\, \tau \tag{1.6}$$

where in the last step use again has been made of the fact that $\tau \ll t$.

By combining the general attenuation expression in Equation A.17 with the considerations of the present section, it is possible to record here the working expression for the total EM atten-

uation near a nuclear detonation (Equation A.18) as

$$\Omega = -8.686\ (\omega/c)\ K\ \tau\ Q_e(t) \int_{z_T}^{z_R} Q_e(z)\ dz \qquad (1.7)$$

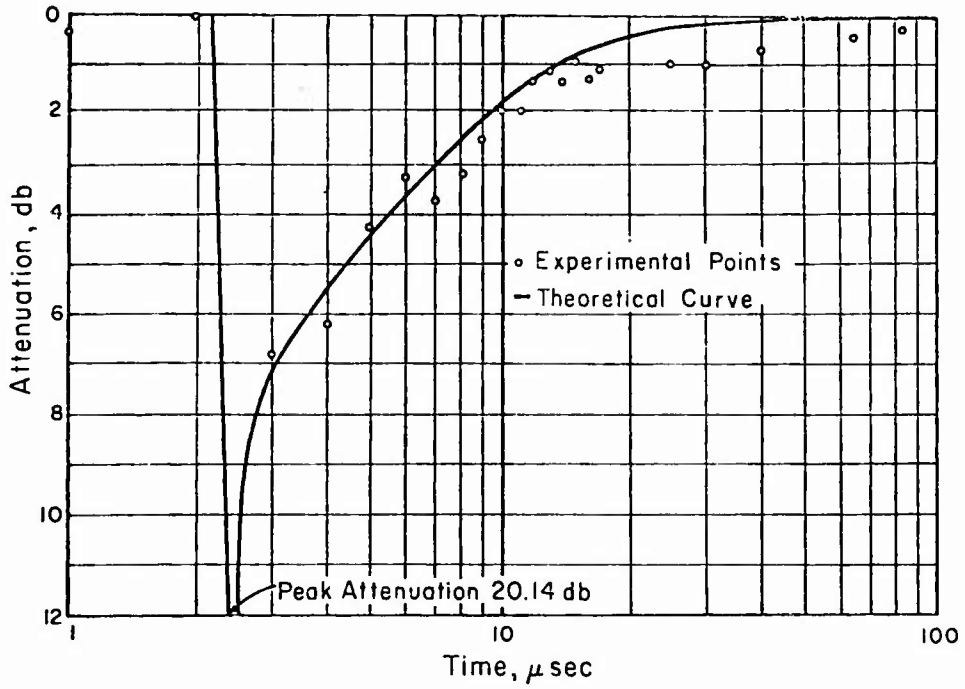

Figure 1.1 Attenuation results for Shot Osage, Operation Redwing.

Chapter 2

PROCEDURE

2.1 FIELD INSTALLATION

The installation consisted of two essential parts: transmitting and/or gamma ray measuring equipment, generally located near ground zero, and receiving and general support equipment at Building 400. The major portion of equipment to be located near ground zero was installed in rudimentary protective bunkers, with only gamma ray detectors and antennas exposed. Time and budget limitations required that all bunkers be placed in one shot area. Area 9 was chosen, because the type of shots scheduled there seemed to be appropriate to the goals of the experiments. Figure 2.1 shows the position plan for the bunkers, and Figure 2.2 shows the relative position of the bunkers and receiving station.

The bunkers consisted of 6-foot-diameter concrete drain tiles placed deep enough to provide 6 feet of earth above the bunker (Figure 2.3). The bunker manholes were filled with cans of earth after the bunker was buttoned up, to shield the installation from gamma rays. The interior of the bunkers was lined with $\frac{1}{32}$-inch copper to reduce the effects of the EM signal.

Power was supplied to the bunkers by an external source during preparations. During the period from about H−4 hours through shot time the bunkers operated as self-contained units, with power supplied by a 5-kw, gas-engine-driven generator installed beneath the floor of the bunker. The bunker was ventilated by a 2,000-cfm blower fan. Time signals provided by Edgerton, Germeshausen, and Grier, Inc. (EG&G) were used to perform the necessary operations within the bunker.

Figure 2.4 is a block diagram of a typical bunker installation. The transmitter provided EM radiation directed by the antenna to the receiving installation at Building 400. The transmitter output was monitored, and the monitor signal was recorded in the bunker on the oscilloscopes and an oscillograph. Three gamma ray detectors are shown. One of these was used to provide a fast pulse to trigger the oscilloscopes. The actual measurement of the gamma rays was the function of the other two, which were used at different scintillation efficiencies to extend the dynamic range (Section 2.4.3). Several oscilloscopes at different sensitivities were used with each detector to extend the sensitivity range further. The H−5 second and H−1 second signals were used to turn off the fan, arm the scope sweeps, open the camera shutters, and initiate a time-delay circuit to shut off all equipment at approximately H+1 second. At H−1 second, a mechanism was activated that disconnected the bunker from external power and EG&G signal wires to reduce the possibility of an EM signal entering the bunker.

The receiving equipment was installed in a trailer van located at Station 400; Figure 2.5 shows a typical arrangement. The receiver output signals were presented on three time scales: 100 μsec, 18 msec, and several seconds. Camera shutters and sweep-arming circuits were controlled by EG&G time signals. Sweeps were triggered by a fiducial-marker (FIDO) pulse. (A more detailed description of instrument functions is given in Section 2.4.)

2.2 SHOT PARTICIPATION

Project 2.7 participated in nine shots.

2.2.1 Shot Boltzmann. One of the objectives was to observe the attenuation of radio waves when transmitted through the fireball; Shot Boltzmann was selected for this experiment. The

point on Banded Mountain at which the transmitter should have been located was inaccessible. A compromise transmitter location on Banded Mountain (Figure 2.6) was employed such that the line of sight from the transmitter antenna to the receiver antenna was within 100 feet of the device cab.

Transmitters at frequencies of 160, 960, and 9750 Mc were used. The signal level was recorded at Station 400 with a Century oscillograph recorder, a drum camera, and oscilloscopes, thus providing time scales in the order of seconds, milliseconds, and microseconds, respectively.

2.2.2 Shot Franklin. The Boltzmann instrumentation was used again during Shot Franklin. In this case, the propagation path came within 1,200 yards of the shot tower.

2.2.3 Shot Lassen. The work planned for Lassen included preliminary experiments designed to check intensity, response, and calibration for later shots. The bunker installations were not completed in time for participation during Lassen; most of the experiments intended for Lassen were included in later shots.

2.2.4 Shot Wilson. The experiment planned for Wilson was the measurement of attenuation at X-band frequencies as a function of range, with a simultaneous gamma ray measurement. Time was available to install only three of the four transmitters originally planned. They were installed in Bunkers .01, .03, and .04, and gamma ray detectors installed in Bunker .02. Attenuation data was taken at Station 400 with oscillograph, drum camera, and oscilloscopes.

2.2.5 Shot Priscilla. The experiment during Priscilla was to observe reflections from the fireball, to find the reflection coefficient (radar cross section) as a function of frequency and time, and to attempt to relate this to electron density gradient. Because Priscilla was delayed to a date approaching that for Shot Hood, only the X-band equipment could be spared for this installation. The transmitter (Figure 2.7) was installed on a line from ground zero to Station 400. The transmitting and receiving antennas were oriented on the burst point by survey.

2.2.6 Shot Hood. The experiment planned for Hood was the measurement of attenuation versus frequency, with a simultaneous gamma ray measurement. Transmitters at 160, 960, and 9600 Mc were installed along with the gamma ray measuring equipment in Bunker .05 (Figure 2.8). Monitoring devices were installed, with an additional X-band system (9750 Mc), in Bunker .03 (Figure 2.9).

2.2.7 Shot Diablo. The recording equipment at Station 400 was used to observe EM signals in the frequency bandwidths of receivers at 160, 960, and 9850 Mc.

2.2.8 Shot Kepler. During Kepler, the EM signal at Station 400 was measured with a vertical dipole.

2.2.9 Shot Owens. The purpose of the experiment during Owens was to measure both the radio wave attenuation and the gamma ray flux with high time resolution, to place a smaller upper limit on the mean life of the electron. A 4700-Mc system was provided for this purpose. The primary installation was in Bunker .05 and consisted of the 4700-Mc transmitter, X-band time correlation transmitter, and gamma ray equipment. Gamma ray detectors were also installed in Bunker .04. The EM signal was again measured with a vertical dipole.

2.3 REQUIRED DATA

In terms of the objectives of Project 2.7 and the background outlines in Section 1.2, data was required on attenuation as a function of time and frequency. In addition, auxiliary data

was needed to separate effects that interfere with the direct measurement of radio wave attenuation. One of these was the EM signal that may find its way into either the transmitter or receiver, or both.

The attenuation data desired falls, on the basis of required time resolution, into two groups. Most of the objectives could be met with data of 1-μsec resolution, since the important factor is the relationship between the magnitudes of the attenuation and gamma ray pulses, while the shape of the attenuation curve only had to be known to about 1-μsec accuracy. For this reason, all of the transmitters used, with the exception of the two in the high-resolution experiment during Shot Owens, were modulated with 1-Mc square waves. The RF signal transmitted thus consisted of 1-μsec-long pulses with a 1-Mc repetition rate. The receiving system used for these experiments had a bandwidth such that these pulses were obtained essentially undistorted. One advantage of this type of transmission is that the data is obtained with an inherent time scale.

The data required from the high-resolution experiment made it necessary to reproduce the shape of the attenuation curve to an accuracy of 1 shake (0.01 μsec). To accomplish this by the means outlined above would have required extremely short pulses with a much higher repetition rate. The technical problems were formidable, so a continuously radiated signal was used—4700 Mc for the attenuation measurement, and about 9700 Mc for the time correlation link. The receiver would then see the attenuation as a modulation on the intensity of the 4700-Mc radiation and treat it as it would any other pulse.

Since the attenuation was assumed to be the result of free electrons produced by the nuclear radiation from the detonation, the measurement of the gamma ray flux as a function of time was a fundamental requirement.

2.4 INSTRUMENTATION

Project 2.7 included a variety of experiments that required a large amount of specialized equipment. Commercial components were used when possible, but many items required special design and fabrication. Those of the special items that bear on the accuracy or validity of the experimental results, or appear to be of general utility, are described below.

The propagation measurements, with the exception of the high-resolution experiment, were made with combinations of the same "building block" components. These components are discussed in Sections 2.4.1 and 2.4.4. The high-resolution experiment was sufficiently different to warrant a separate discussion in Section 2.4.2. The gamma ray equipment was common to all of the installations and is discussed in Section 2.4.3.

2.4.1 Radiofrequency Propagation Study Link. Transmitters. A block diagram of the Band 1 transmitter (152 to 160 Mc) is shown in Figure 2.10. The essential components of this transmitter are a General Radio (GR) 1208B variable-frequency oscillator, Airborne Instruments Laboratory (AIL) gated amplifier, Hewlett-Packard 211-A square-wave generator, AIL power amplifier, and an M. C. Jones directional coupler and power indicator. The oscillator was used as a source of RF energy; its output was fed into the gated amplifier, which acted as a modulator. A 1-Mc square wave from the square-wave generator was mixed with the RF signal in the gated amplifier to produce, at its output, an RF carrier modulated at a 1-Mc rate. The difference in the power level from "off" to "on" was such that the "off" level was greater than 60 db below that of the "on" level. This difference in level between "on" and "off" is important, since it is one of the factors determining the maximum dynamic range of the measurement. This signal was then amplified by the power amplifier to a peak power output of 7 watts. The output signal from the power amplifier was coupled through the directional coupler to the antenna. The purpose of the directional coupler was to provide continuous monitoring of the power output from the transmitter by the power indicator. Tube and circuit operating voltages were supplied by Lambda power supplies.

A block diagram of the Band 2 transmitter (890 to 960 Mc) is shown in Figure 2.11. A GR 1208B oscillator served as a source of RF energy. Its output was fed to a gated amplifier where the RF signal was modulated in the same fashion as for the Band 1 transmitter. The RF output signal from the gated amplifier was then multiplied to the desired operating frequency by means of a tripler and doubler (AIL). The output signal from the doubler was then fed to a driver amplifier where the power in the RF signal was raised to a sufficient level to drive the final power amplifier (AIL). The peak power output from this amplifier was about 8 watts. This signal was fed through the directional coupler to the antenna. The power indicator continuously monitored the output from the transmitter. All tube and circuit voltages were supplied from Lambda power supplies.

The block diagram for the Band 4 transmitter (9800 to 10,200 Mc) is shown in Figure 2.12. A Varian V-55 klystron oscillator was the source of RF energy. It delivered an 800-mw peak-power output and was square-wave modulated at its repeller by a 1-Mc signal from a 211-A square-wave generator. The RF signal output from the klystron was waveguide coupled to a ferrite isolator that reduced the effect of loading of the following circuitry on the klystron. A Hewlett-Packard X530A cavity wave meter was used to measure the frequency of the RF energy. A Hewlett-Packard X750E directional coupler and 430-CR power meter were used to monitor the power output.

Receiving Equipment. A block diagram of the Band 1 receiver is shown in Figure 2.13. The signal from the antenna was coupled through RG8/U coaxial cable to the RF amplifier. This amplifier was fixed-tuned to the center of the 152- to 160-Mc band and had an overall bandwidth of approximately 10 Mc. The output signal from the RF amplifier was fed to the grid of the mixer tube along with a loosely coupled signal from the local oscillator. The 30-Mc intermediate frequency signal from the mixer was fed through two stages of preamplification and then coupled through a short coaxial cable to the logarithmic intermediate-frequency (IF) amplifier. From this point on, the AIL receivers were identical. Each had a logarithmic intermediate-frequency amplifier, video detector, video amplifier, and monitor scope.

To handle the wide range of signal levels expected in the attenuation measurements, it was decided that the IF amplifier should have a logarithmic response. That is, the detected output signal of the IF amplifier should be proportional to the logarithm of the input RF power. The IF amplifiers, as finally developed by AIL, were not true logarithmic amplifiers but were more a combination of a linear and logarithmic response. Since this type of amplifier was adequate and could be calibrated, it was accepted. In its final form, the IF amplifier had approximately 50 db of dynamic range and a bandwidth of about 2 Mc. The detected video output of this amplifier was approximately 0.6 volt at maximum RF signal input to the receiver. A video amplifier with a gain of about 70 was used to bring the video signal up to an amplitude sufficient for recording purposes.

A block diagram of the Band 2 receiver is shown in Figure 2.14. The RF signal was fed from the antenna through RG11/U coaxial cable to the input of the receiver. Here it was mixed in an Empire Devices CM 1015 crystal mixer with the signal from the local oscillator, a GR 1209-B variable-frequency oscillator. The 30-Mc IF was then amplified by the IF preamplifier and fed through a short piece of cable to the logarithmic IF amplifier. The remaining portion of the receiver was identical to that described in the previous paragraph.

A block diagram of the Band 4 receiver is shown in Figure 2.15. The RF signal was waveguide coupled from the antenna to the input of the receiver. Here it was mixed in a balanced crystal mixer with the signal from the local oscillator, a Varian VA-6314 reflex klystron. A balanced mixer was used because, in the ideal case, it should improve the noise figure of the receiver by 3 db. The IF output from the mixer was then fed through an IF preamplifier to the logarithmic amplifier in the fashion previously described.

Antennas. The antennas used in the Band 1 system were Andrew 3645 corner reflectors with two bays of two sections each stacked vertically. The gain provided by each of these antenna was 12.5 db, and the beam width was approximately 15°.

The Band 2 receiving antenna was a 6-foot parabolic dish, center-fed from a half-wave dipole, with a gain of 23.2 db and a beam width of 11°. The transmitting antenna was a 2-foot parabolic reflector fed in the same fashion, with a gain of 14 db and a beam width of 33°.

The Band 4 receiving antenna was a 6-foot parabolic reflector fed from a waveguide, with 43 db of gain and a beam width of 2°. The transmitting antenna was a 2-foot parabolic reflector fed from a waveguide, with a gain of 32.3 db and a beam width of 6°.

Calibration. Since the receiver contained a logarithmic element (lin-log IF amplifier), special consideration had to be given to the method of calibration. Most commercial signal generators provided for variable modulation percentage. An indicated modulation of 100 percent meant nearly 100 percent. A good generator with square-wave modulation usually gave a ratio of 20 db between the peaks and valley of the square wave for nominal 100-percent modulation. Since the dynamic range of the IF amplifiers used was greater than 40 db, the amplifiers could see only the 20-db-modulation depth and could give a 20-db output signal, which was constant over a wide range of input power. Thus, it was necessary that the modulation depth be greater than the dynamic range of the lin-log IF amplifier. The modulation used on the transmitting klystron was designed to carry the klystron completely out of oscillation and thus provided modulation ideally suited for calibration.

Since all components in the receivers except the logarithmic IF amplifiers operated in linear fashion, their calibration as part of an X-band receiver was adequate. Therefore, the X-band transmitter was set up as a signal source, and calibrated attenuators with the necessary range were used. Calibration curves of the four logarithmic IF amplifiers are shown in Figures 2.16 through 2.19.

2.4.2 High-Resolution Equipment. 4700-Mc System. In the high-resolution experiment, it was decided that a wide band RF link was necessary in order to make the attenuation measurement with the desired 1-shake time resolution. To this end, a portion of a high-resolution radar operating at 4700 Mc was borrowed from the Civil Aeronautics Administration. A block diagram of the transmitter is shown in Figure 2.20.

The transmitter consists of a 2K22 klystron driving a traveling wave tube (TWT) power amplifier with a CW power output of approximately 500 mw. A cross-guide 20-db coupler was inserted at the transmitter output to couple a small portion of the output to a crystal detector. This provided a means of monitoring the power output from the transmitter. All tube and circuit voltages were supplied from self-contained power supplies in the transmitter.

A block diagram of the receiver is shown in Figure 2.20. The RF signal was fed from the antenna through an RG8/U coaxial cable to the input of the receiver. The first stage of the receiver was a TWT amplifier operating at 4700 Mc with a gain of approximately 40 db. To limit the bandwidth of the receiver and thereby reduce interference from undesired signals, a passive filter network was placed ahead of the TWT. This network was tuned to 4700 Mc and had a bandwidth of approximately 175 Mc. The output of the TWT was fed directly to a video crystal detector. From here, the video signal was amplified by several stages of a distributed-line-type amplifier. This amplifier had an overall gain of about 33 db and a bandwidth of 50 Mc. The output of the receiver was taken from a cathode follower and fed through coaxial cable to the recording equipment.

The transmitting and receiving antennas used here were parabolic reflectors fed from a waveguide. They had a gain of 35 db and a beam width of 4°.

X-Band Time Correlation System. Since it was the purpose of the high resolution experiment to obtain a time correlation between the instantaneous gamma ray field and the RF attenuation, a time correlation system was developed. A portion of this system was an X-band RF link between the bunkers at Station 9-2.7-9009.05 and the van at Station 400.

A block diagram of the transmitter is shown in Figure 2.21. It is essentially the same as discussed in Section 2.4.1, the difference being that it was operated without modulation until the arrival of the gamma ray field at the bunker. At this time, the klystron was driven out of oscillation by a signal that was obtained from a gamma ray trigger photomultiplier located di

rectly above the bunker. Thus, a step-function change in the RF carrier whose time of occurrence was established by the gamma rays was transmitted back to the receiving van with a known total delay.

A block diagram of the receiver is shown in Figure 2.21. It is a special wide-band superheterodyne receiver developed at the Naval Research Laboratory (NRL). The waveguide input to the receiver feeds a single ended crystal mixer operating as a first detector. The local oscillator is a 2K25 klystron. The IF is 100 Mc, which is amplified by three Spencer Kennedy Lab 202P chain amplifiers with a bandwidth of approximately 200 Mc. The crystal video second detector feeds three Hewlett-Packard 204B chain amplifiers with a bandwidth of approximately 150 Mc. The output from the receiver is a negative step function of about 20-volt amplitude with a 10^{-8} second rise time and a signal-to-noise ratio of about 20 to 1.

The transmitting and receiving antennas used here were the same as the Band 4 antennas described in Section 2.4.1.

Time Markers. To establish a 1-shake time correlation between the instantaneous gamma ray field and the RF attenuation, a time marker whose time of occurrence relative to prompt gamma ray pulse was known must be displayed along with the data. In both the bunker and the van recording systems, the time reference marker was established by the output signal from a photomultiplier looking at a Pilot B scintillator located in the immediate vicinity of the bunkers at Station 9-2.7-9009.05. At the arrival of the prompt gamma ray flux, the output from the photomultiplier is driven rapidly to saturation and then remains fairly constant for a time that is long compared with the sweep time on the scopes. Hence, a step function of voltage is developed across the anode load resistor of the photomultiplier. This signal turned off the time correlation transmitter carrier, as discussed above, and was used to provide time markers in the bunker.

The time marker for the bunker recording system was fed into the bunker through a length of RG8/U cable. This signal went directly to three scope trigger inputs where each scope was triggered successively with about 0.002-μsec delay between the starts of the sweeps. The signal was then delayed 0.095 μsec and fed into two Hewlett-Packard 204B chain amplifiers connected in series. The 52-ohm anode load resistor of the photomultiplier was located at the input to the first amplifier. These amplifiers each had a voltage gain of 20 db, rise time of 0.003 μsec, and a bandwidth of approximately 150 Mc.

The output of the amplifiers was fed to the deflection plates of the three scopes and then through a length of cable shorted at the far end. This shorted cable formed a pulse on each scope, which established a time-reference marker for the data presented on that scope.

2.4.3 Gamma Ray Detectors. Since radio wave attenuation is caused by electrons, the rate of production of these electrons is important for quantitative analysis of observed attenuations. At early times after the detonation of a nuclear device and at radial distances of 0.5 mile and farther, electrons are produced by the action of gamma rays on the surrounding air. At somewhat later times (a little less than 30 μsec for 14-Mev neutrons at 1 mile from the device), some of the electrons are produced by the neutrons. For this experiment the roentgen is a natural unit for measurements of the gamma rays, since the roentgen is defined in terms of the number of electrons produced in a cubic centimeter of air.

For gamma ray intensity measurements with a time resolution of 10^{-8} second, the simplest detection system consists of a fast scintillator and some device for measuring the light output as a function of time. The requirement that the scintillator be fast, that is, have a decay time of less than 10^{-8} second, rules out all the inorganic scintillators. A liquid scintillator consisting of a solution of toluene and terphenyl was selected, since this combination has been well tested at previous nuclear tests and seems to work at intensities up to 5×10^{9} r/sec before saturating.

Since toluene, by weight, consists mostly of carbon, its response as a function of gamma ray energy will closely approximate that of air, which averages only a little more than one atomic number higher than carbon.

A vacuum photodiode rather than a photomultiplier was chosen as the light measuring device. The advantage of no variation in gain with supply voltage for the photodiode outweighed the advantages of photomultipliers, e.g., placing the photomultiplier at some distance from the scintillator so that gamma ray shielding could be used around the tube. For reasons of economy and time, a readily available tube, the 935, was selected. This tube has a spectral response that peaks in the near ultraviolet and thus matches the ultraviolet light output from the scintillator.

Photodiode Selection. To test the pulse response of these photodiodes, two types of high-intensity light flashers were used. One was an FX-1 flash tube manufactured by EG&G. The flash tube was fired by charging a 0.2-μfd capacitor to 8 to 15 kv and then discharging it through the flash tube by firing a 5C22 hydrogen thyratron. This unit gave a pulse whose half-width was approximately 1 μsec. The other consisted of a similar unit containing a flash tube made at NRL and gave a 30-mμsec pulse when a 500-μμfd capacitor was used.

The 935 photodiode had to meet rather stringent requirements. First, the tubes to be used must have dark currents of the order of 10^{-12} ampere or lower. The reason for requiring such low dark currents was that the gamma ray calibration measurements were made with currents of the order of 10^{-10} ampere. To keep down the dark currents, measurements were made with only 67 volts applied across the tube. Calibration measurements were made at the same voltage. Since some of the tubes were to be used at 3,000 volts, a test was performed to see if the tube gave the same pulse output when the voltage was changed from 67 to 3,000 volts. Only tubes whose output varied by 15 percent or less were used. This test was made by connecting the tube to a coaxial cable, RG114/U, whose characteristic impedance is 185 ohms, and terminating the cable with a resistance of 185 ohms at the oscilloscope on which the pulse was displayed. Care was taken to use light pulses that did not raise the photodiode output above the linear region when 67 volts were used.

The next test rejected all the tubes that broke down when subjected to a number of light pulses that would give a 1-ampere output with the voltage at 5,000 volts. These tests eliminated three tubes out of four.

A major problem of high-intensity gamma ray measurements is the fact that the intensities involved are much higher than those that can be produced in the laboratory. In particular, the Co^{60} source available for the calibration of the detectors gave detector current outputs that were about 10^{10} times smaller than the peak output expected. Extrapolation of the calibration measurements by 10 orders of magnitude is a problem of some concern. As far as is known, photo surfaces emit electrons directly proportional, in number, to light intensity (for a fixed spectral distribution). This is true only if the photo surface has a low electrical resistance as is the case for the 935 tube. It would be expected, then, that the output current would be limited only by space charge saturation of the tube.

A test was made by placing the photodiode close enough to the 1-μsec flash tube, the FX-1, so that the tube was saturated at all voltages. A plot of the peak current versus photodiode voltage showed that the output was approximately proportional to $V^{3/2}$; thus, the effect was clearly that due to space charge. Next, the FX-1 tube was shielded except for a small portion so that the light source approximated a point source, and the voltage was varied to give a non-saturating pulse when the photodiode was 1 foot away. Since the FX-1 intensity varies very little from flash to flash, it was possible to move the photodiode farther and farther away and check the output versus the distance. A variation of 10^4 in the square of the distance was covered. The photodiode output, as measured by an oscilloscope, varied inversely as the distance squared, as would be expected if it were linear. The limits of accuracy were approximately ± 5 percent.

Various tubes were tested at 3,000 volts to determine their linear output current range. At 3,000 volts, all tubes gave a linear output up to more than 0.5 ampere. An easy rule of thumb for the 935 tubes is that their output is linear up to currents of half their saturation current.

Since some of the tubes were to be used to measure gamma rays at a time after those tubes had been saturated, a test was made to find the effects of saturation on a pulse that occurred

somewhat later. To do this the FX-1 flash tube was placed at a distance that would have given a maximum current from the 935 of about 0.5 ampere if the tube were not saturating. The 935 voltage was only 100 volts, which limited the current to 0.01 ampere. Another pulse from the 30-mμsec flash was timed to occur when the current from the 935 had dropped to about a third of the saturation value. No apparent differences between the short pulses were visible, whether they occurred after the FX-1 saturation pulse or were triggered separately. From this it was concluded that, as soon as the 935 current drops to about half the saturated value, the tube is responding linearly despite being saturated a few microseconds before.

Calibration. To calibrate the detectors with accuracy, it was necessary to use a radioactive source, although a pulsed gamma beam would have more closely approximated operating conditions of the tube. This calibration technique made it necessary to consider the question of the response of the 935 photodiode to a continuous light and to a pulsed light of the same intensity. To test this response, an intense light source was beamed at a rotating mirror and then focused by a lens system on a slit. The 935 tube was placed at a distance behind the slit so that approximately half of the photocathode was illuminated. The output from the 935 was measured by an oscilloscope and resistor system. With the scope set for dc input, the mirror was rotated by hand until the maximum deflection of the cathode ray tube beam occurred. This gave the steady-state current. Then, the motor was started and run up to a speed to give about 25-μsec light pulses through the slit onto the 935. The pulse height observed corresponded to the dc deflection of the oscilloscope beam.

The gamma ray detectors were designed for two sensitivities. The low-intensity detectors consisted of a pyrex glass cell about 3 inches in diameter and 3 inches long. The 935 photodiode was placed as close to the end of the cell as possible. With the cell filled with a solution of ⅓ percent terphenyl in toluene, the detector sensitivities ranged from 2 to 3×10^{-8} amp/(r/sec). Since the 935's were linear to 0.5 ampere, the most intense field that could be measured with this type of detector was about 2×10^{7} r/sec. To measure intensities greater than this, a high-intensity type of detector was designed. This consisted of a scintillator cell of approximately the same size, but with the photodiode placed 15 inches from the end of the cell. The cell and the photodiode were connected by a 2-inch-diameter black anodized aluminum tube. The sensitivity of this type of detector was approximately one-hundredth that of the low-intensity type. Thus, 0.5 ampere corresponds to about 2×10^{9} r/sec.

The detectors were calibrated at NRL using the facilities of the Radiation Calibration Section. Among these facilities is a 20-foot well containing a movable Co^{60} source of about 140 curies. Gamma ray intensities from 0.36 to 0.0036 r/sec could be readily obtained by changing the source-detector distance. The field in this well has been calibrated in terms of the Co^{60} standard field at the National Bureau of Standards (NBS) and is known to ±3 percent. Current from the detectors was determined by measuring the voltage across a standard resistor with a vibrating reed electrometer. The resistor used had been checked by NBS to ±0.1 percent.

A 300-kv, constant-potential, X-ray machine whose output is measured by a standard air chamber was used to determine the energy response of the detectors to lower energy radiation. Table 2.1 shows the response of a typical detector in terms of its Co^{60} gamma ray sensitivity. The median energy is defined as the energy that separates the number of photons into two equal groups.

The field from a Navy-type UDM-1 gamma ray calibrator containing 5 curies of Co^{60} was checked against the laboratory standard Co^{60} field, shipped to NTS, and used for a check on the detectors just before they were installed at the bunkers.

The gamma ray response of the phototubes without a scintillator was measured to be approximately one-hundredth that of the low-intensity detector. Thus, for the high-intensity detector, the response of the tube would have been equal to that due to light from the scintillator. For gamma ray measurements at NTS, the phototube of the high-intensity detector was shielded by about 4 inches of lead and buried in the ground 1 foot deep. Thus, the response of the tube itself to gamma rays being measured was kept to a small percentage of the tube-scintillator response.

Since the preceding calibration measurements were for steady-state conditions, it was desirable to check the detectors with gamma ray pulses. To do this, the detectors were placed 1 meter from the target of the NRL 20-Mev betatron. Photographs were taken of individual pulses displayed on an oscilloscope. These pulses were 0.1 to 0.2 μsec long, depending on the setting of the betatron controls. Next an r-chamber enclosed in lucite was used to measure the average field at the detector position. Thus, it was possible to determine the number of roentgens per pulse and compare this value with that obtained by measuring the area under the pulse given by the detector. The two measurements were made several times and checked to ±25 percent, which is about the limit of accuracy of the experiment.

Field Installation. The complete gamma ray measuring equipment at the NTS was made up as follows. At each position where a measurement was to be made, two or three detectors with the scintillators at ground level were used. The number used depended on the range of intensities to be covered. The detector outputs were connected to Tektronix 541 oscilloscopes, and the display was photographed by a Dumont 298 camera. The signal lines to the oscilloscopes consisted of approximately 12 feet of RG114/U coaxial cable terminated at the oscilloscopes in the bunker with 185-ohm resistors. In general, each detector's output was viewed by two oscilloscopes whose sensitivities were set a factor of 10 apart. To keep from heavily overloading the more sensitive oscilloscope, the detector voltage was set so that the detector current space charge saturated at a value that would give approximately 20 times full-scale deflection on the Tektronix 541 oscilloscope. It was found that the 541 would take twice this overload, but that more than this caused difficulties. To give a clearer idea of the apparatus, a typical installation is described below.

Detector 1, a high-intensity detector, was run at 3,000 volts. At this voltage, the space-charge-limited saturation current would give about 160 volts across the 185-ohm termination. The output of Detector 1 was connected to Scope 1 set at 20-v/cm deflection sensitivity. From there, the pulse went to Scope 2 where the signal line was terminated. The sensitivity of Scope 2 was set at 2 v/cm. Thus, full-scale deflection of 4 cm for Scope 2 was 8 volts, or about one-twentieth of the maximum possible pulse from the detector. A 0.4-cm deflection on Scope 2 is one-hundredth the signal for full-scale deflection on Scope 1. Therefore, if only signals of 0.4 cm or greater are considered, the detector system is capable of recording a range of 100 in intensity.

To cover the next range in sensitivity below that covered by the Detector 1 system, Detector 2, a high-intensity detector, was operated at 100 volts. At this voltage, it was limited by space-charge saturation to a maximum pulse of 1.6 volts. The output was viewed by Scopes 3 and 4 set at 0.2 and 0.05 v/cm, respectively. The maximum sensitivity of the 541 scope with the type preamplifier used was 0.05 v/cm so a setting of 0.02 v/cm was not available. Here, the intensity range covered is only 40.

Detector 3, a low-intensity detector whose sensitivity was 100 times that of Detectors 1 and 2, was connected to Scopes 5 and 6. These scopes were set at 0.5 and 0.05 v/cm, respectively. The voltage of Detector 3 was set at 150 volts to limit the pulse to about 4 volts. The entire system of three detectors and the associated scopes covered an intensity range of 4×10^5.

Trigger Generator. To correlate the sweeps of the various scopes in time, all were triggered externally by the pulse from the gamma ray trigger detector. This detector was made up of a 931A photomultiplier with the voltage distributed along the dynodes so that the latter stages were run at higher voltages to give larger output currents before space-charge saturation. The 931A looked at a Pilot B scintillator. The output of the tube was connected to the scopes by an RG8/U coaxial line terminated by its characteristic impedance of 52 ohms. This combination gave a pulse of about 20 volts when the photomultiplier was operated at 1,300 volts.

2.4.4 Recording and Control Equipment. To obtain as much information as possible from each shot, it was found desirable to make recordings that covered a wide range of time intervals

beginning approximately at detonation time referred to the recording station. The recording methods decided upon consisted of three main types.

The first of these was a high-speed recording. These were photographic and made from high-speed oscilloscopes to cover a range of from 1 to 100 μsec, beginning at detonation time.

The second was a medium-speed recording; again, it was done photographically from cathode ray tubes. The time interval covered here was about 15 msec, with 1-μsec resolution, beginning slightly before detonation time.

The last was a slow-speed recording covering a time interval of about 2 to 15 seconds, with 250-μsec resolution, starting slightly before detonation time.

All recording systems were designed so that the operation was automatic with timing signals supplied by EG&G and triggering or time markers from either an EG&G FIDO or special time-mark generators developed at NRL.

High-Speed Recording. The high-speed recording of data occurring immediately after the detonation and up to H + 100 μsec was done with a Dumont 298 camera looking at a single sweep presented on the face of a Tektronix 541 oscilloscope. To insure that the recording oscilloscopes displayed only the desired information, a sweep-lockout chassis was devised. This circuit was used both in the bunkers and in the receiving station at Building 400.

The recording oscilloscopes were set up to be triggered from the output signal of a photomultiplier tube. Therefore, the possibility existed that the scopes could be triggered at other than the desired time by extraneous pulses. The operation of the sweep circuits in the scopes was such that, once the sweep had started, the stability control could be turned all the way back without interfering with the sweep. However, the sweep could never be triggered again until the stability control was readjusted for proper operation. This property was used for lockout-circuit operation.

The sweep-lockout circuit prevented extraneous signals from triggering the scopes in the following fashion: Before the signal arrived at H − 1 second, the lockout circuit and scope sweep circuits were unarmed, and triggering of the scopes was prevented. At H − 1 second, the lockout circuit and scope sweep circuits were armed, and the scopes were ready to be triggered. At the reception of a trigger signal from the gamma ray trigger photomultiplier or from FIDO at the receiving station, the scope sweep began displaying the desired information, and the sweep-lockout circuits were disarmed by a signal obtained from the scopes.

The circuit diagram for the sweep lockout is shown in Figure 2.22. The input signal to the lockout circuit at J-1 was the plus gate output from the scope. It occurred synchronously with the sweep voltage applied to the cathode ray tube. Tube V-1A inverted this signal and formed a sharp negative spike that was coupled to the left-hand grid of V-2, a bi-stable multivibrator that generated the desired waveform to lock out the sweep circuits in the scope. During the time interval when the sweep was locked out, the left-hand triode of V-2 was cut off, and the right-hand triode was conducting. This condition was indicated on the front panel by a light, which was extinguished. As previously indicated, at H − 1 second a relay-contact closure was applied from the control panel, or from the EG&G lines directly at the receiving station, to J-3, which dumped the charge on a condenser. This brought V3-A out of cutoff very rapidly, applying a sharp negative spike to the arming bus. This spike was applied to each lockout circuit, and the circuits became armed, a condition indicated by lighting of I-1 (Figure 2.22). The control voltage was taken from the left-hand plate of V-2 and applied to the voltage divider. This divider was returned to the − 150-volt supply that established the necessary dc voltage level at the grid of cathode follower V1-B. The output signal was then taken from the cathode of this tube and applied through a diode to the grid of the stability cathode follower in the recording oscilloscope. The purpose of this diode was to disconnect the sweep-lockout circuits from the scope sweep circuits during the triggering interval and, thereby, allow proper operation of the sweep circuits.

During the planning stages of the high-resolution experiment, it was decided that a means should be provided for calibrating the sweep speed of the scope traces. Therefore, a 5-Mc, crystal-controlled oscillator (V-4) was included in the sweep-lockout chassis.

Medium-Speed Recording. The medium-resolution attenuation data was recorded on a 4-channel drum camera designed and fabricated at NRL for neutron time-of-flight measurements. It was used both because of its immediate applicability and to test its utility for field operations.

This recorder consisted of four 5-inch oscilloscope tubes mounted in quadrants above a 20-inch-diameter drum. The inner surface of the drum was grooved to accept 70-mm photographic film. The optical system of this instrument consisted of a 45° first-surface mirror and a 25-mm-focal-length lens (F1:1.5 Wollensak Cine-Raptar) mounted to project the image of the scope tube face on the film surface. The drum was rotated by a $\frac{3}{4}$-hp motor at a speed variable from 3,600 to 4,200 rpm. The oscilloscope tube was operated with only a radial deflection, since the sweep was accomplished by the motion of the drum. The scope tube was chosen to have a phosphor whose persistence was less than 1 μsec, in order to resolve two signals 1 μsec apart. The tube used was the T51P24. To fit four records on the 70-mm film, a demagnification of about 7:1 was used. The tubes and lenses were mounted at different levels to stagger the records across the film without overlap between adjacent channels. Figure 2.23 shows one of the four optical sections.

With these components, the speed required to barely resolve a 1-Mc signal could be calculated. The spot diameter on the cathode ray tube was 0.010 inch; allowing half again the width of the line for spacing, a value of 0.015 in/cycle was applicable. Using the 7:1 optical reduction involved, approximately 0.002 in/μsec was the required speed of the film. This required that the film used have a resolution of about 500 lines/in, a reasonable requirement, since Kodak Tri-X panchromatic film has a resolution of about 700 lines/in. The speed of 0.002 in/μsec, when converted to the necessary angular speed of a 20-inch-diameter drum, yielded about 2,000 rpm. Therefore, the operating speed of the drum was twice the minimum speed required for barely resolving a 1-Mc signal. For loading and unloading, the drum could be removed from the housing that held the tubes and optical system. A dark slide, which could be raised or lowered while the drum was in place, provided the light seal for the film while the drum was being transported to the darkroom for loading or unloading.

The following considerations governed the design of the electronics for the drum camera system. The drum camera recorded for only 1 revolution, or about 15 msec; since a 1-Mc signal was to be recorded, the system had to turn the beam on to full intensity in less than 1 μsec, and after 1 revolution of the drum, the spot had to be extinguished in a few microseconds. A FIDO provided a trigger pulse for a Tektronix 161A pulser, which then produced an intensifier pulse of the correct width and amplitude to operate the cathode ray tubes. Because of the possibility of extraneous pulses triggering the intensifier circuit, a safety circuit or lockout was provided to prevent a spurious trigger pulse from firing the trace. The operation of this lockout system was similar to the system described previously in this section. The lockout was armed by the EG&G timing signal at H−1 second and was automatically locked out after a single intensifier pulse.

The inputs to the vertical amplifiers came from 1-μsec delay lines connected to the receiver outputs. The purpose of this delay was to insure that the cathode ray beam was fully on before the signals to be recorded deflected the scope beam. The outputs of the amplifiers were connected directly to the vertical deflection plates of the cathode ray tubes. The amplifiers were essentially duplicates of a conventional oscilloscope vertical deflection amplifier, and had a response from 20 cycles to 5 Mc.

The drum speed was measured by a tachometer making use of a Magmeter—a special transformer that saturated at low currents. The output of the Magmeter consisted of pulses of constant amplitudes as long as it was operated in a saturated condition. The input to the tachometer came from a magnetic pickup next to the shaft of the rotating drum. The Magmeter output was then rectified and metered.

Slow-Speed Recording. Longer period changes were measured by Century recording oscillographs capable of recording rise times slower than about 300 μsec, and with a flat frequency response from dc to 2,000 cycles. The recorder had a paper speed of about 40 in/sec

and an internal 100-pulse/sec time marker from which the actual paper speed could be determined to ±2 percent. The instruments were used in the bunkers to monitor various power supplies and transmitter power outputs, and in the receiver van to monitor the receiver signals, during the period from H−1 to H+10 seconds. In both applications, a precise timing mark corresponding to zero time was recorded by stretching either a gamma ray or FIDO trigger pulse sufficiently to be registered by the instrument.

Timing and Control Panel. In the original concept of the bunker control system, the bunker installations were to be prepared for a shot and left, operating from station power, in a standby condition until the EG&G time signal at H−2 hours. This was done to allow starting the bunker motor generator and initiating the operation of the installation automatically. Two advantages would result from this approach: the amount of gasoline to be stored in the bunker would be reduced to a minimum and the bunkers could be closed up well in advance of shot time.

The complete sequence of functions to be performed by the control circuitry in the bunkers was, in chronological order:

H−2 hours:	Start motor generator.
H−1 hour:	Transfer bunker from external (station) power to internal (motor generator) power.
H−5 seconds:	Turn off ventilating fan.
H−1 second:	Start the paper drive on a recording oscillograph and arm the oscilloscope sweep and lockout circuits.
H−0.95 second:	Open the oscilloscope camera shutters and disconnect the station from power and signal wires.
H+0.05 second:	Close camera shutters.
H+1 second:	Shut down motor generator, turning off all apparatus.

The operations performed at H−0.95 second were initiated by the EG&G signal at H−1 second and delayed about 0.05 second by using two sequentially closing relays. The operations after zero time were initiated by a relay in the sweep-lockout circuit that operated at the termination of the oscilloscope sweep. This relay operated another relay that closed the shutters at about H+0.05 second and initiated a 1-second delay circuit that in turn shut off the motor generator.

In some experiments, oscilloscopes were not used in all of the bunkers, and therefore, the signal from the sweep-lockout circuit was not available in some bunkers. An additional 1.25-second delay circuit, initiated by the EG&G signal at H−1 second, was included to initiate the after-zero-time sequence. This circuit was left operative at all installations to protect the data against failure in the sweep-lockout circuit.

Before the first scheduled shot, the time signal at H−2 hours became unavailable, for the duration of the operation, in the area containing these bunkers, and a revision of the plan was required. About a 7-hour supply could be held in the gasoline storage space available. Approximately 3 hours were required to warm up the equipment and close up the bunkers, so if the buttoning-up process were completed at about H−3 hours, a 1-hour safety margin of gasoline was left. This eliminated the need for the time signals at the H−2 and H−1 hours. This approach was the one finally adopted. The circuit originally concerned with the signal at H−1 hour was retained and operated manually to transfer the bunker from station power to motor-generator power before the bunker was buttoned up.

Functionally, the control circuitry consisted of two distinct parts: the first was associated with incoming signals (e.g., the EG&G timing signals) and the second with the things being controlled (e.g., the oscilloscope camera shutters). Since the control system was disconnected from the EG&G signals at H−0.95 second, each EG&G signal actuated an electrically latching relay that remained closed during automatic operation, i.e., until the motor generator was turned off. A 3-position switch was associated with each EG&G signal lead such that one position connected the control circuits to the EG&G relay, the center position disconnected all leads, and the other position simulated the closing of the EG&G relay. The position of each

switch, except for "off," and each EG&G relay was indicated by pilot lights, so that the state of the control system was readily apparent. A similar arrangement was used in the output part of the control system, so that the thing being controlled could be operated manually, disconnected from the control system, or operated automatically by the control system. Pilot lights were used in the same way here, permitting the condition of each controlled circuit to be quickly determined.

The various bunkers were used for different functions on different shots, and the control circuits were designed to handle all of these functions. For a given experiment, this sometimes left surplus circuits in the control system, but these could be disabled from the front panel. To set up the control system for an experiment, it was only necessary to throw the appropriate switches into the automatic position.

The only control functions required in the van control system were those involved in opening and closing the oscilloscope camera shutters and arming the sweep-lockout chassis and the drum-camera sweep circuit. These were performed directly with the EG&G relay contacts at H−1 second.

TABLE 2.1 ENERGY SENSITIVITY OF DETECTORS

Median Energy	Fraction of Co^{60} Sensitivity
kv	
200	0.86
145	0.86
95	0.71

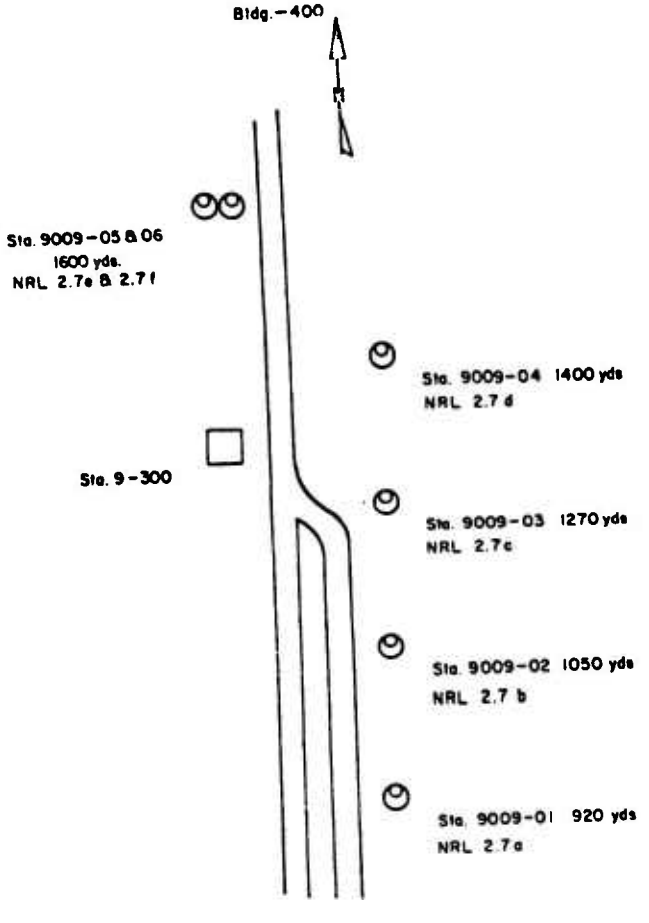

Figure 2.1 Position plan for bunkers.

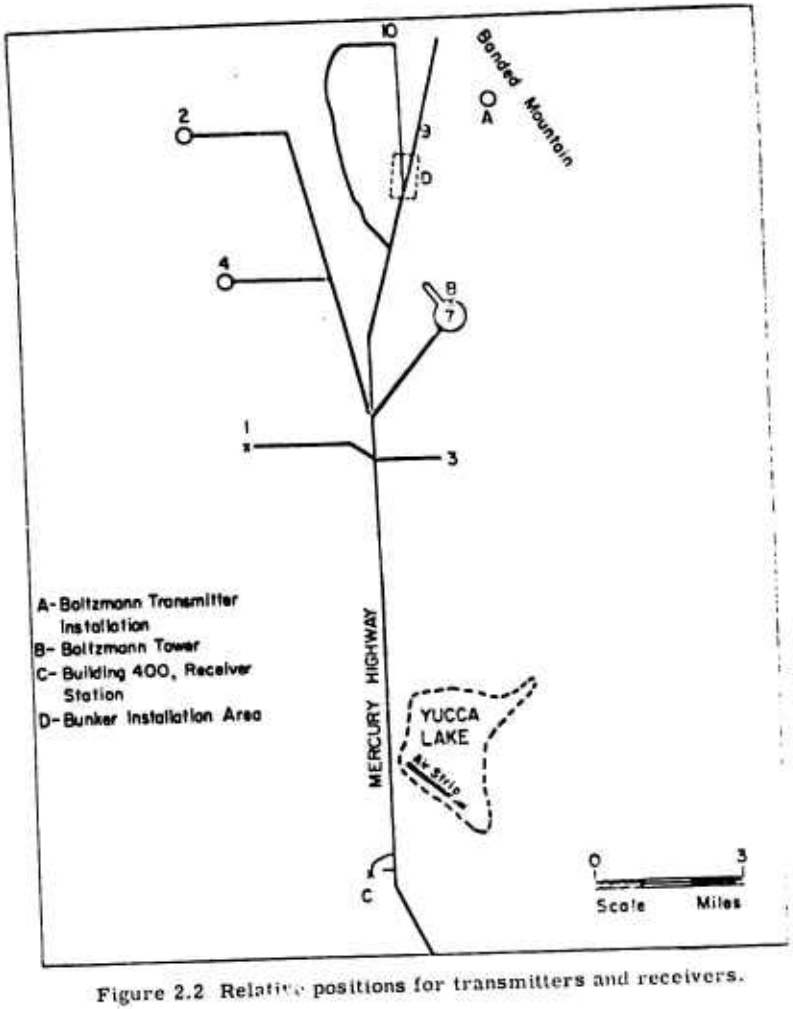

Figure 2.2 Relative positions for transmitters and receivers.

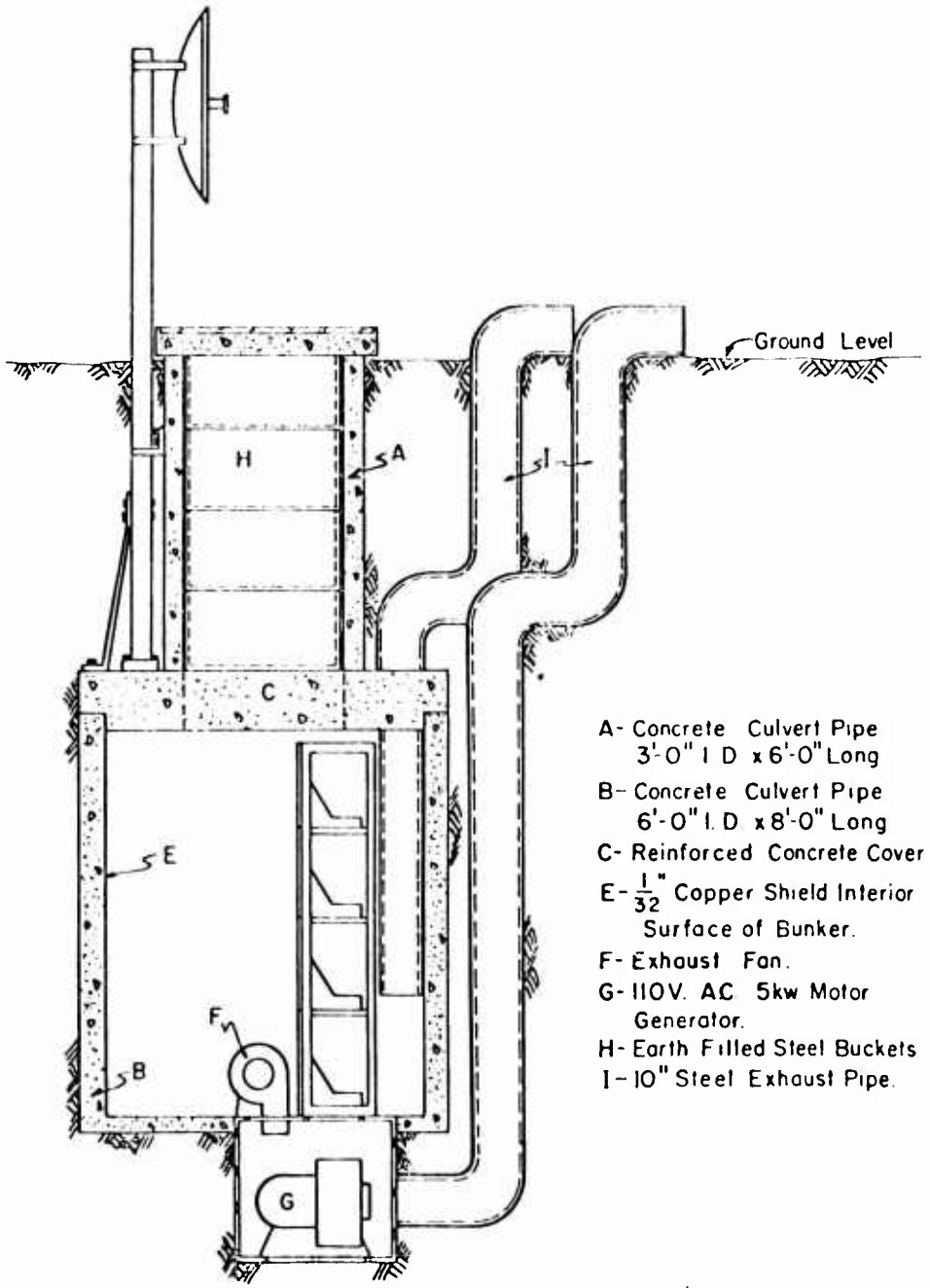

Figure 2.3 Typical bunker installation.

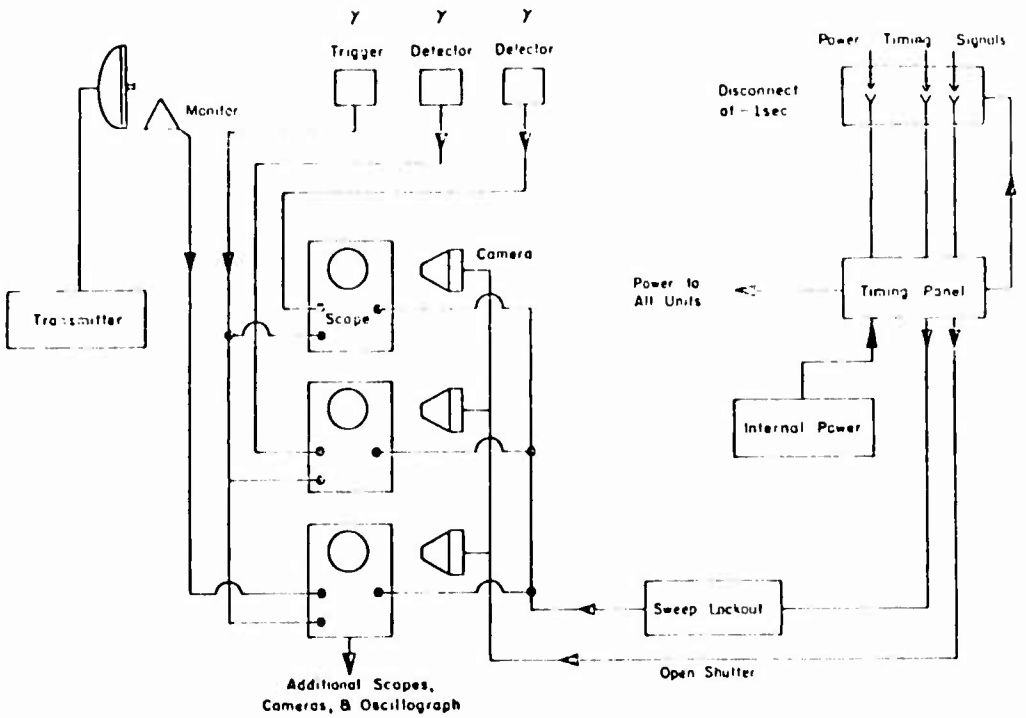

Figure 2.4 Block diagram for typical bunker installation.

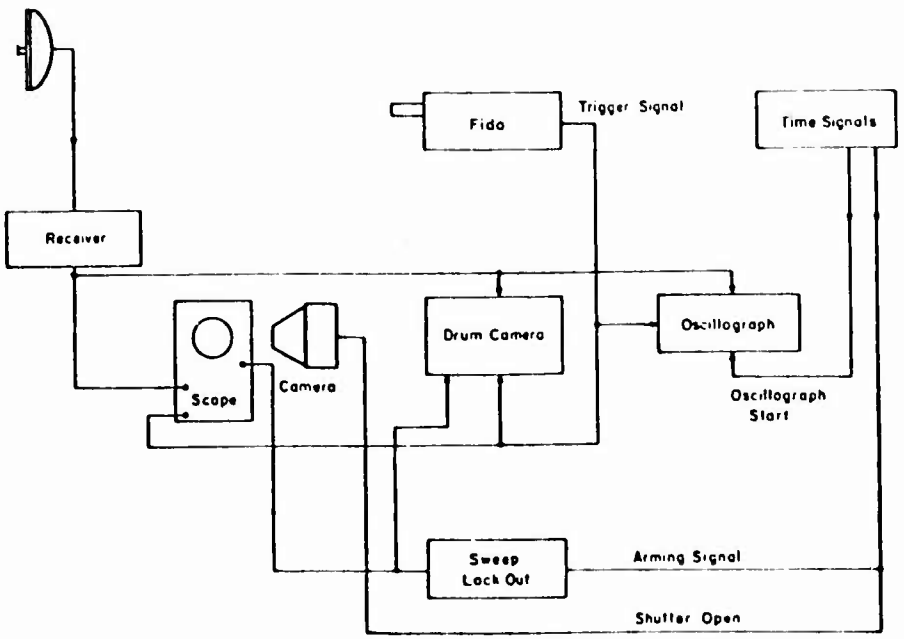

Figure 2.5 Typical receiver installation.

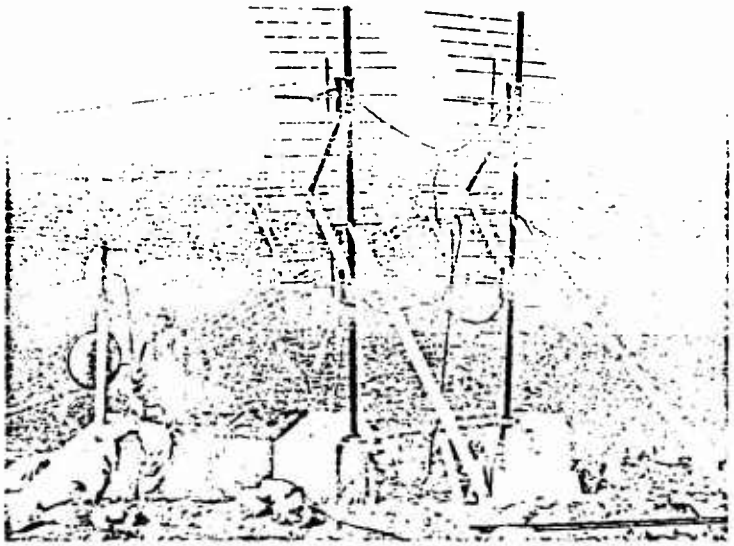

Figure 2.6 View of transmitter installation on Banded Mountain.

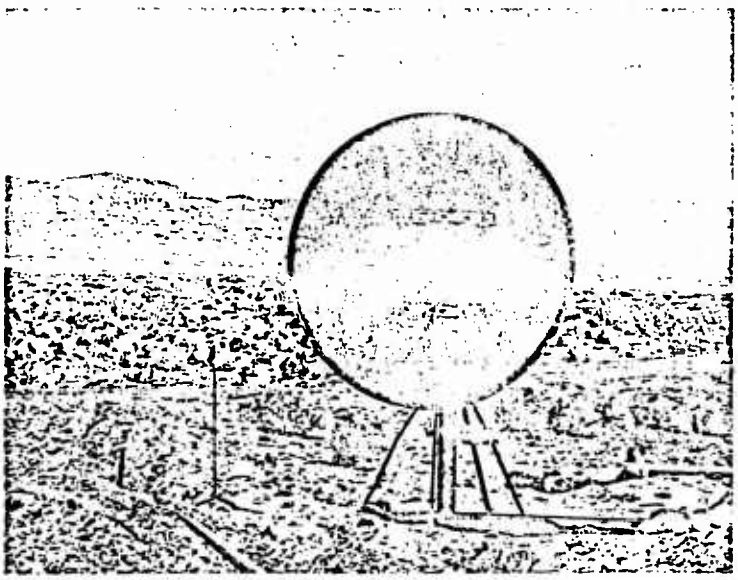

Figure 2.7 Transmitter installation, Shot Priscilla.

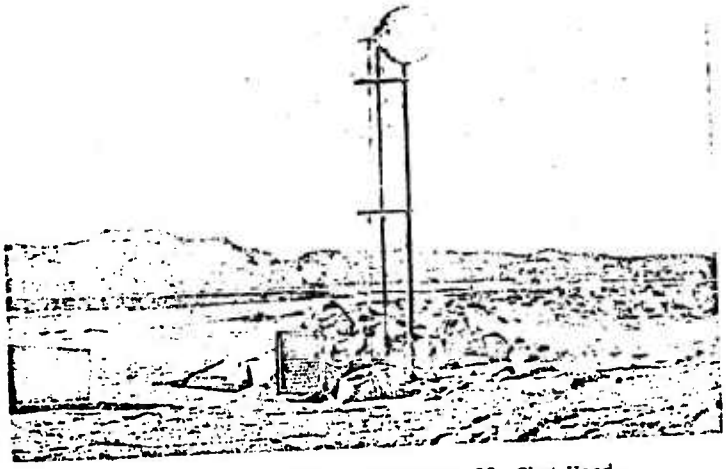

Figure 2.8 Installation at Bunker .03, Shot Hood.

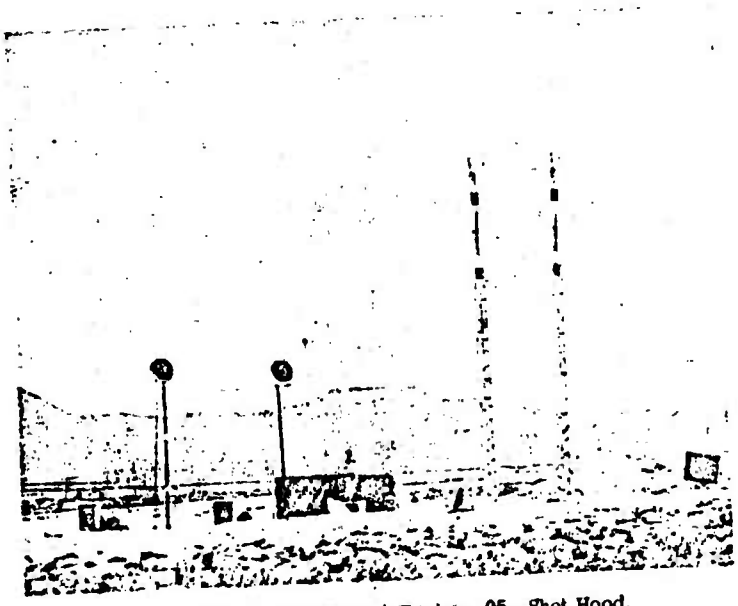

Figure 2.9 Installation at Bunker .05, Shot Hood.

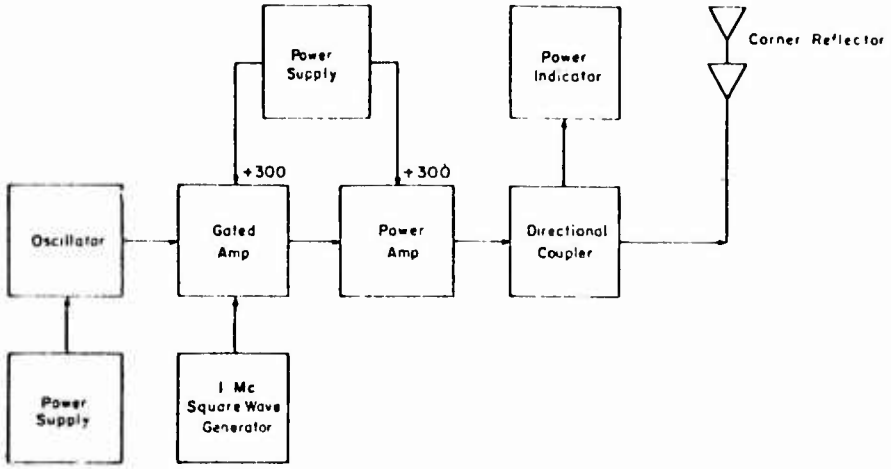

Figure 2.10 Block diagram of Band 1 transmitter (152 to 160 Mc).

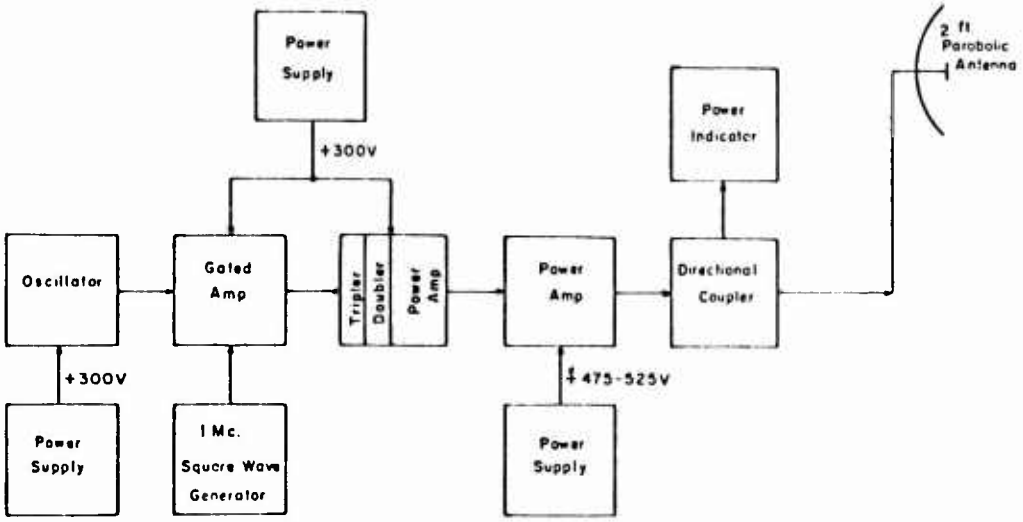

Figure 2.11 Block diagram of Band 2 transmitter (890 to 960 Mc).

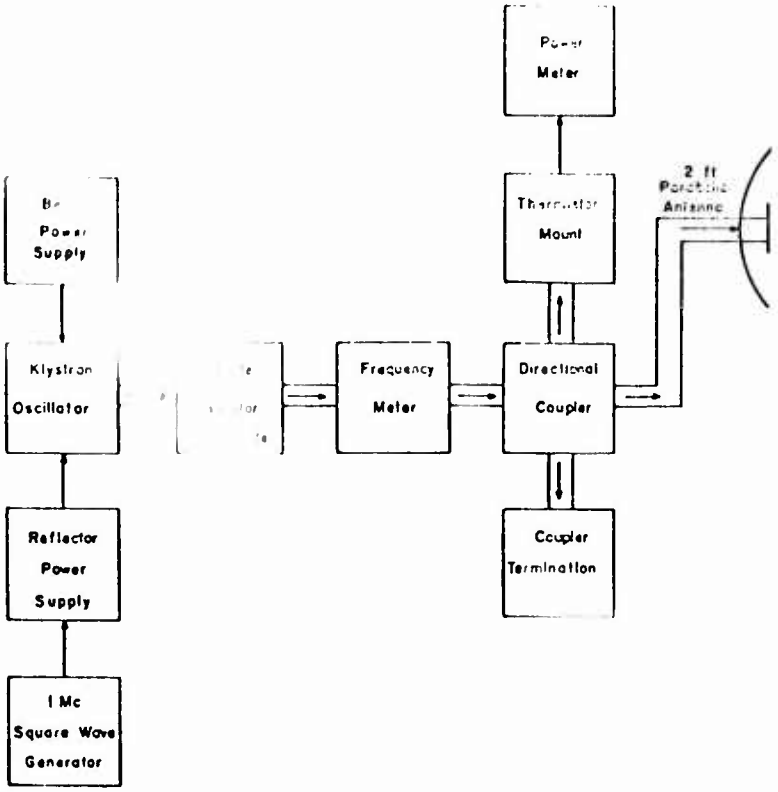

Figure 2.12 Block diagram of Band 4 transmitter (9800 to 10,200 Mc).

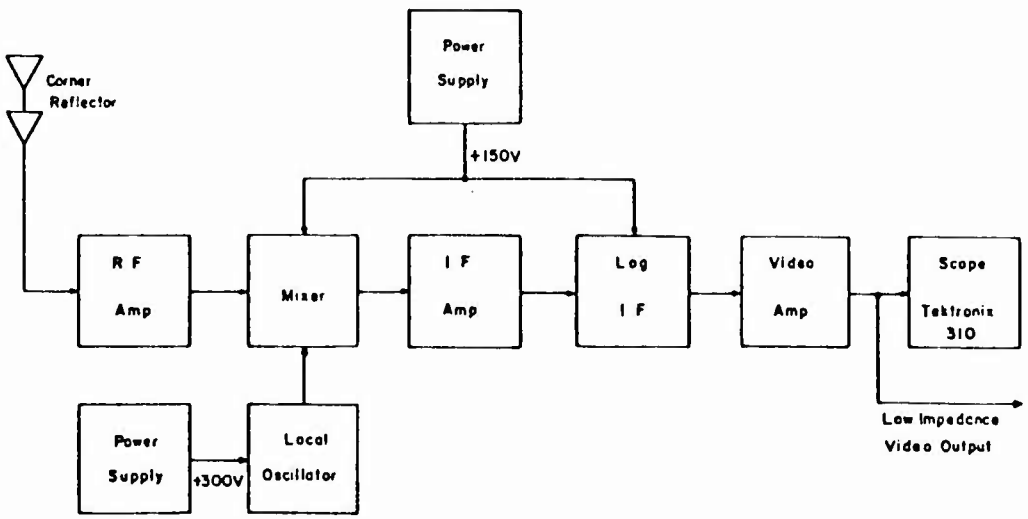

Figure 2.13 Block diagram of Band 1 receiver (152 to 160 Mc).

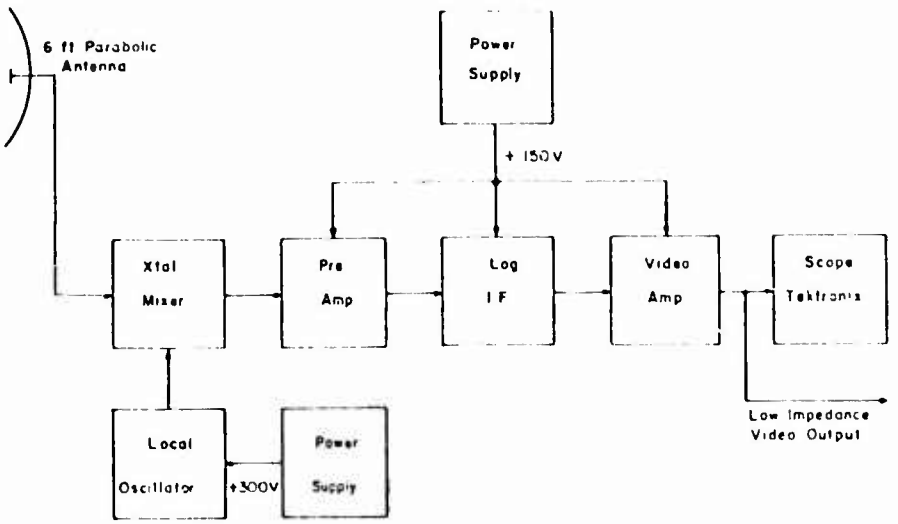

Figure 2.14 Block diagram of Band 2 receiver (890 to 960 Mc).

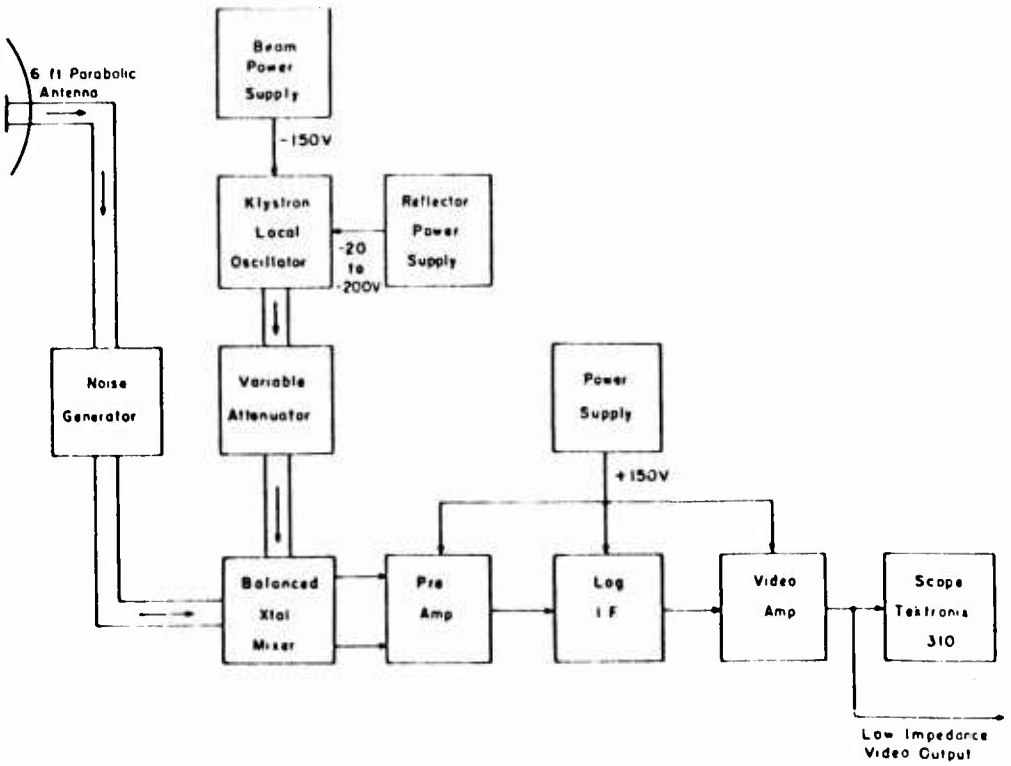

Figure 2.15 Block diagram of Band 4 receiver (9800 to 10,200 Mc).

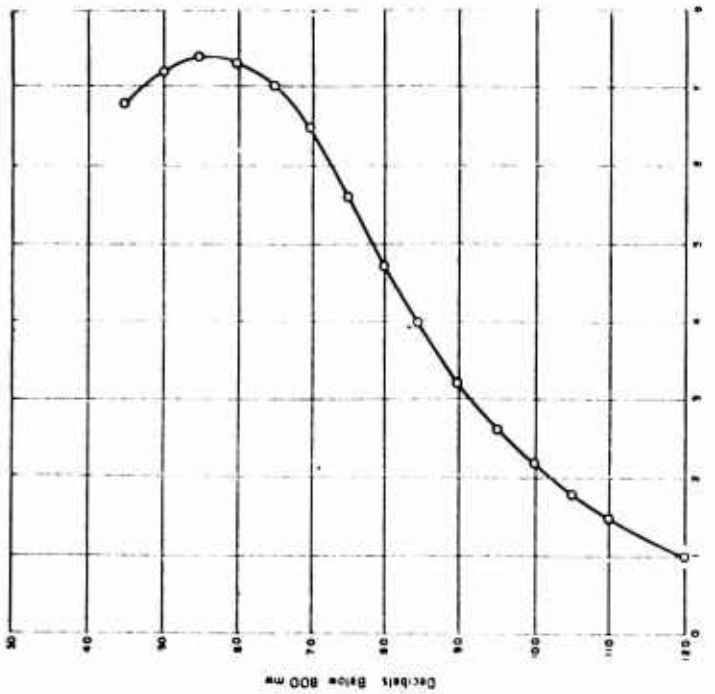

Figure 2.17 Calibration curve for Band 4 Receiver 2.

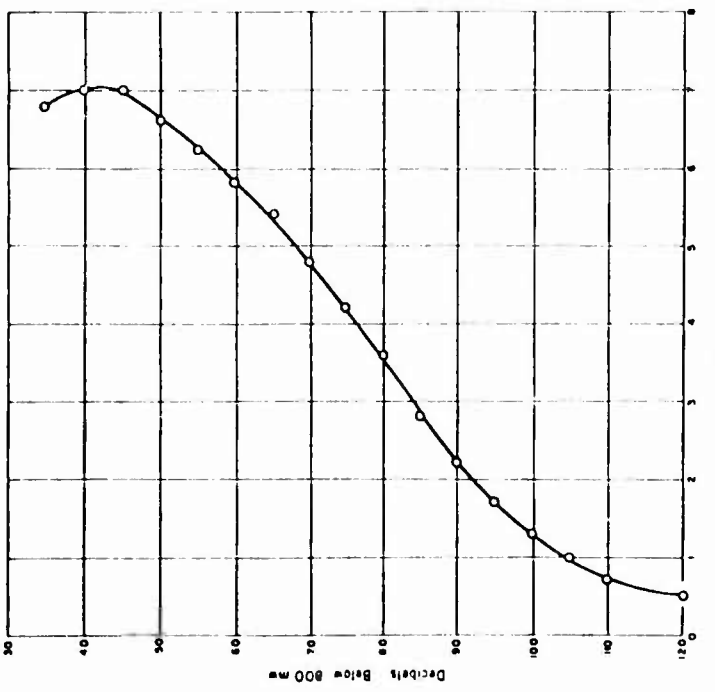

Figure 2.16 Calibration curve for Band 4 Receiver 1.

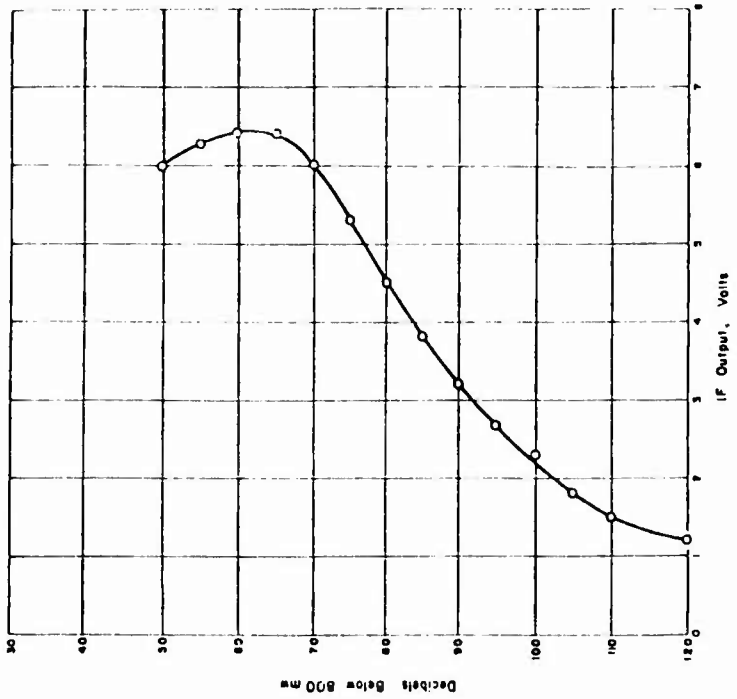

Figure 2.19 Calibration curve for Band 4 Recciver 4.

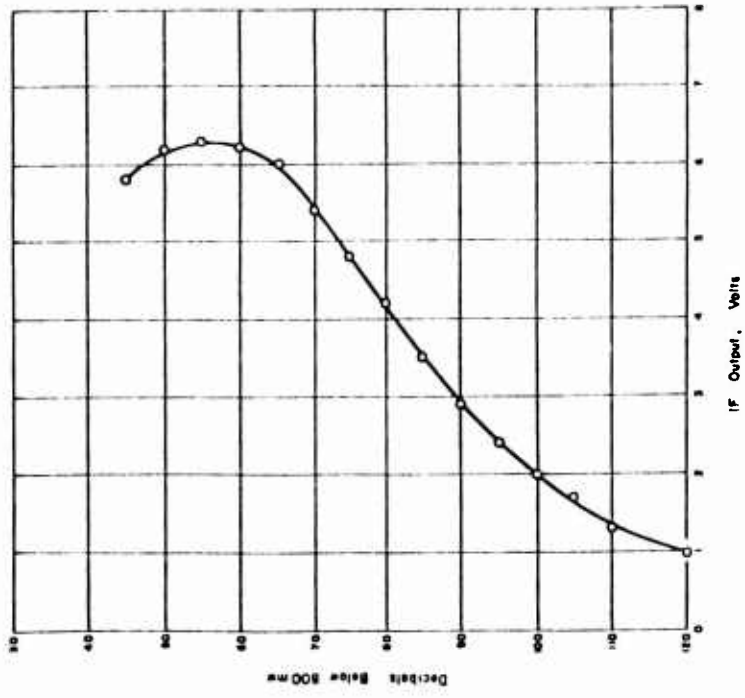

Figure 2.18 Calibration curve for Band 4 Receiver 3.

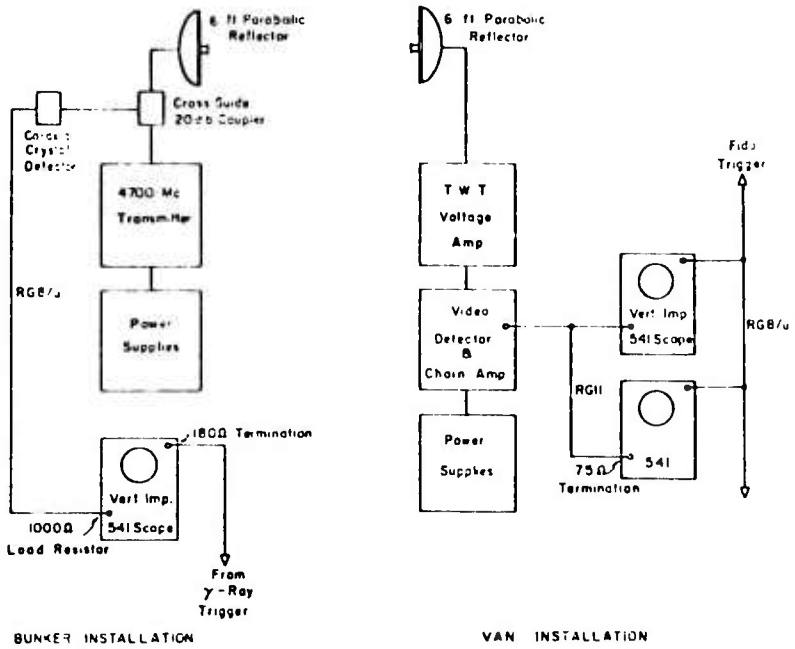

Figure 2.20 Block diagram of 4700-Mc transmitter and receiver.

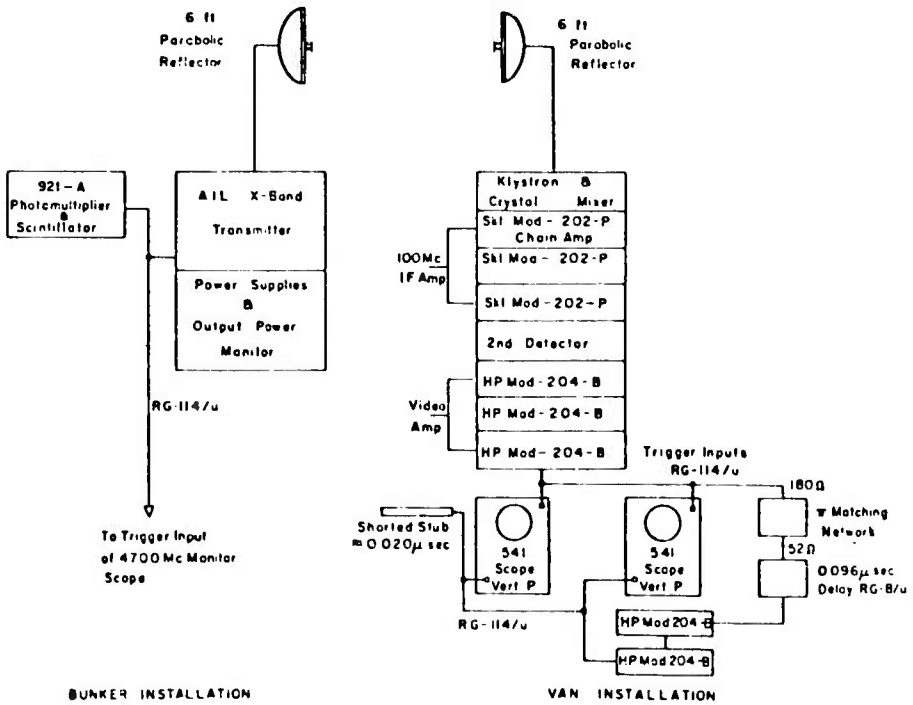

Figure 2.21 Block diagram of X-band time correlation transmitter and receiver.

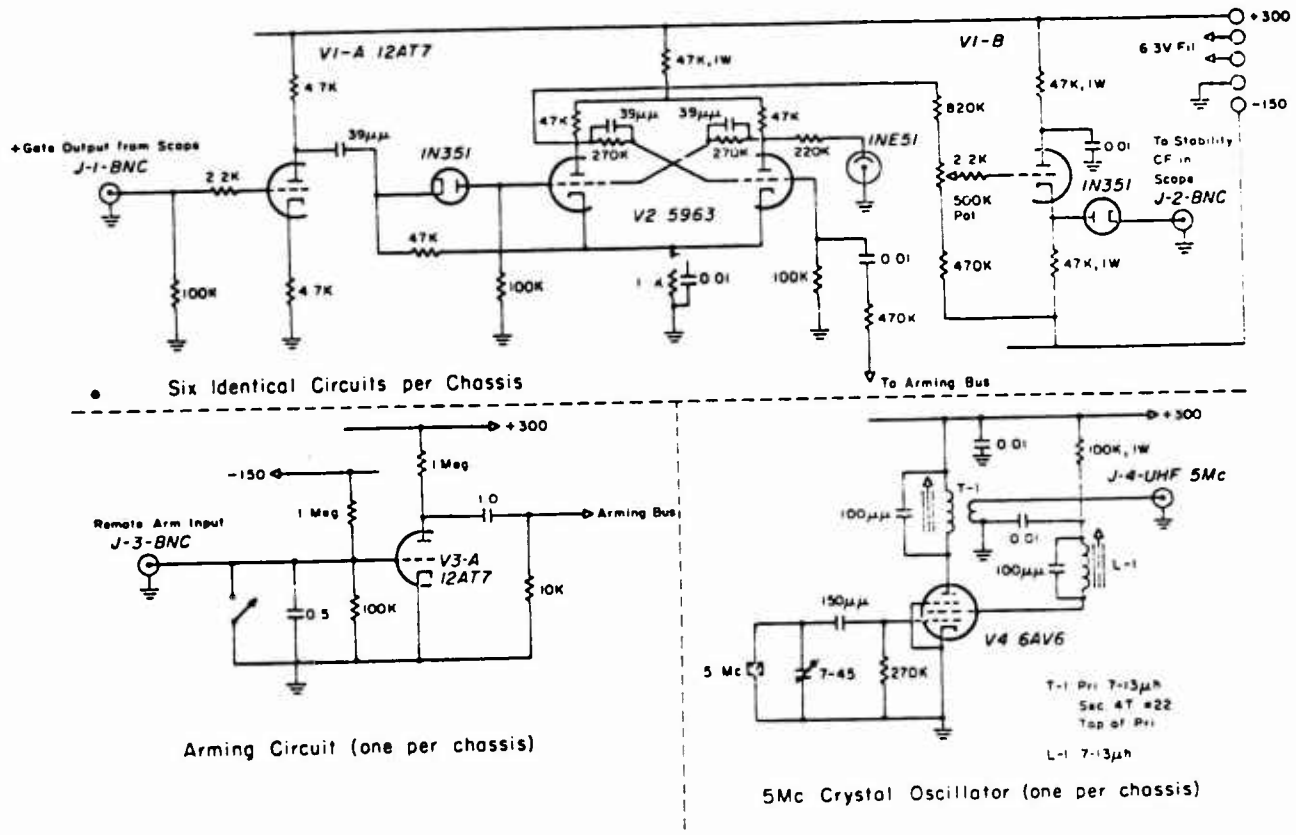

Figure 2.22 Sweep-lockout chassis.

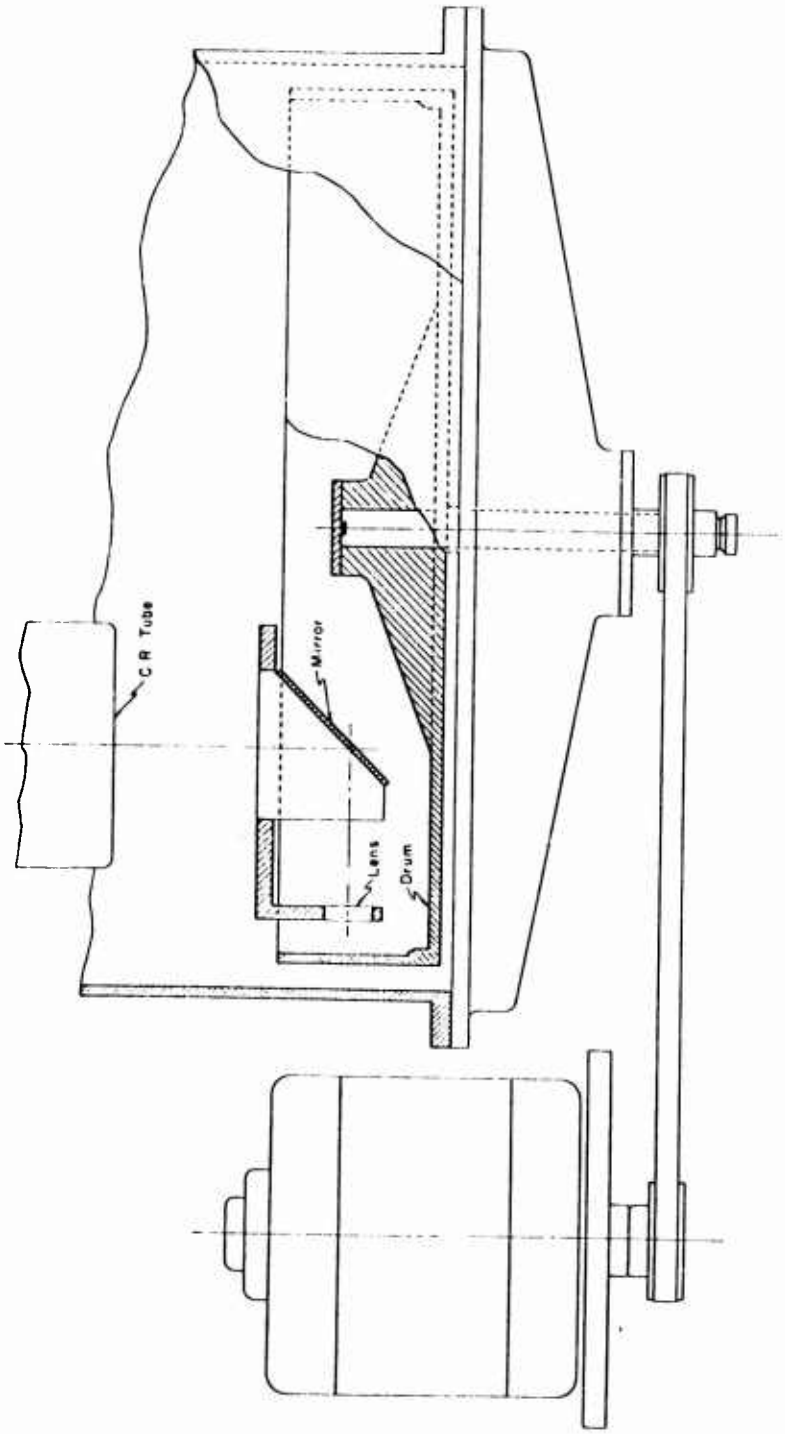

Figure 2.23 Drum camera.

Chapter 3

RESULTS

This chapter will be devoted to a presentation and evaluation of the data obtained. The analysis of and conclusions resulting from the data will be discussed in the next chapter. Where appropriate, additional details of the experimental arrangement will be given.

Table 3.1 gives a summary of the measurements performed and the equipment locations for the various shots. The receiving antennas, with the exception of the 160-Mc antenna, were mounted on top of the receiver van at Station 400, giving an antenna height of about 15 feet above ground level. The 160-Mc antenna was mounted on top of Building 400, giving an antenna height of about 40 feet (Figure 3.1).

3.1 SHOT BOLTZMANN

Participation in Shot Boltzmann was a measurement of attenuation through the fireball. This was done at frequencies of 160, 960, and 9750 Mc generated by transmitters located on Banded Mountain. The location of the transmitters was such that the line of sight from the transmitting antennas to the receiving antennas at Building 400 passed within about 85-foot radius of the center of the cab (detonation on 500-foot tower). The 160- and 960-Mc measurements were made with horizontal polarization. The 9750-Mc measurement was made with a horizontally polarized transmitting antenna but was received with both vertically and horizontally polarized antennas, each having its own receiving and recording channel. All of the receivers used on this shot, and on the following shots, were set to an IF gain such that the log-IF amplifiers were operating on the same portion of their calibration curves for the unattenuated signal. The small differences in output voltage resulting from this procedure were compensated for by adjusting the video gain.

Figures 3.2 through 3.5 show the signals from the oscilloscope cameras during the first 100 μsec. The several pulses at the left of the sweep represent the signal amplitude before the shot. These were obtained by triggering the oscilloscope with the FIDO pulse and delaying the video signal from the receiver by about 5 μsec in a lumped constant delay line. The appearance of the trace at the right of the sweep results from multiple-path signals combining in essentially random phase. The calibrated dynamic range of the system was 50 db. The complete absence of the transmitted pulses implies an attenuation of 65 db or greater. However, with the possible exception of one pulse, the signal is present during the entire attenuation period. This signal is so small, probably more than 60 db down, that it is outside of the calibration range.

The records from the drum camera, of which only the first few milliseconds are reproduced, are shown in Figures 3.6 through 3.9. There is some overlap of late data on the early data. This was caused by the intensifier gate not turning off right on time.

The early portion of the record from the slow recorder (Century) is shown in Figure 3.10. A composite graph of all of the data is shown in Figures 3.11 through 3.14. This gives attenuation in db, obtained from the appropriate receiver calibration curves, on a logarithmic time scale. The dotted portion of the curve (Figure 3.11) indicates the period during which the signal was incoherent because of the multiple-path propagation mentioned earlier.

The Boltzmann data appears to be quite reliable. All of the equipment operated satisfactorily, and there was no interference from the EM effect. There was, however, some pulse-type interference in the 160-Mc channel. The source of this could not be definitely located.

It is unfortunate that the 2.7 bunkers were so far from the Boltzmann tower. As it was, no significant gamma ray data could have been obtained. If this information were available, it would allow the analysis of the propagation data to be made more quantitative in some respects.

3.2 SHOT FRANKLIN

The Boltzmann installation was left intact for Franklin. However, the line of sight from the transmitting antenna to the receiving antenna was about 1,200 yards from the Franklin cab. This, combined with the low yield of the shot, led to no significant data being obtained. The only change observed was a slight fluctuation, beginning at 10 μsec and lasting about 200 μsec, observed in the 160-Mc link. It is doubtful that any significance can be attached to this. The records are not reproduced here.

3.3 SHOT LASSEN

The primary purpose of participation in this shot was to check the calculations of expected attenuation and gamma ray signals. As noted previously, the bunkers were not completed in time to allow finishing the installation of the project instrumentation before the shot. Since the yield was so low, it is unlikely that the data would have been significant.

3.4 SHOT WILSON

3.4.1 Gamma Ray Measurement. The installation for this shot was made in Bunker .02, 1,050 yards from ground zero, and consisted of the detectors and recording oscilloscopes shown in Table 3.2.

No gamma ray data was obtained because of a failure in the timing channel at H−1 second. The precise cause of the failure could not be determined; however, it appeared that the signal did not get to the bunker.

3.4.2 Attenuation Measurement. This experiment was designed to obtain attenuation data at X-band for transmitters located at various ranges from the detonation. This would permit comparison with attenuation calculated from the gamma ray measurement. Transmitters were installed as listed in Table 3.3. Horizontal polarization was used, and the antennas were about 12 feet above ground level at the bunkers.

Figures 3.15 through 3.17 show the data obtained for the first 100 μsec from the high-speed oscilloscope cameras. The presentation here is similar to that used at Boltzmann, i.e., the group of pulses at the left represents the signal level before the detonation, and the baseline represents 50 db below the unattenuated signal level. The termination of the data at about 14 μsec in Figure 3.17 was apparently caused by a malfunctioning of the intensifier circuit in the oscilloscope. Again, there appears to be a small signal present during most of the attenuation period; however, as in the Boltzmann case, it is below the calibration range.

The data obtained from the drum camera could not be satisfactorily reproduced. However, it generally corresponds with that from the high-speed recordings and extends the information to somewhat later times.

No significant data was obtained from the Century recorder; therefore, its record is not reproduced here.

The data in Figures 3.16 and 3.17 has been reduced to attenuation in db versus time through the use of the appropriate receiver calibration curves. These results are shown in Figures 3.18 and 3.19. The data in Figure 3.15 is suspect and has not been analyzed. The remaining data appears to be quite reliable. No interference from the EM effect was apparent, with the possible exception of Bunker .01.

3.4.3 Bunker Monitoring. It had been intended to monitor transmitter output and power supply voltages in the close-in bunker (.01) at this shot, but there was not sufficient time available to complete the installation.

3.5 SHOT PRISCILLA

3.5.1 Gamma Ray Measurement. No bunkers were available near ground zero; therefore, no attempt was made to measure gamma rays from this shot.

3.5.2 Reflection from Fireball. This measurement was designed to give the EM wave reflection coefficient of the fireball at 160, 960, and 9750 Mc. This data would allow an estimate of the electron density gradient to be made. Because of the approach of the time for Shot Priscilla to that for Hood, only an X-band (9750-Mc) system could be spared. Ground zero was 20,400 yards from the receiver at Building 400. The transmitter and antenna were 5,280 yards from ground zero, on the line of sight from the receiver to ground zero. The geometry of the link is shown in Figure 3.20. Horizontal polarization was used.

The reflected signal was so small that it was below the receiver noise level. Therefore, a value of the 9750-Mc reflection coefficient was not obtained. An upper limit can be set, however, and this will be discussed in the next chapter.

3.6 SHOT HOOD

3.6.1 Gamma Ray Measurement. The installation for this shot was made at Bunker .05, 1,600 yards from ground zero, and consisted of the detectors and recording oscilloscopes shown in Table 3.4.

The scope whose deflection sensitivity was set for 20 v/cm failed for unknown reasons; however, the data was reasonably complete without this record. The data from the four recording scopes is shown in Figures 3.21 through 3.24. Examination of the photograph of the 2-v/cm scope (Figure 3.21) indicates some ringing in the circuit. This raises some question as to whether the tops of the two peaks observed are actual peaks or steps on the way down caused by this ringing. The purpose of this measurement was to look at the gamma rays at later times, so the uncertainty of the peak amplitudes is not critical. The intensity scales for these figures can be seen by comparing these photographs to the points on the graphs of the data shown in Figures 3.25 through 3.27.

These graphs show the degree of internal consistency that would be expected. Since it is difficult to determine an accurate baseline from which to measure the deflection, the accuracy of this determination depends on the magnitude of the deflection. Thus a 0.4-cm deflection probably cannot be determined more accurately than ±25 percent whereas full-scale deflections would have about 10 times this accuracy. This accounts for the spread in the data from two different scopes. The time scale was determined by using the Tektronix 541 scope sweep speed as the calibration. This accuracy is dependable to ±3 percent. In addition to these possible errors, there are the errors involved in reading the data from the photographs, though the errors involved here are small compared to those previously mentioned.

The detector's response to neutrons is probably several times that of an equivalent mass of air, since the toluene contains comparatively large amounts of hydrogen. The hydrogen atoms absorb more energy per neutron than do the nitrogen and oxygen; therefore, the values of r/sec given on the graphs are upper limits on the ionization at times after about 23 μsec.

The data from the 0.5-v/cm recording should not be used above a deflection of 0.8 volt, since the detector was operated at 100 volts instead of a required 150 volts. A deflection of 0.8 volt is the largest linear deflection that can be expected from this channel.

3.6.2 Attenuation Measurement. The experiment during Hood was designed to measure the EM wave attenuation as a function of frequency. Transmitters at 160, 960, and 9600 Mc were installed in Bunker .05, 1,600 yards from ground zero. A transmitter at 9750 Mc was installed in Bunker .03, 1,270 yards from ground zero, to allow comparison of measurements made in the bunker of its power output and power supply voltages during the detonation with its signal

received in Building 400. Horizontal polarization was used in all cases. The 9600- and 960-Mc antennas were about 12 feet above ground level at the bunkers. The 160-Mc antenna was about 20 feet above ground level.

The data obtained on the high-speed oscilloscope cameras at the receiving station are shown in Figures 3.28 through 3.31. A severe baseline shift can be observed in these pictures. This was apparently caused by the EM signal entering the receiving station van on the powerlines and disturbing the receiver and recording system. Most of the data is hopeless, but something can be resurrected, as discussed in the next chapter.

The data from the drum camera was somewhat less perturbed by the EM effect, but it is no more informative than that from the high-speed oscilloscope cameras. The results are, therefore, not reproduced here.

There was no apparent long-term signal on the Century record. The record is, therefore, not reproduced here.

3.6.3 Bunker Monitoring. A monitoring system was installed in Bunker .03 to record the high-voltage power supply on the 9750-Mc transmitter and the RF output of the transmitter. The voltage monitor consisted of a voltage divider, across the power supply, whose output was recorded on an oscilloscope camera and on one channel of a Century recorder. The RF output monitor consisted of a small horn about 1 foot in front of, and looking at, the transmitting antenna. The horn output was brought into the bunker via a waveguide and rectified in a crystal detector. The crystal current was then recorded on an oscilloscope camera and on another channel of the Century recorder.

The exciter lamp in the Century recorder failed; therefore, no long-term record is available.

The oscilloscope record of the voltage monitor showed no change greater than 0.1 volt at the input to the divider. It is not reproduced here.

The oscilloscope record of the RF monitor is shown in Figure 3.32. A severe baseline shift is apparent here too, indicating that the EM effect penetrated the bunker shielding. It also appears that there was either an interference with the transmitter output or severe attenuation between the transmitting antenna and the monitor horn. This appears to be a separate phenomenon (from the changes caused by the EM effect), since the time constants in the RF monitor and the transmitter itself make it difficult to reconcile the short period variations (not the 1-Mc pulse modulation rate) with the EM effect signal. These short period variations are probably due to ionization in the waveguide connecting the antenna to the bunker. The second decrease in monitor signal strength visible in Figure 3.32 coincides with the arrival time of the 14 Mev neutrons at the bunker, tending to support the local ionization explanation. The effect of ionization (and the resultant attenuation in the waveguide feeding the transmitting antenna) on the atmospheric attenuation measurements are discussed in the next chapter.

3.7 SHOT DIABLO

The only participation by this project in this shot was a measurement of the EM radiation from the detonation that fell in the pass bands of the same receiving equipment that was used in the attenuation measurements. Three receivers were used: 160, 960, and 9850 Mc. Horizontal polarization was used in all cases. The signals from the 160- and 960-Mc channels are shown in Figures 3.33 and 3.34, respectively. No signal was observed in the 9850-Mc channel, and its record is not reproduced here.

3.8 SHOT KEPLER

The only participation by this project in this shot was a measurement of the EM signal from the detonation. A 2-meter-long vertical probe was installed on the roof of the van at Building 400 (the bottom of the probe was about 10 feet above ground level). The signal was conducted

to an oscilloscope by an RG8/U coax terminated in its characteristic impedance at the oscilloscope. The outer conductor of the coax was connected to the aluminum body of the van at the base of the probe.

Figure 3.35 shows the oscilloscope camera recording of the signal, and Figure 3.36 is a calibrated graph.

3.9 SHOT OWENS

3.9.1 Gamma Ray Measurement. Detectors were installed in two bunkers for this shot. Table 3.5 gives the details of this installation. The first two detectors were in Bunker .04, 1,400 yards from ground zero, and the others were in Bunker .05, 1,600 yards from ground zero.

No data was obtained in Bunker .04 because of failure of the motor generator between the final buttoning-up and shot time.

The equipment in Bunker .05 functioned satisfactorily. The raw data is shown in Figures 3.37 through 3.40, and the graphs of the analyzed data are reproduced in Figures 3.41 and 3.42.

The Tektronix 541 oscilloscope and Dumont camera recording system did not have sufficient writing speed to show the rise of the gamma ray burst, so the data is somewhat inconclusive as to whether there exists a secondary peak of approximately a tenth of the amplitude of the primary peak. At times longer than 0.25 μsec after the initial peak, the record appears to be unambiguous.

3.9.2 Attenuation Measurement. The goal of this experiment was to measure the shape of the attenuation pulse with a resolution of 1 shake and correlate it with gamma ray measurements of the same resolution. The apparatus has been fully described in Section 2.4 and will not be discussed further here. The 4700-Mc link installed for this measurement failed. A trace was recorded at Station 400 but contained no data; the trace is not reproduced here. Figure 3.43 is the monitor trace of the 4700-Mc transmitter output taken in the bunker.

The failure of the 4700-Mc link is inexplicable. The large fluctuations in the output power recorded in the bunker have no apparent correlation with the gamma rays, neutrons or EM signal.

3.9.3 Electromagnetic Signal. The experimental arrangement described in Section 3.8 was also used during Owens. The oscilloscope camera recording is shown in Figure 3.44, and Figure 3.45 is a calibrated graph.

As a check on EM signal disturbances, the powerline was monitored by an oscilloscope triggered by a FIDO. The signal was obtained from the powerline through a high-pass filter having a 1-kc cutoff frequency. This would show most of the EM effect but would suppress the 60-cycle power frequency. The data obtained showed violent excursions of greater than 40 volts (the limit of the oscilloscope deflection system). The excursions had a rather surprisingly high and somewhat random frequency, probably related to the several periods of the entire power distribution system. Since the data is not quantitative, it is not reproduced here. It is felt that these excursions are the cause of the baseline shifts in the oscilloscopes used in the receiving station.

TABLE 3.1 SUMMARY OF MEASUREMENTS

Shot	Yield	Location	Experiment	Instrumentation					Remarks
		Bunker		.01	.02	.03	.04	.05, .06	
		Range from ground zero, yds		920	1,050	1,270	1,400	1,600	
	kt								
Boltzmann	11.5	500-foot tower Area 7	Attenuation through fireball versus frequency.						Transmitters at 160, 960, and 9750 Mc on Rainier Mountain.
Franklin	0.138	300-foot tower Area 3	Same as for Boltzmann.						Same as for Boltzmann.
Lassen	0.47×10^{-3}	Balloon, 500 feet Area 9	Calibration.	Installation not completed.					
Wilson	10.3	Balloon, 500 feet Area 9	(a) X-band attenuation versus range. (b) Gamma ray measurement.	9550-Mc transmitter	Gamma ray detectors	9650-Mc transmitter	9750-Mc transmitter		
Priscilla	36.6	Balloon, 700 feet Frenchman Flat	Reflection from fireball versus frequency.						9750-Mc transmitter between ground zero and Building 400.
Hood	71	Balloon, 1,500 feet Area 9	(a) Attenuation versus frequency. (b) Gamma ray measurement.			9750-Mc transmitter		(a) 160-, 960-, and 9600-Mc transmitter (b) Gamma ray detectors	
Diablo	17	500-foot tower Area 2	EM signal from detonation versus frequency.						160-, 960-, and 9850-Mc receivers at Building 400.
Kepler	10.3	500-foot tower Area 4	EM effect field strength.						Vertical 2-meter dipole at Building 400.
Owens	9.7	Balloon, 500 feet Area 9	(a) High-resolution attenuation experiment. (b) Gamma ray measurement. (c) EM effect field strength.				Gamma ray detectors	(a) 4700- and 9600-Mc transmitters (b) Gamma ray detectors	Vertical 2-meter dipole at Building 400.

TABLE 3.2 GAMMA RAY DETECTOR INSTALLATIONS, SHOT WILSON

Detector Range	Detector Voltage	Number of Scopes	Deflection Sensitivities
	volt		v/cm
High intensity	3,000	2	20, 2
Low intensity	3,000	2	20, 2
Low intensity	100	2	0.2, 0.05

TABLE 3.3 TRANSMITTER INSTALLATIONS, SHOT WILSON

Bunker	Range from Ground Zero	Frequency
	yards	Mc
.01	920	9550
.03	1,270	9650
.04	1,400	9750

TABLE 3.4 GAMMA RAY DETECTOR INSTALLATIONS, SHOT HOOD

Detector Range	Detector Voltage	Number of Scopes	Deflection Sensitivities
	volt		v/cm
High intensity	3,000	2	20, 2
High intensity	100	2	0.2, 0.05
Low intensity	100	1	0.5

TABLE 3.5 GAMMA RAY DETECTOR INSTALLATIONS, SHOT OWENS

Detector Range	Detector Voltage	Number of Scopes	Deflection Sensitivities
	volt		v/cm
High intensity	3,000	2	20, 2
High intensity	100	1	0.2
High intensity	3,000	2	20, 2
High intensity	100	2	0.2, 0.05

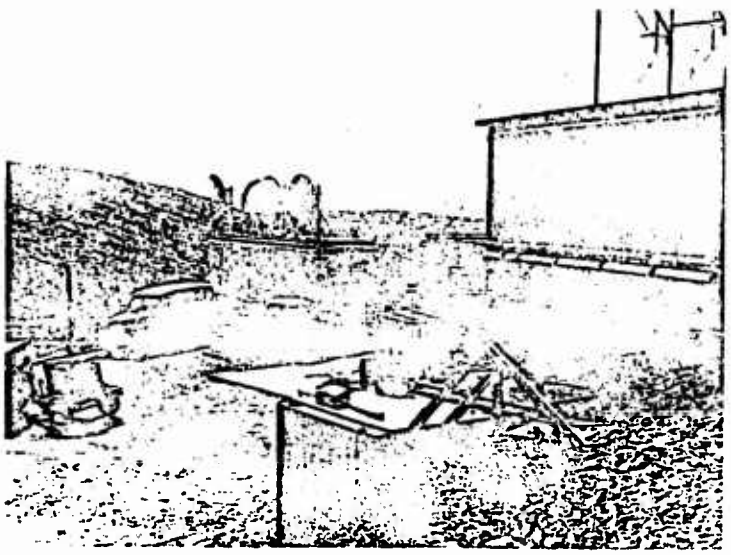

Figure 3.1 Receiving station, Building 400.

Figure 3.2 Signal recorded for first 100 μsec on 160-Mc receiver, Shot Boltzmann.

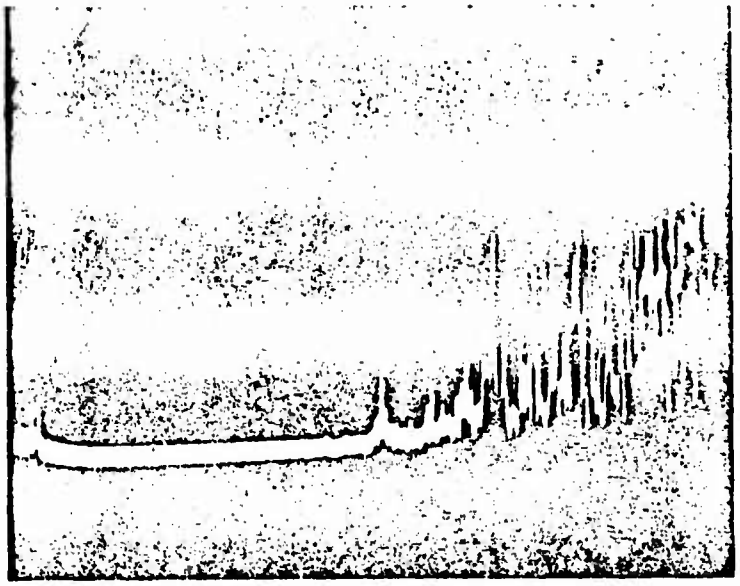

Figure 3.3 Signal recorded for first 100 μsec on 960-Mc receiver, Shot Boltzmann.

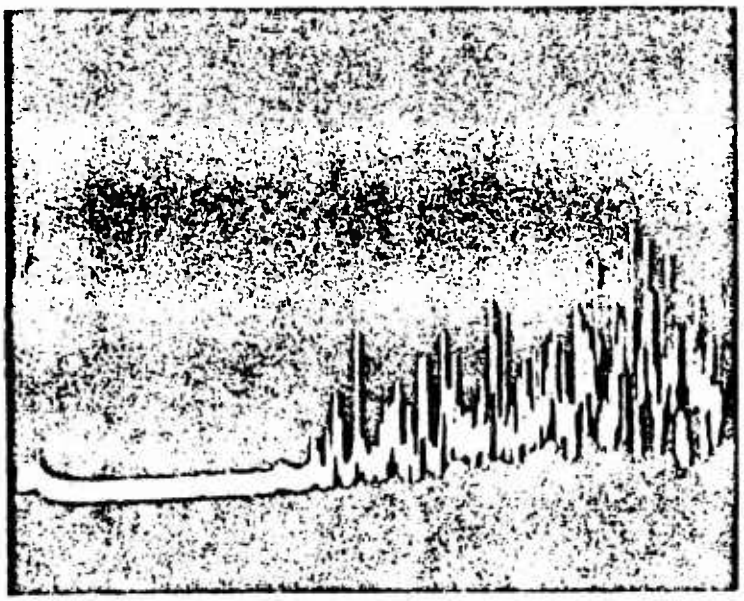

Figure 3.4 Signal recorded for first 100 μsec on 9750-Mc receiver with horizontally polarized antenna, Shot Boltzmann.

Figure 3.5 Signal recorded for first 100 μsec on 9750-Mc receiver with vertically polarized antenna, Shot Boltzmann.

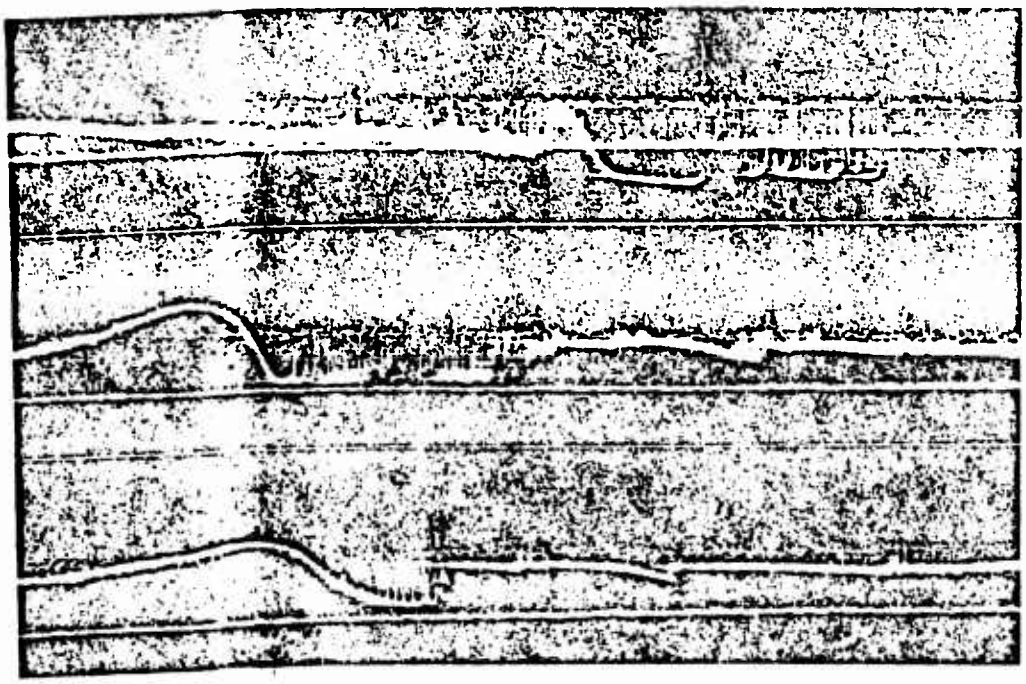

Figure 3.6 Initial portion of drum camera record from 160-Mc receiver, Shot Boltzmann.

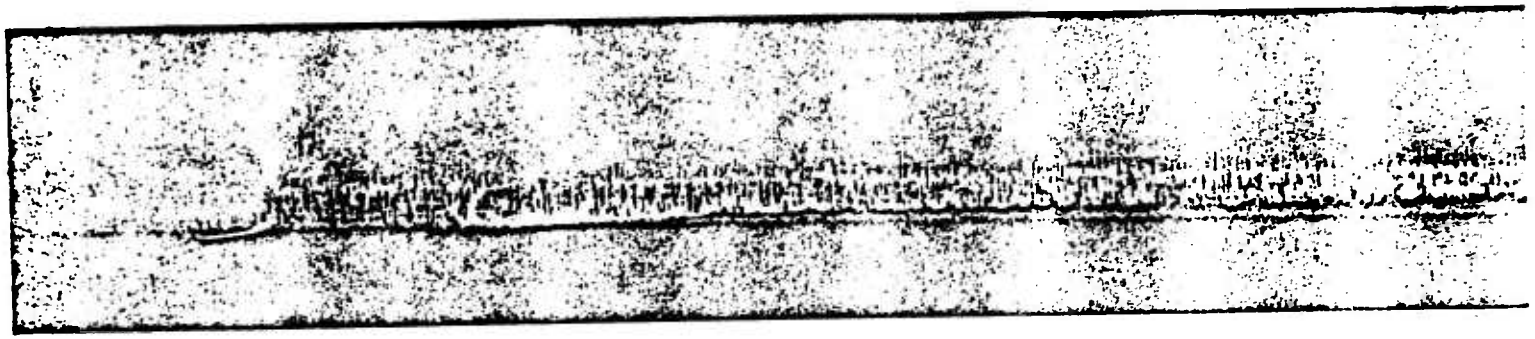

Figure 3.7 Initial portion of drum camera record from 960-Mc receiver, Shot Boltzmann.

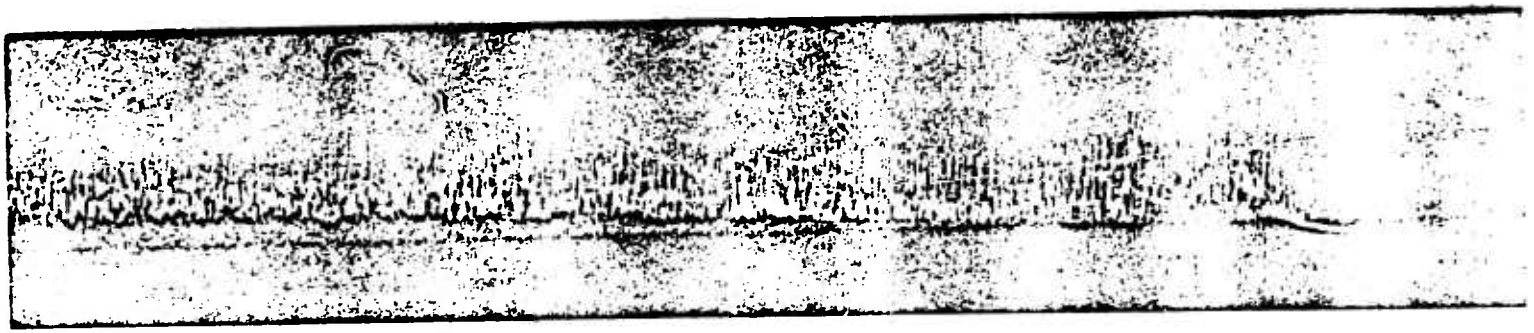

Figure 3.8 Initial portion of drum camera record from 9750-Mc receiver with horizontally polarized antenna, Shot Boltzmann.

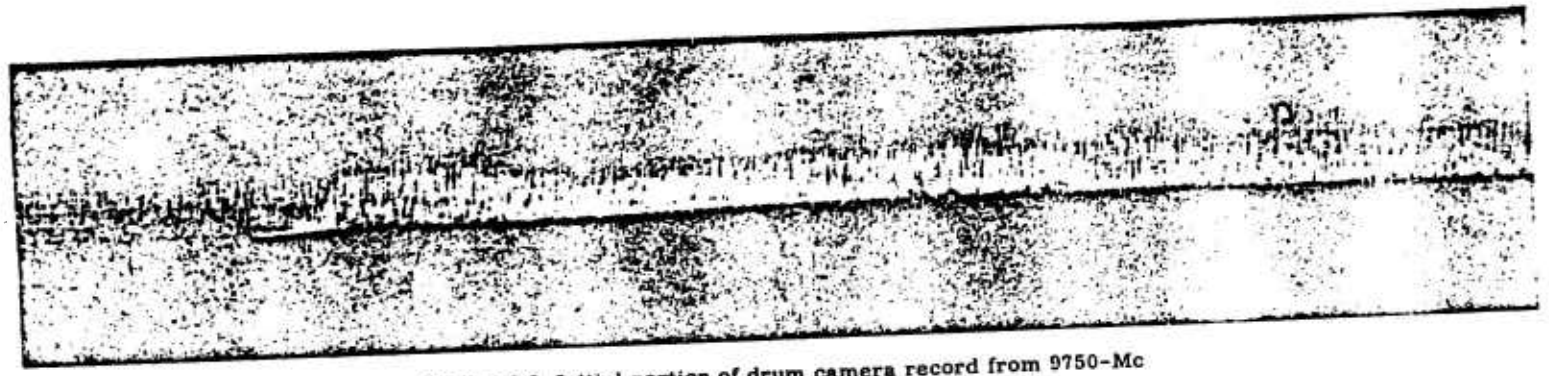

Figure 3.9 Initial portion of drum camera record from 9750-Mc receiver with vertically polarized antenna, Shot Boltzmann.

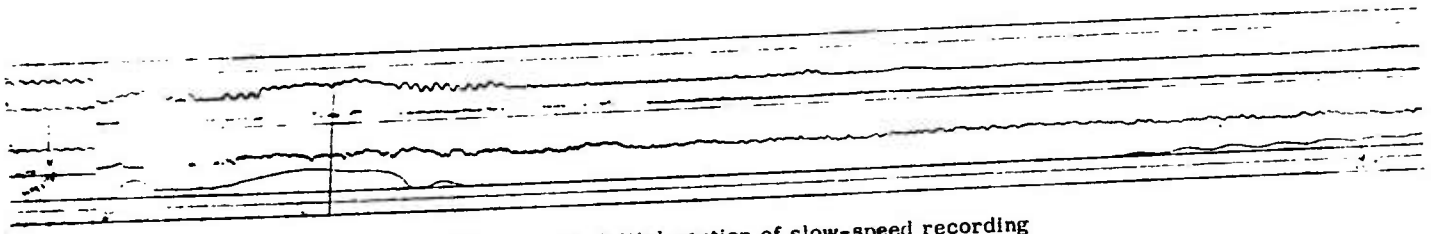

Figure 3.10 Initial portion of slow-speed recording of signal level on all four channels, Shot Boltzmann.

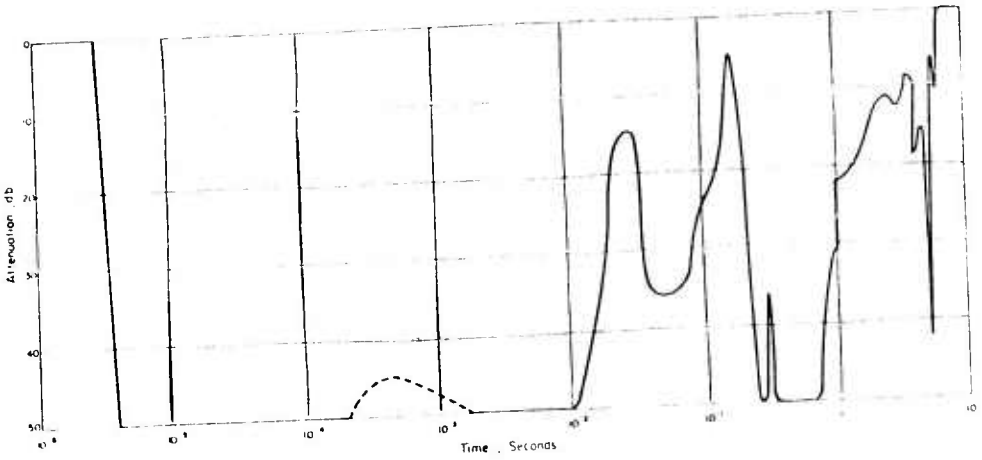

Figure 3.11 Signal level from 160-Mc receiver, Shot Boltzmann.

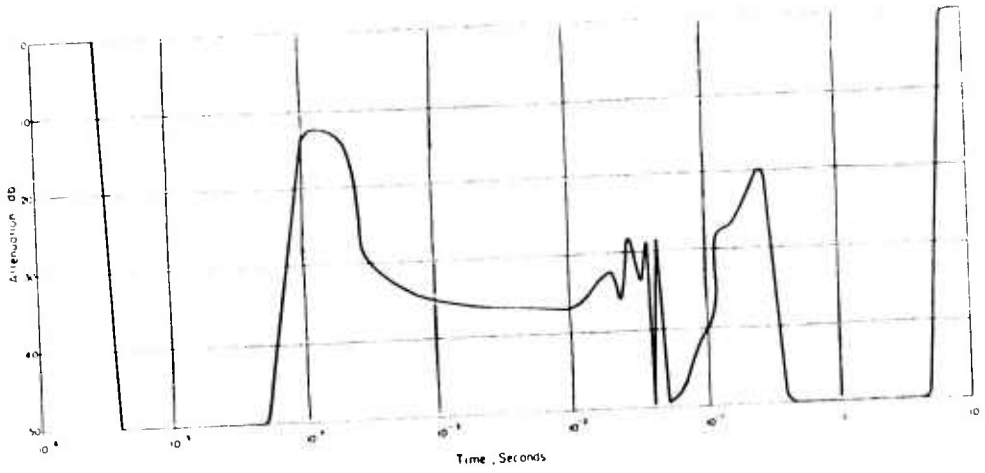

Figure 3.12 Signal level from 960-Mc receiver, Shot Boltzmann.

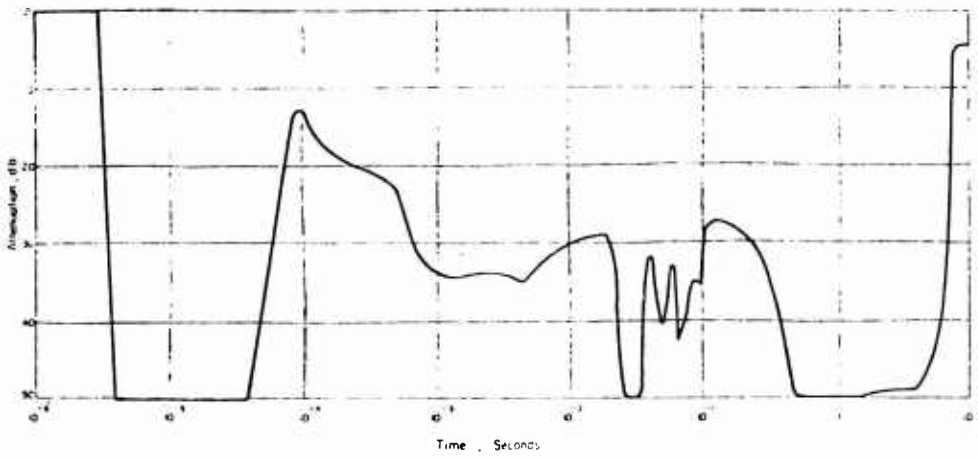

Figure 3.13 Signal level from 9750-Mc receiver with horizontally polarized antenna, Shot Boltzmann.

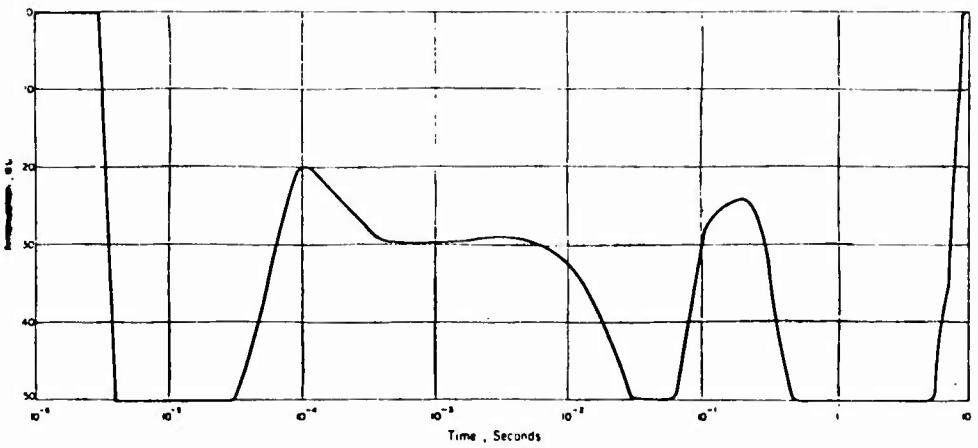

Figure 3.14 Signal level from 9750-Mc receiver with vertically polarized antenna, Shot Boltzmann.

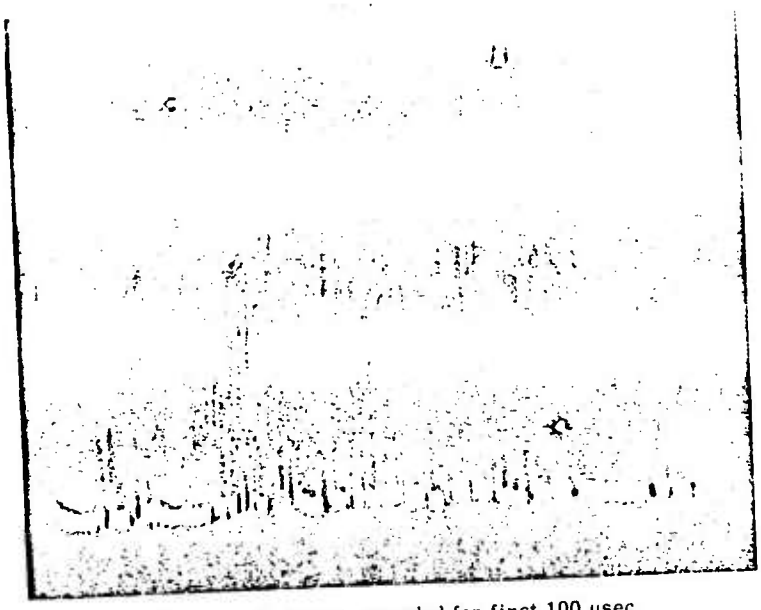

Figure 3.15 Signal recorded for first 100 μsec from Bunker .01, Shot Wilson.

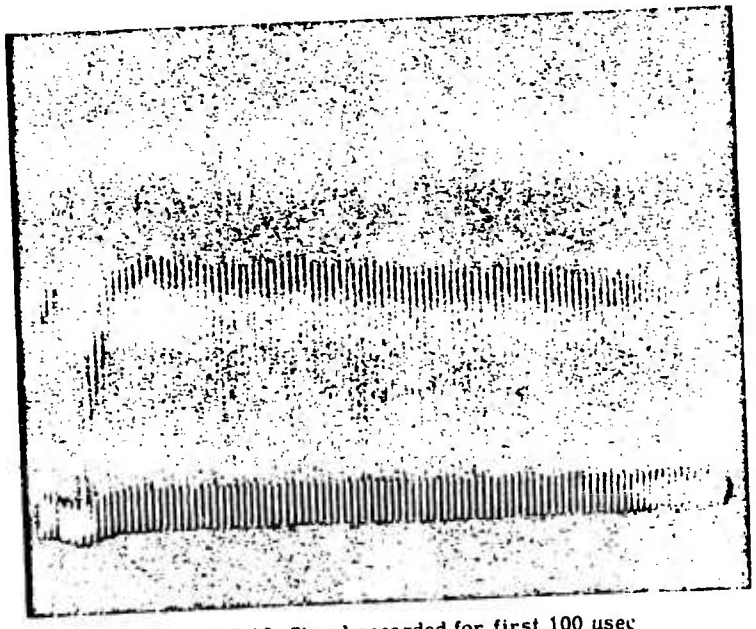

Figure 3.16 Signal recorded for first 100 μsec from Bunker .03, Shot Wilson.

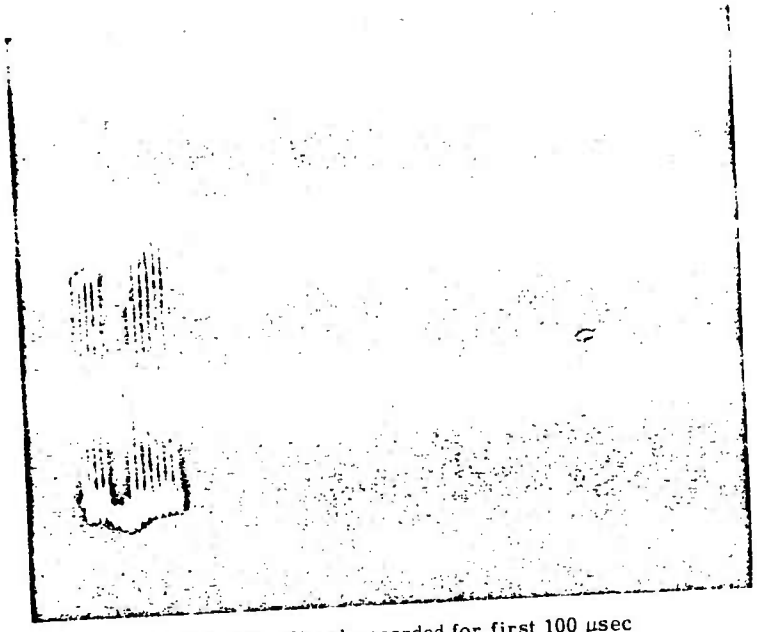

Figure 3.17 Signal recorded for first 100 μsec from Bunker .04, Shot Wilson.

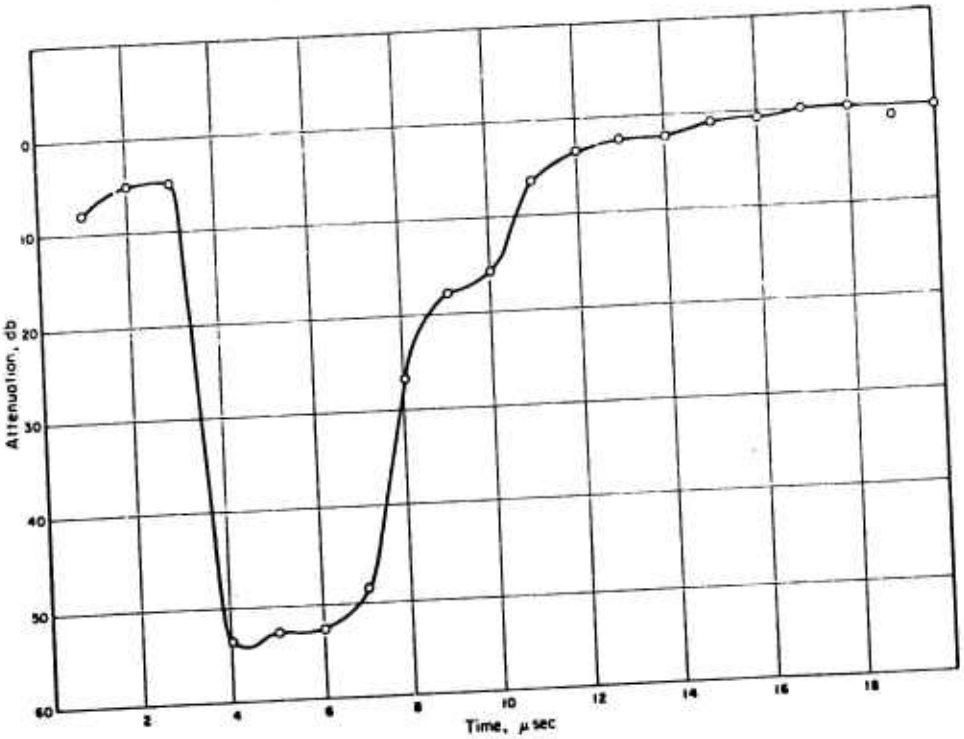

Figure 3.18 Attenuation as measured from Bunker .03, Shot Wilson.

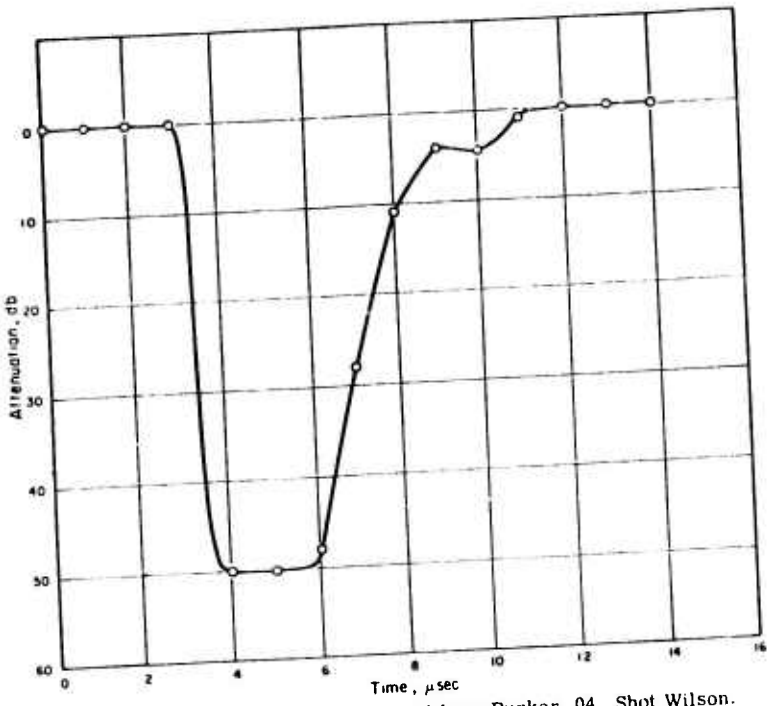

Figure 3.19 Attenuation as measured from Bunker .04, Shot Wilson.

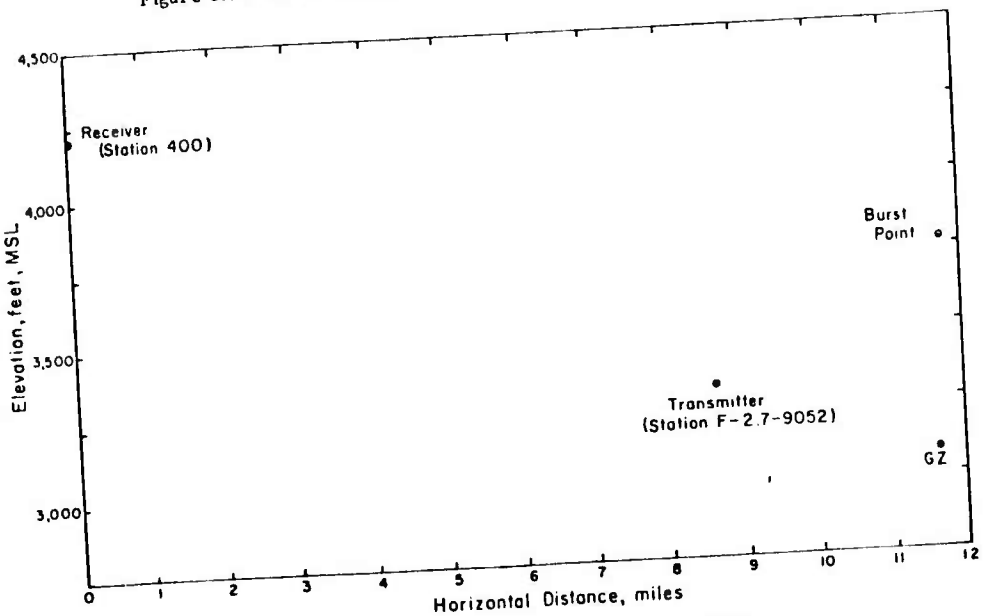

Figure 3.20 Relative positions of the transmitter, reflecting sphere, and receiver, Shot Priscilla.

Pages 59 and 60 have been deleted.

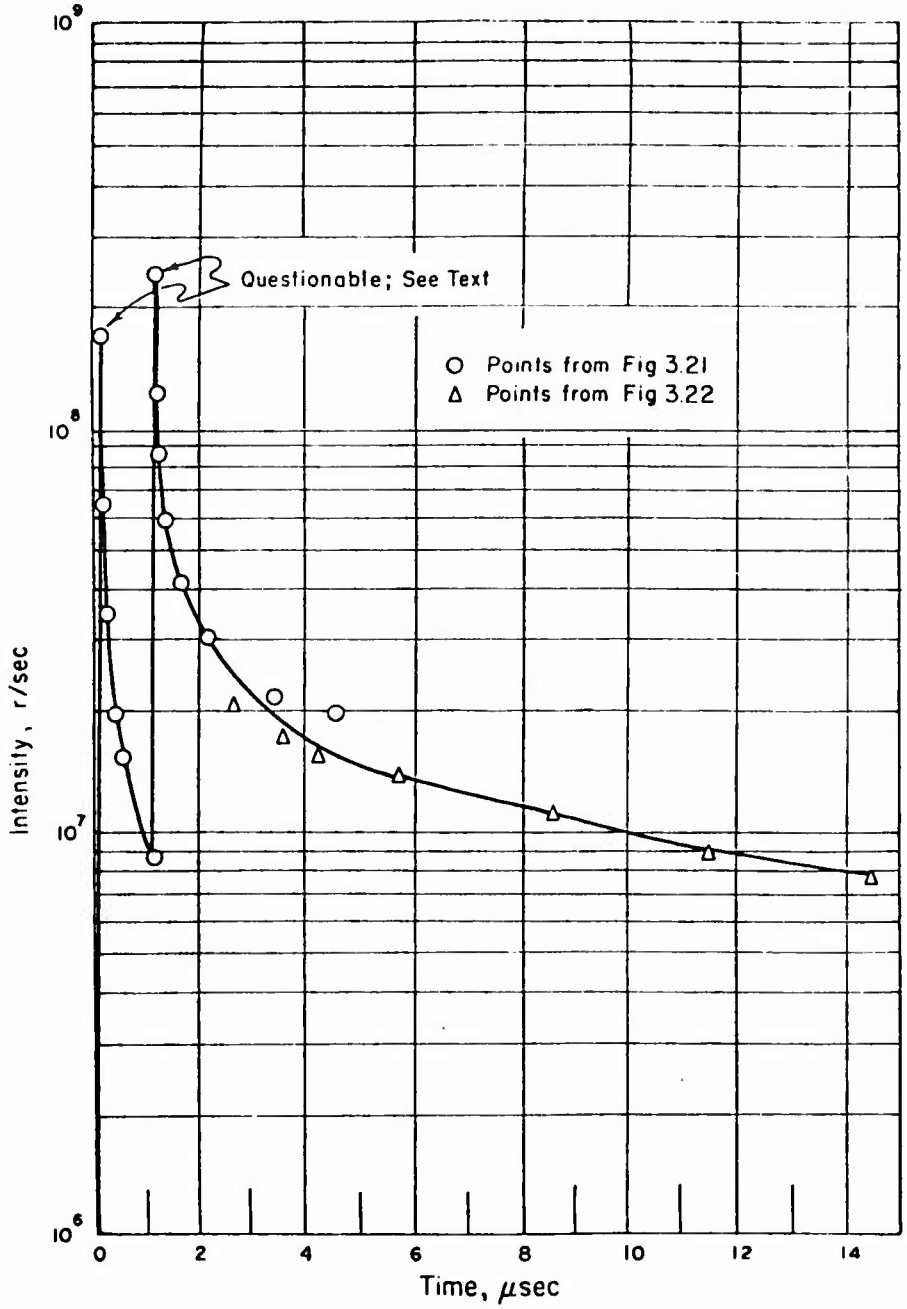

Figure 3.25 Gamma ray intensities at 1,600 yards for first 15 μsec, Shot Hood.

Page 62 has been deleted.

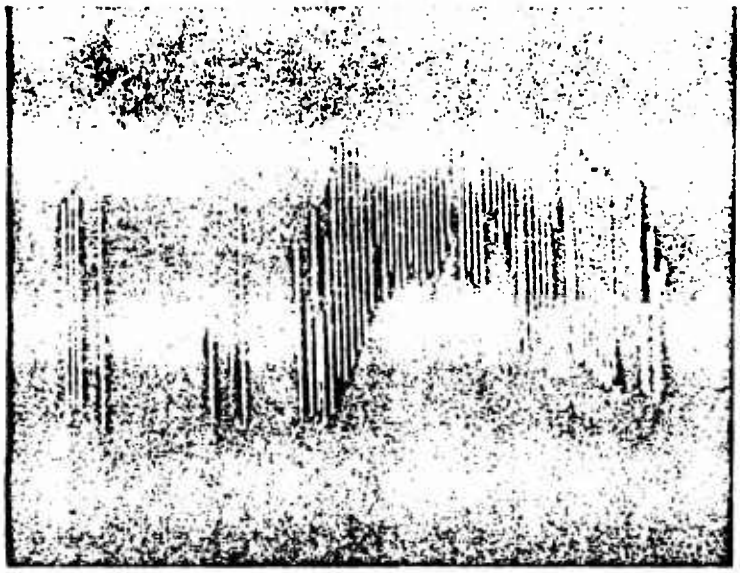

Figure 3.28 Signal received from 160-Mc transmitter in Bunker .05, Shot Hood.

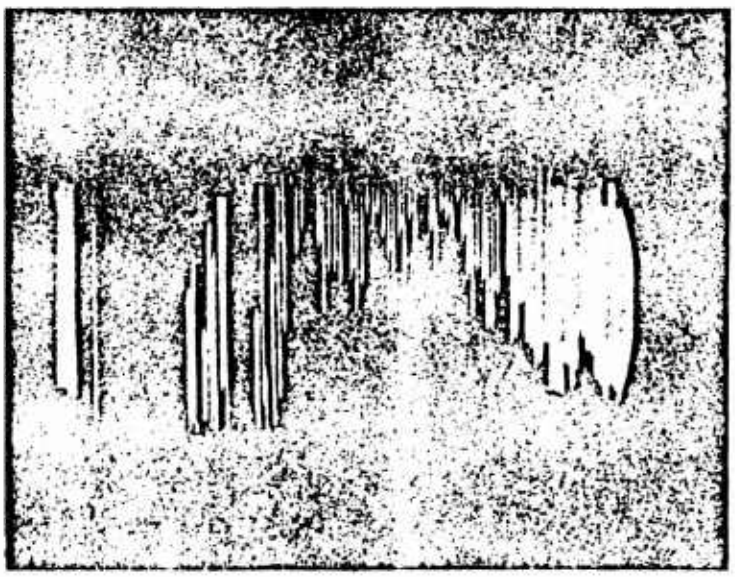

Figure 3.29 Signal received from 960-Mc transmitter in Bunker .05, Shot Hood.

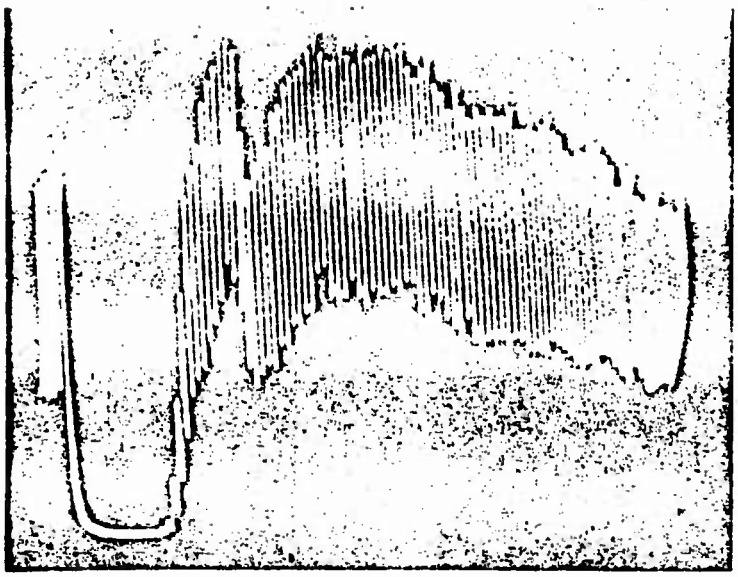

Figure 3.30 Signal received from X-band transmitter in Bunker .05, Shot Hood.

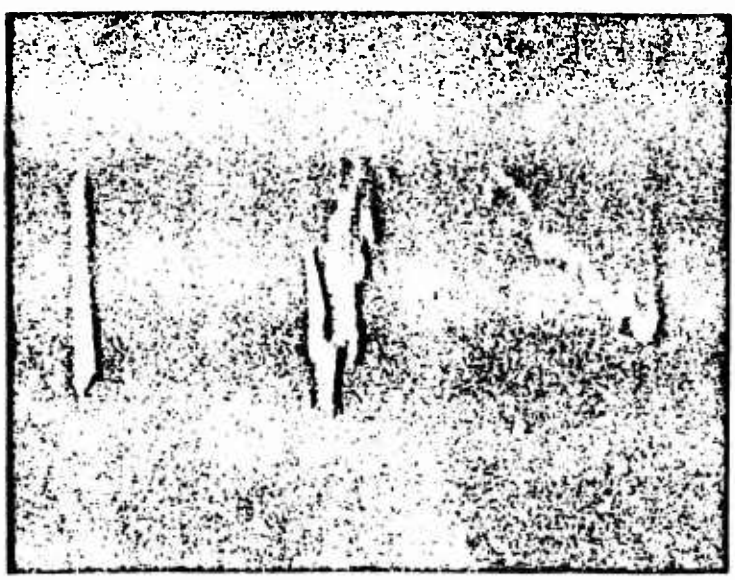

Figure 3.31 Signal received from X-band transmitter in Bunker .03, Shot Hood.

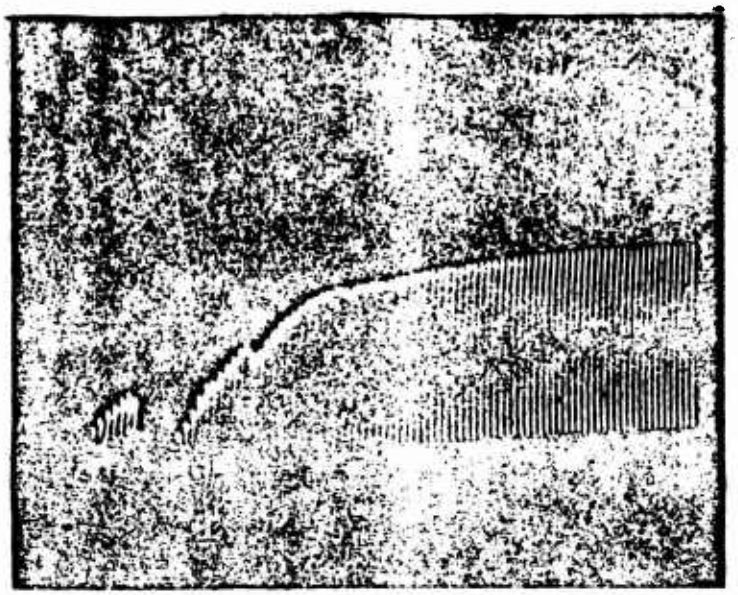

Figure 3.32 Signal recorded on X-band monitor scope in Bunker .03, Shot Hood.

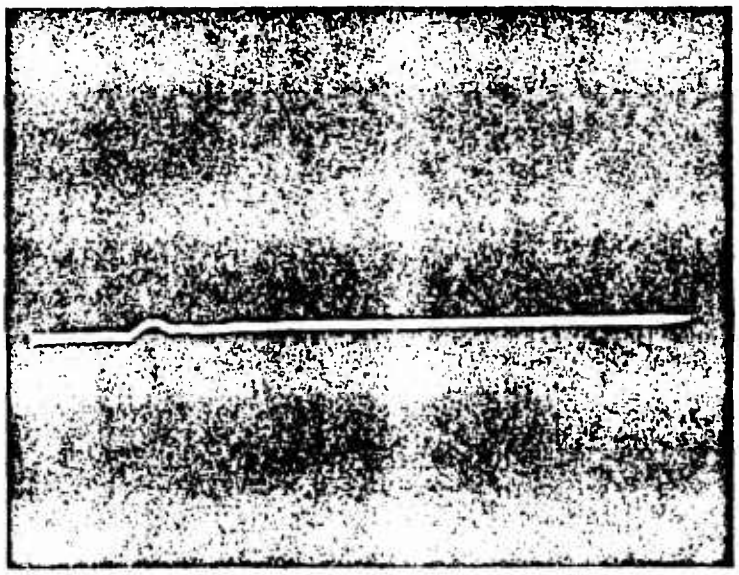

Figure 3.33 Signal from 160-Mc receiver for first 100 μsec, Shot Diablo.

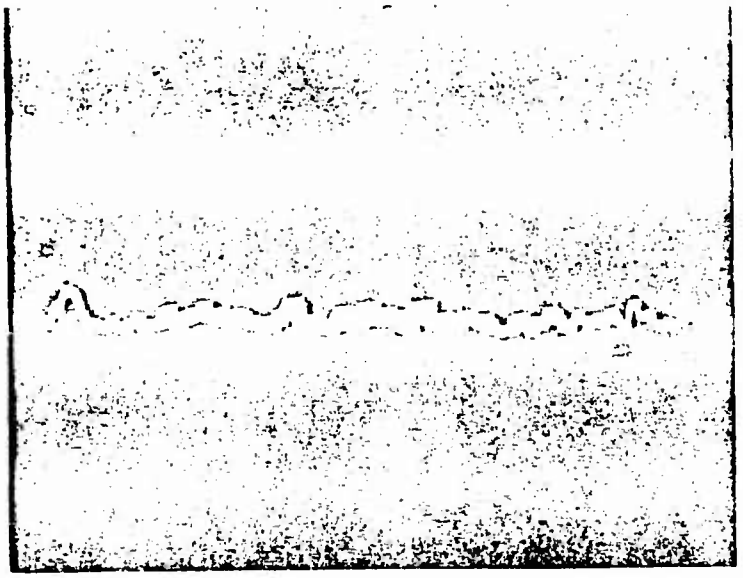

Figure 3.34 Signal from 960-Mc receiver for first 100 μsec, Shot Diablo.

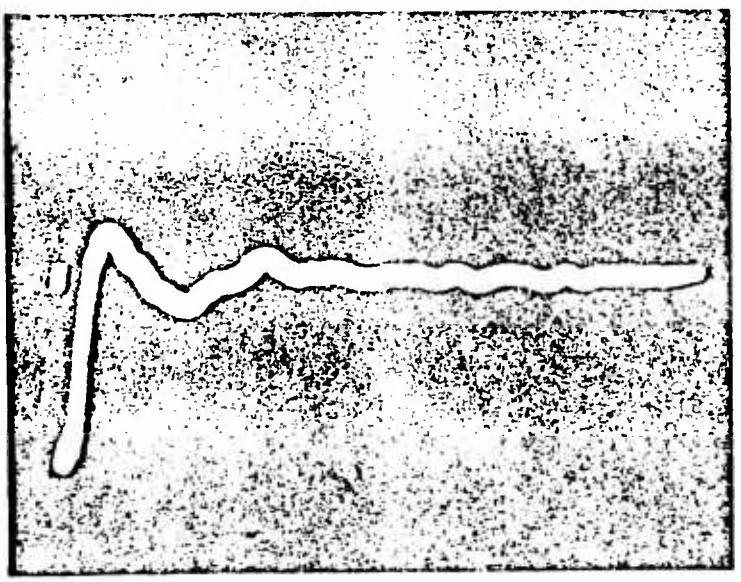

Figure 3.35 Recording of EM signal for first 100 μsec, Shot Kepler.

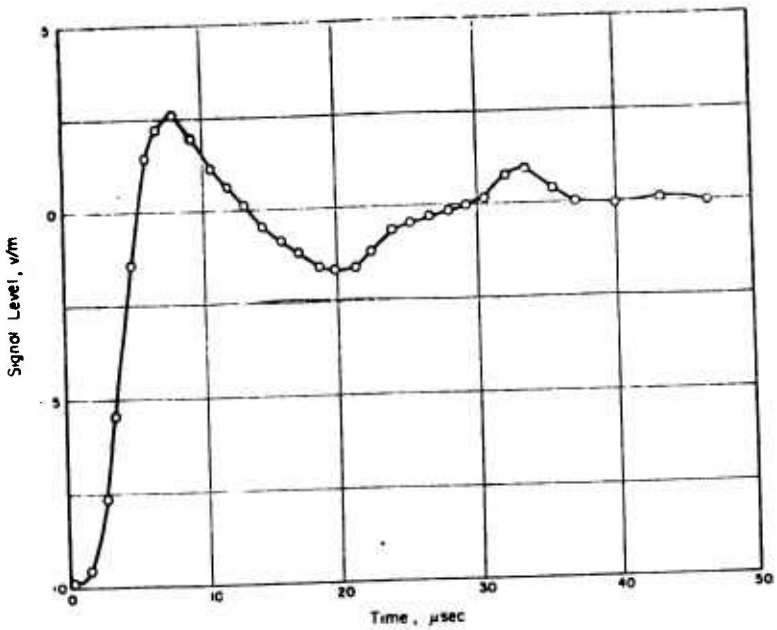

Figure 3.36 EM signal versus time, Shot Kepler.

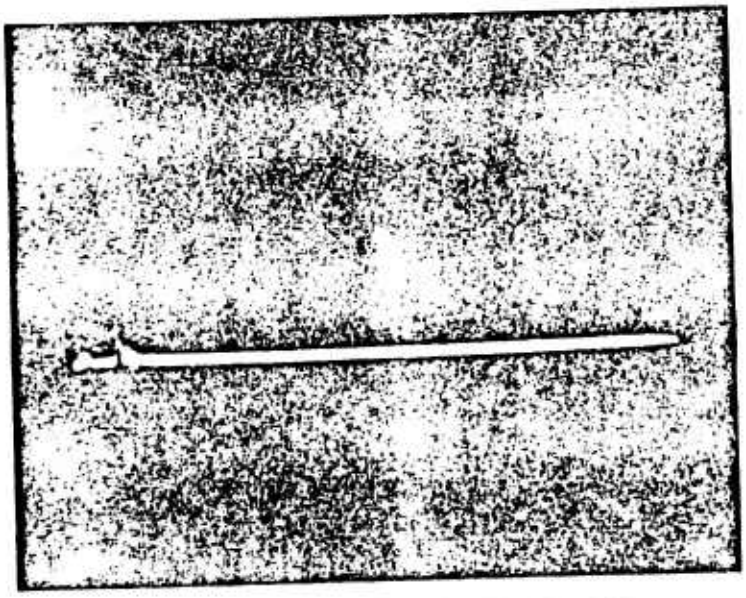

Figure 3.37 Gamma rays from Bunker .05 on high-intensity channel with 20-v/cm sensitivity for first 5 μsec, Shot Owens.

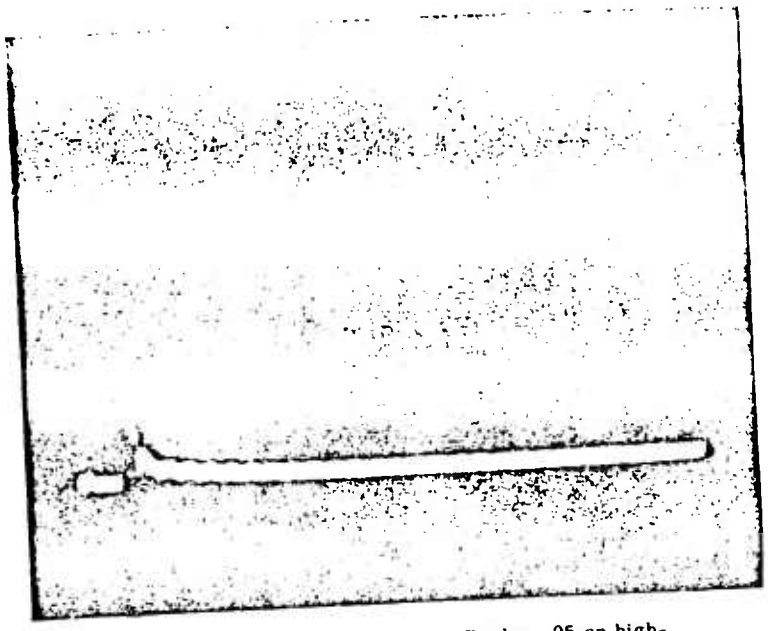

Figure 3.38 Gamma rays from Bunker .05 on high-intensity channel with 2-v/cm sensitivity for first 5 μsec, Shot Owens.

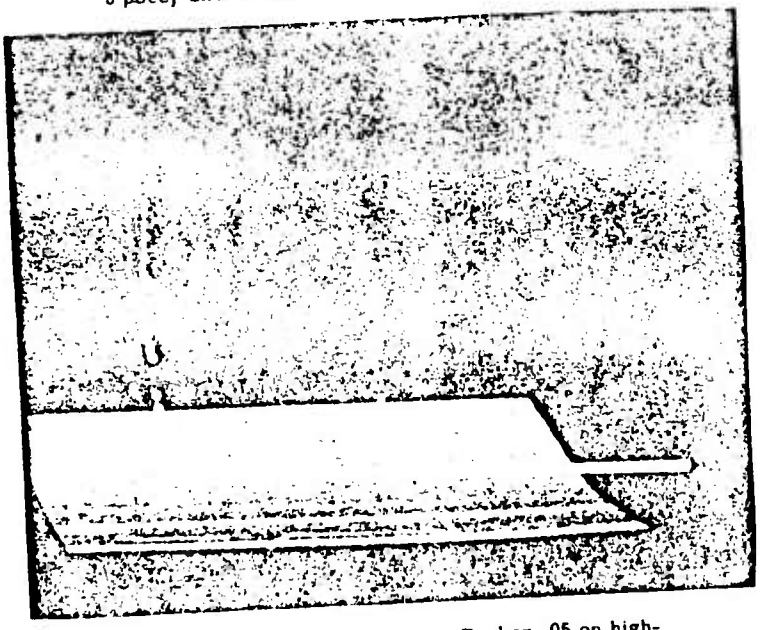

Figure 3.39 Gamma rays from Bunker .05 on high-intensity channel with 0.2-v/cm sensitivity for first 10 μsec, Shot Owens.

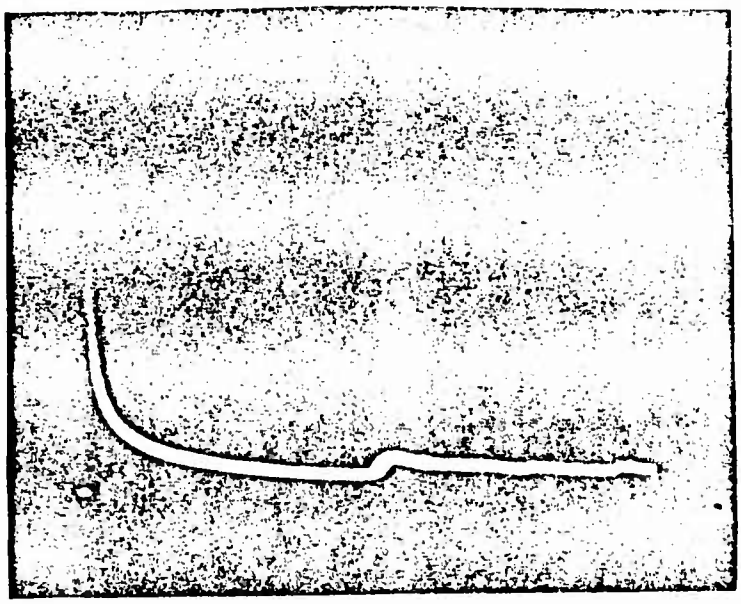

Figure 3.40 Gamma rays from Bunker .05 on high-intensity channel with 0.05-v/cm sensitivity for first 50 μsec, Shot Owens.

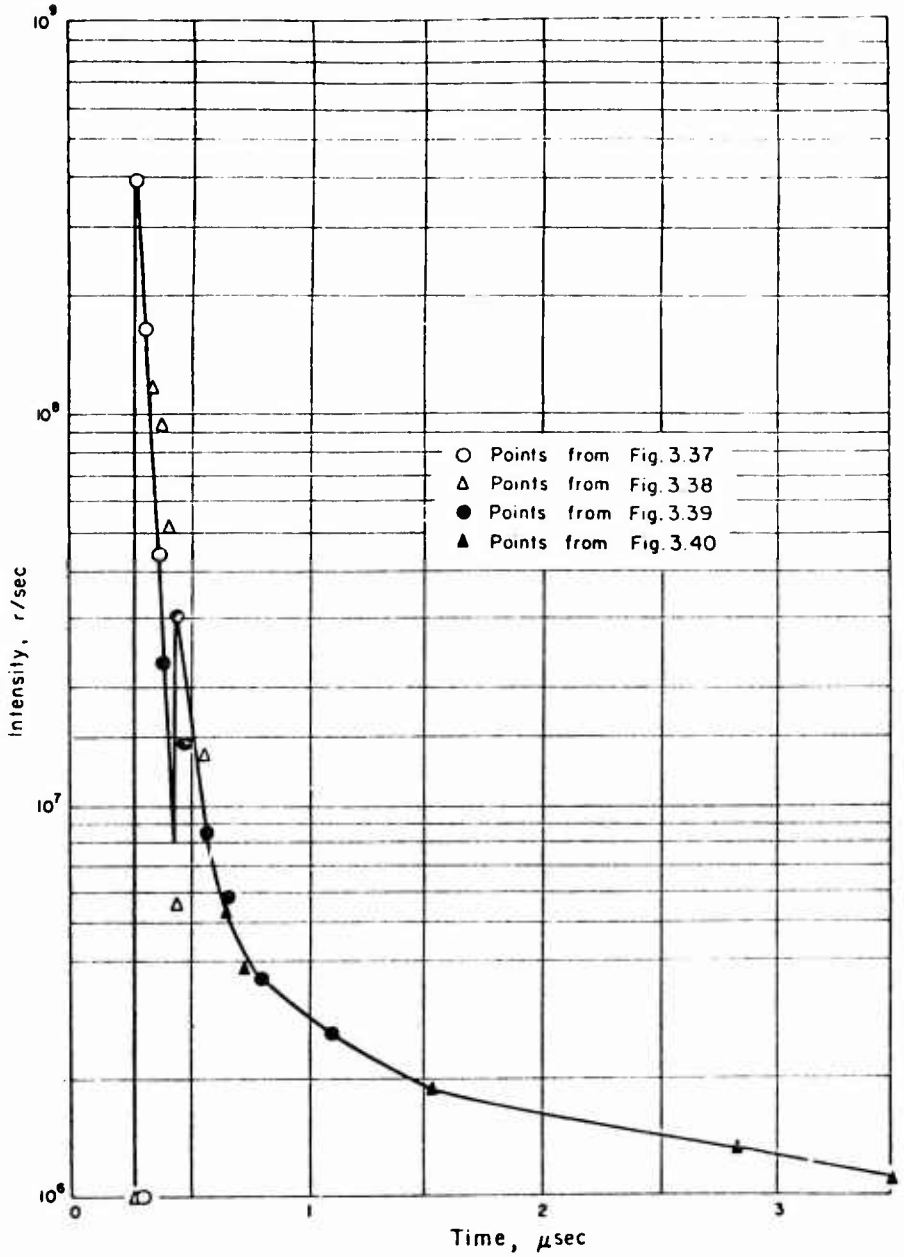

Figure 3.41 Gamma ray intensities at 1,600 yards for first 3 μsec, Shot Owens.

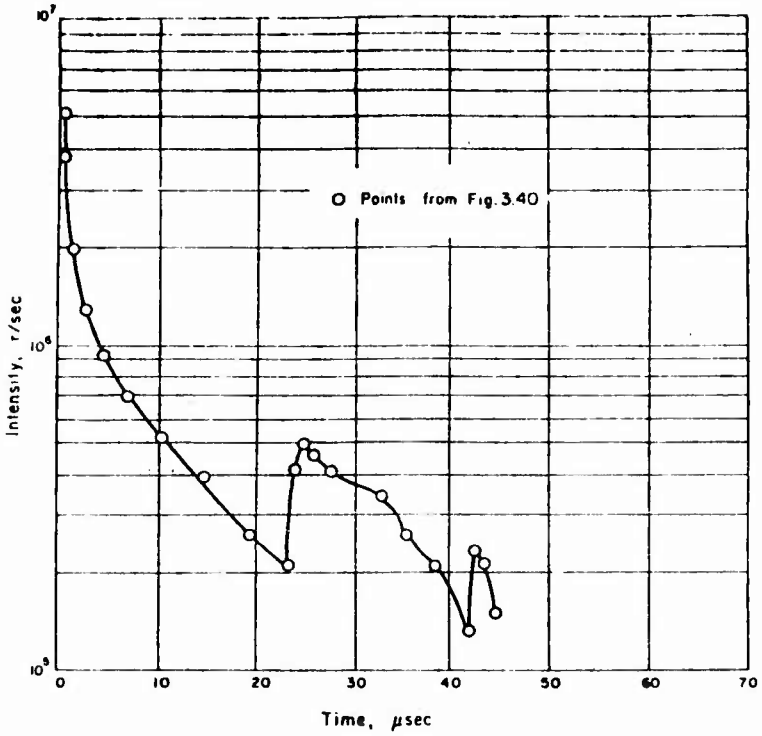

Figure 3.42 Gamma ray intensities at 1,600 yards for first 50 μsec, Shot Owens.

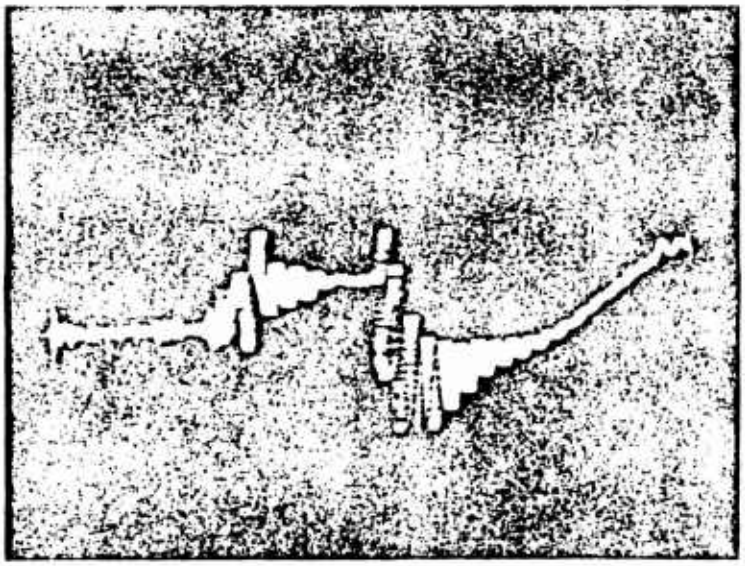

Figure 3.43 Monitor record in Bunker .05 of the 4700-Mc transmitter output.

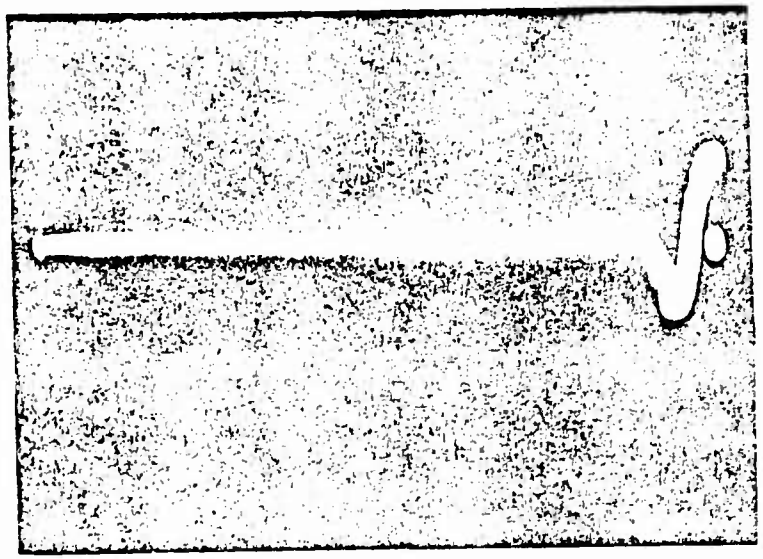

Figure 3.44 Recording of EM signal for first 50 μsec, Shot Owens.

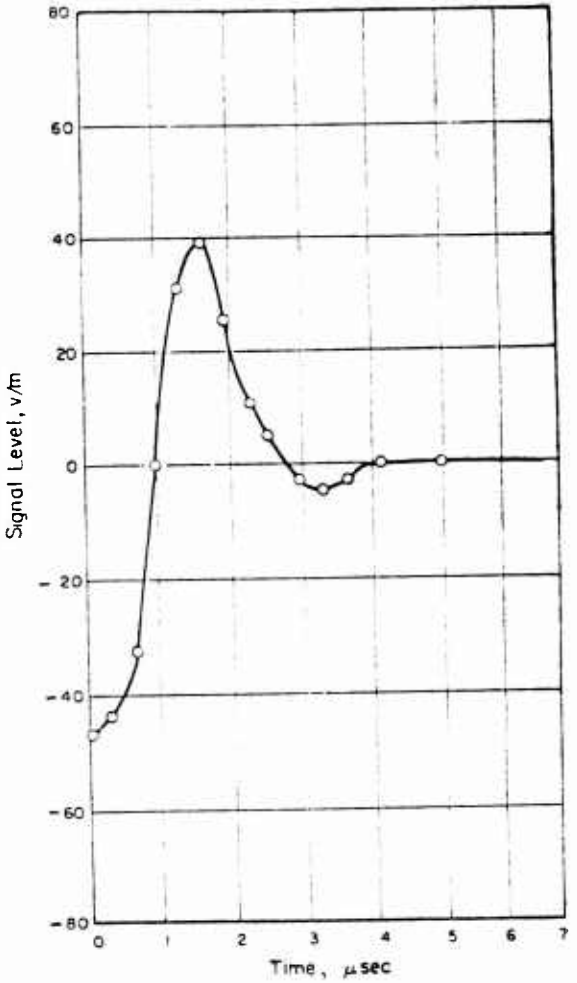

Figure 3.45 EM signal versus time for first 7 μsec, Shot Owens.

Chapter 4

DISCUSSION

4.1 ATTENUATION MEASUREMENTS

4.1.1 Gamma Rays. The gamma ray intensity as a function of time was measured during Shots Hood and Owens. No gamma ray information was obtained during Shot Wilson because of the failure of the timing signal at H−1 second (Chapter 3).

The ratio of the measured gamma ray intensities of Hood and Owens was approximately constant and about 20 to 1 over the time region from 2 to 45 μsec. However, the yield of Hood (71 kt) was only 7.3 times that of Owens (9.7 kt), so that the intensities apparently do not scale linearly with the yield. For reference, these results have also been compared with the results from Shot Easy during Operation Greenhouse as given in Reference 2. To scale the Easy curve to 1,600 yards and convert it to the units in which Hood and Owens were measured (r/sec), it was necessary to assume an average energy for the gamma rays. This was taken to be 1 Mev. To determine the validity of scaling the gamma ray intensity directly with the yield of a device, each of the three curves was reduced to a yield of 1 kt by dividing the measured intensity by the measured yield. The results of this comparison are shown in Figure 4.1.

4.1.2 Attenuation. Radial attenuation data as a function of time was obtained from Bunkers .03 and .04 during Shot Wilson and from Bunker .05 during Shot Hood. All three of the successful measurements were made at X-band frequencies. In addition to the attenuation data from Shot Hood, a simultaneous measurement of gamma ray intensity as a function of time was obtained. Since the gamma ray intensity measurement during Shot Wilson failed, it was necessary to use the gamma ray production function from Reference 2 scaled to the yield of Shot Wilson.

The attenuation as a function of time was calculated using Equation A.19 from Section A.1. This attenuation equation can be evaluated for a given range; however, the factors τ (electron mean lifetime) and K (a parameter that depends on the radio frequency, the electron energy distribution, and the collision frequency) must be evaluated. Chapter 1 contains a description of a Monte Carlo program that was used in calculating the value of these parameters. At the time this report was written, only preliminary values had been obtained. Since Equation A.19 involves only the product of these parameters, let the quantity $K\tau$ be called A. They are $\tau = 1.7 \times 10^{-8}$ sec, $K = 1.77 \times 10^{-19}$, giving $A = 3.0 \times 10^{-27}$.

The attenuation due to ionization in the copper waveguide leading from the transmitter in the bunker and the transmitting antenna, approximately 12 feet above ground level, has been taken into account. The ratio of electron density (for 1-Mev gamma rays) inside the waveguide to that in air was found to be 1.2. Since the attenuation in the waveguide is less than 1 percent of the attenuation over the remainder of the transmission path, it was neglected.

Figures 4.2 and 4.3 show the experimental data points from Shot Wilson, Bunkers .03 and .04, respectively. The calculated attenuation using $A = 3 \times 10^{-27}$ for each bunker is included on the figures. In addition, curves that were considered best fits (using A as an adjustable parameter) over the time between the earliest readable signal and full recovery are included in the figures. These fits result in values for A of 7.0×10^{-27} and 7.7×10^{-27}, respectively. The agreement between these values indicates that the radial dependence of the gamma ray intensity as given by Equation A.20 is reasonable.

Figure 4.4 shows the experimental data points from Shot Hood, Bunker .05. Since, in this case, a simultaneous measurement of gamma ray intensity as a function of time was obtained,

it was used as the electron production function in Equation A.19. Using $A = 3.0 \times 10^{-21}$, the calculated attenuation is shown on the same figure; however, the fit is not satisfactory. The best fit, which is still far from satisfactory, is also shown. This curve was obtained by using $A = 9.0 \times 10^{-21}$.

This discrepancy is apparently not due to an anomalous gamma ray measurement, since its general features are in agreement with both of the other gamma ray measurements shown in Figure 4.1. Therefore, the assumptions involved in the derivation of Equation A.19 and its applicability to the present case must be questioned.

The major difference between Shot Hood and those which have been analyzed using Equation A.19 (Plumbbob Shot Wilson and Redwing Shot Osage, Reference 3) is the fact that the yield of this device was about 7 times as large as the largest of the others. It is apparent that the rate of recovery of the experimental attenuation curve is more rapid than the rate of recovery of the calculated attenuation curve.

The assumption leading to Equation 1.5 (Chapter 1) may well be questioned. Since a large fraction of the gamma rays produced is due to (n, γ) reactions in air, constituting a distributed source, the gamma ray source function may have a more complicated distance and time dependence. It should be kept in mind that, during the recovery phase, the most energetic neutrons (14 Mev) have not yet reached the transmitter. An additional complication would result if the gamma ray energy distribution were a function of time and distance.

A second possible explanation of this discrepancy could be that the electron production function is obtained only from the gamma ray intensity measurement. However, as pointed out in Chapter 1, the most prominent mechanism for the removal of free electrons is attachment to neutral oxygen molecules, which gives rise to negative ions. The electron is bound in this configuration by about 1 ev. It is conceivable that there exists enough light energy of sufficiently short wavelength to detach electrons from the negative oxygen molecular ions and thereby make it necessary to add another production term into Equation 1.1. This would make the attenuation dependent not only on the gamma ray intensity but also on the intensity of the light over the transmission path.

A final possibility is that this discrepancy may be due to the EM signal produced by the burst. The mean lifetime of a free electron, τ in Equation A.19, could be affected by a sufficiently intense electric field. This parameter depends on the time required for the electron energy to be reduced to thermal, and to the capture cross section, since this cross section is small for higher energies. An electric field causes longer moderation times, because the electrons can gain energy from the field between collisions. Any increase in τ causes a corresponding increase in the attenuation. There is evidence from the behavior of the baseline that the electric field is decreasing at the same time that the signal recovers.

4.2 ELECTROMAGNETIC SIGNAL EFFECTS

The measurements made by this project of the EM signal generated by the detonation of a nuclear device fall into two categories: The first concerns only the frequency components of the EM signal that lie in the acceptance bands of the receivers used for the attenuation measurements; the second concerns the entire EM signal and its effect on the equipment used by the project.

The minimum detectable signal in measurements of the first type mentioned above may be calculated from the parameters of the receivers used. The signal power at the receiver input terminals, P_R, is given by

$$P_R = \omega G \sigma \text{ watts}$$

Where: ω = free-space energy flux at antenna, w/m^2
G = numerical power gain of antenna with respect to an isotropic radiator
$\sigma = \lambda^2/4\pi$, the cross section in square meters of an isotropic radiator at wavelength λ meters.

The inherent receiver noise, which determines the smallest signal that can be detected, is normally described by two parameters: the Johnson noise power, P_j, which is the thermal noise power appearing across an impedance, e.g., the antenna, or receiver input impedance; and the "noise figure," N_f, of the receiver, into which can be lumped all other sources of noise in the receiver. The noise figure can be expressed as the ratio by which the thermal noise would have to be increased to produce the same total noise signal. This "equivalent" noise power at the receiver input terminals, P_N, is then

$$P_N = P_j N_f$$

A rather optimistic estimate (for the recording methods used here) of the minimum detectable signal can be obtained by assuming that a signal equal to the receiver noise can be detected, i.e., that the minimum detectable signal is

$$P_R = P_N$$

The energy density required at the antenna can now be calculated from

$$\omega \sigma G = P_j N_f$$

P_j can be found from the expression

$$P_j = 4 k T \Delta f$$

Where: k = Boltzmann constant
T = absolute temperature
Δf = bandwidth, cycles/sec (2 Mc for these receivers)

So that $P_j = 3.29 \times 10^{-14}$ watts

The other parameters for the receivers used are given below:

Frequency Mc	N_f	σ	G
160	13	0.28	16.2
960	32	0.008	205
9850	160	0.00008	20,000

The electric field intensity required may be found from ω by using the expression

$$\omega = \frac{1}{2} \sqrt{\frac{\epsilon}{\mu}} E_0^2$$

where ϵ and μ are the dielectric and permeability constants of free space, and E_0 is the peak electric field intensity in volts per meter.

The minimum detectable signals, based on the criteria previously mentioned, are given below in terms of both ω and E_0.

Frequency Mc	ω w/m^2	E_0 v/m
160	9.4×10^{-14}	8.4×10^{-6}
960	6.4×10^{-13}	2.2×10^{-5}
9850	3.3×10^{-12}	5.0×10^{-5}

The signals recorded during Shot Diablo are shown in Figures 3.33 and 3.34. The 9850-Mc receiver signal did not show above the noise; therefore, its record was not reproduced. An upper limit of about 50 μv/m can be placed on the 9850-Mc intensity. The 960-Mc signal appears to be about twice the noise level, so that the peak intensity is about 40 μv/m. The 160-Mc record shows a small pip, but it appears at the wrong time. This could have been produced by pretriggering in the sweep circuit, but the data must be regarded as suspect. If it is taken as valid, it leads to a peak intensity of about 25 μv/m.

The data resulting from the EM effect measurements made during Kepler and Owens with vertical dipoles are shown in Figures 3.36 and 3.45, respectively. These recording channels were direct-coupled all the way from the dipoles to the deflection plates of the oscilloscopes, and the transmission-line-antenna system was carefully terminated and checked with a pulse generator exciting the dipole. There should be no distortions due to coupling capacitors, or to ringing in the system. The results of these measurements will not be analyzed here; they are presented as general information only.

The effects of the EM signal generated by a nuclear detonation on equipment in close-in bunkers can be severe and difficult to avoid. The bunker-monitoring system was first used during Hood. The oscilloscope record (Figure 3.32) showed a large baseline shift that is apparently due to penetration of the shield of Bunker .03 by the EM signal.

Each bunker installation was 6 feet below ground level, completely shielded by a $\frac{1}{32}$ inch copper sheet with soldered joints, and electrically disconnected from the outside world (with one exception) from H−1 second on.

The exception mentioned consisted of waveguides soldered to the copper shield at the point of entry to the bunker and coaxial cables similarly treated. The waveguide should not give trouble, but the case for the coax is not as clear. The majority (4 or 5) of the coax cables were connections to the gamma ray detectors. These detectors were completely shielded electrically and just under or just above ground level. There seems to be no evidence in any of the gamma ray recordings of any interference from the EM effect. The only other coax cables involved were those used to connect the 160- and 960-Mc transmitters and transmitting antennas in Bunker .05. These antennas used dipole feeds, thus exposing a small portion of their center conductors. However, the cables were driven by coupling networks in the transmitters that provided dc short circuits to ground and extremely low impedances at frequencies more than about 20 percent different from the operating frequency. If the electrical bond between the transmitters and the copper shield were faulty, or the inductance in that path were high, this could be a vulnerable point.

Large magnetic fields are known to have been present in the bunker area from measurements made by Project 6.2 (Reference 11) in the same general area. Fields could have been induced in the interior of the bunker, particularly by the lower frequency components of the EM signal where the skin depth in the copper shield becomes comparable to or greater than the shield thickness, that would be large enough to produce the effects noted. A very remote possibility is that the disconnect mechanism used to isolate the bunker from power and timing lines at H−1 second did not operate. However if this had failed, the damage to the bunker would probably have been severe, and its operation completely disrupted. There is at present no clear way to account for the penetration. When the effects of the EM field generated by the detonation are better understood, it may be possible to calculate the fields that could have been expected due to induction through the bunker shield. It is apparent that the precautions observed in this installation were not adequate at this range from a device with this large a yield.

This bunker was the only source of valid monitoring information. However, there was no indication in the records obtained at the receiving station of interference by the EM effect with the operation of the bunkers used during Wilson. (The indications at Bunker .01 during Wilson were that the timing signal at H−1 second was not received; therefore, the disconnect mechanism did not operate.) As has been previously mentioned, the situation during Owens is inexplicable.

Now for a discussion of the difficulties in the receiving van (at Building 400) during Shot Hood. Signals on the powerline of the magnitude observed (greater than 40 volts) were completely unexpected, even though this possibility had been investigated. Interference with the receiving and recording system was observed only at this shot. This raises the possibility that the line voltage regulators in the van could handle the signals from the other shots, but their capability was exceeded for this large-yield detonation.

4.3 REFLECTION BY FIREBALL

The experiment during Shot Priscilla consisted of measuring the X-band energy reflected from the fireball. A 9750-Mc transmitter with a 6-foot parabolic antenna was used to illuminate the fireball, and a receiver with a 6-foot antenna at the receiving station was directed toward the burst point to measure the reflected signal strength. The results given in Section 3.5.2 indicate that the reflected signal was less than the minimum detectable signal throughout the time of the measurement.

At times before 0.01 second, the ionization produced by the gamma rays is sufficiently intense so that the attenuation over the transmission path, as calculated from Equation A.19, is greater than 50 db. At 0.01 second, this gives a signal strength at the receiver of about 10^{-14} w/m^2 or 25 db less than the minimum detectable energy flux (3.3×10^{-12} w/m^2, see Section 4.2). However, an upper limit for the reflection coefficient at times later than 0.01 second can be estimated.

At times greater than 0.01 second, the fireball is so large that it subtends an angle greater than the 2° beam width of the transmitter, and it is possible to assume that the total power of the transmitter is intercepted by the sphere. The power density, S_r, at the receiver position is then approximately given by (assuming reflection into a solid angle of 2π radians),

$$S_r = \frac{P_t C^2}{2\pi R^2}$$

Where: P_t = power output of transmitter
C = reflection coefficient
R = distance from fireball to receiver

Equating S_r to the minimum detectable signal strength (3.3×10^{-12} w/m^2) and substituting 0.8 watt for P_t and 1.87×10^4 meters for R gives 0.095 as the upper limit for the reflection coefficient of the surface of the fireball. This value corresponds to a radar cross section of 190 m^2.

Since there was no detectable signal during the entire time of the measurement (~10 sec), it is apparent that the signal is strongly absorbed in the vicinity of the fireball even after 0.01 second. This result is not unreasonable, since in Figure 4.5 it can be seen that the surface temperature of the fireball at 1.5 seconds is still greater than 3,000° C (Reference 12). On the same figure, the attenuation, in db per meter, for air at the temperature of the fireball surface is also shown (Reference 13). It can be seen, for example, that for times as late as 1.5 seconds the attenuation at the fireball surface is about 270 db/m. Since, by this time, the surface of the fireball is by no means sharp and distinct, it is not unreasonable to assume that the signal would be absorbed in penetrating this surface.

4.4 MEASUREMENTS THROUGH THE FIREBALL

The experiment during Shot Boltzmann consisted of measuring attenuation on line-of-sight transmission paths that passed near the position of the center of the initial fireball. Three transmitters and receivers, each pair operating on a different frequency, constituted the radio links. For convenience in the analysis of the data, the time is divided into the initial phase (0 to 100 μsec), the intermediate phase (100 μsec to 0.5 second) and the final phase (0.5 to 10 sec-

onds). The size and position relative to the ground of the Boltzmann fireball for times of interest are shown in Figure 4.6.

The major effect during the initial phase is attenuation of the signal by free electrons, which are produced by the gamma rays. To make an estimate of the lower limit of the attenuation of a microwave signal propagating through a region near the fireball, the integral of Section A.2 was evaluated for an R_T of twice the maximum fireball radius (≈370 meters). Inserting twice this result (to get the total attenuation from the transmitter to the fireball and then to the receiver) into Equation A.19 and using the gamma ray production function from Reference 2, scaled to the correct yield for Shot Boltzmann (11.5 kt), gives the attenuation as a function of time. This result is shown in Figure 4.7. During the initial phase, the gamma ray intensity is seen to be sufficiently high and so extended through space that the line-of-sight signal path has a peak attenuation of more than 2,000 db. The signal then recovers to within 10 db of the normal signal level in about 50 μsec. This is consistent with the experimental results, since the signal is completely absent (attenuated by more than 50 db) during the first 50 μsec (Figures 3.2 through 3.14).

From about 100 μsec to 7 or 8 seconds, the line-of-sight path is obscured by the fireball. During this time, the temperature of the fireball was sufficiently high so that it can be considered virtually opaque to microwaves (Section 4.3). On this basis, any line-of-sight signal would be nonexistent, and the signal that does reach the receiver during this period could be due only to signals reflected from the ground or diffracted by the fireball or a superposition of both of these effects.

As a first attempt to explain the somewhat complicated experimental results, the visible fireball was treated as an opaque sphere and the resulting diffraction patterns, including both the direct and reflected transmission paths, have been examined. The details and results of this calculation can be found in Section A.3. Since the reflection angles are, in general, very shallow and the ground is relatively flat, the actual reflection coefficient should be high (≈1). However, since measurements have been made of this quantity by various investigators (References 14 and 15) and the results of these measurements have not been in accord, the calculation was performed for a series of reflection coefficients between 0 and 1 and a representative set of these results is shown in Figures A.3 and A.4.

In comparing these results to the experimental results (Figures 3.11 and 3.12) it is apparent from the discrepancies observed that, during the intermediate times, there are other effects, which are not taken into account in this calculation. The first and most obvious discrepancy is the fact that the calculated signal levels are, in general, higher than the measured levels. This may be due to the fact that even at late times the electron density near the surface of the fireball is high and any signal that passes near the sphere is attenuated to some extent. For example, the fireball temperature at 2 seconds is still about 3,000° C (Reference 12). The electron density near the surface of the sphere is, therefore, around 10^{11} electrons/cm^3 and for a frequency of 1,000 Mc, this corresponds to an attenuation of about 18 db/m. It is, therefore, not unreasonable to find that the experimental results show lower signal levels than do the calculated curves.

In addition, there exists around the fireball an electron density gradient, which can cause refraction around the sphere. The differences in path length of the various refracted rays produce different time delays in the 1-μsec RF wave trains with the result that they overlap, causing the received signal to be incoherent (Reference 16). This is probably the reason for the distortion of the signal after the initial phase is over (Figures 3.2 through 3.9).

The time at which the signal returns to its preshot level in the calculated curves agrees reasonably well with the measured results. This time corresponds to the time at which the fireball moves out of the line of sight between the transmitters and receivers.

An examination of the results of this measurement shows that there is a strong similarity between the 960- and 9750-Mc records and indicates that there is little or no frequency dependence at these frequencies. The early portion of the 160-Mc record appears to be quite different

from the others; however, there appeared to be some interference on this channel from unknown sources. At later times (10^{-2} to 10 seconds) the signal was clean and appeared to be free from the interference. The 160-Mc signal started to recover at about 0.5 second but did not reach the preshot level until about 7 seconds. This long recovery time can be compared to the 960- and 9750-Mc records where the recovery takes place over a period of about 1 second.

This difference is probably due solely to differences in the diffraction, since, from Equation A.19, assuming a collision frequency of 2×10^{11}/second, it can be seen that there should be no frequency dependence in the attenuation by electrons over the frequency range that was used.

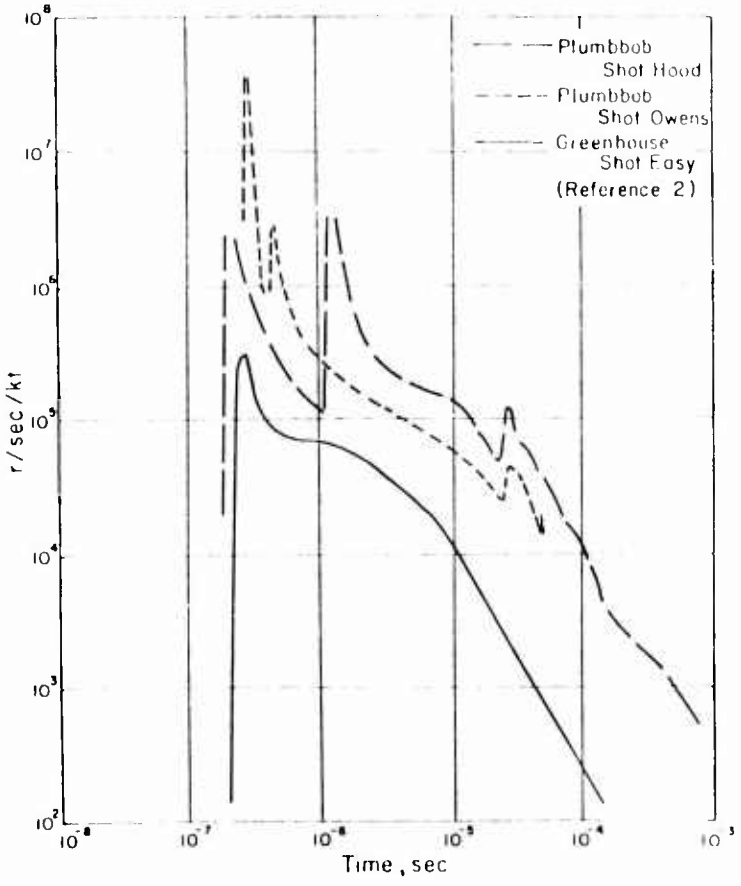

Figure 4.1 Normalized gamma ray intensity measurements at 1,600 yards compared with Greenhouse Shot Easy scaled to the same distance.

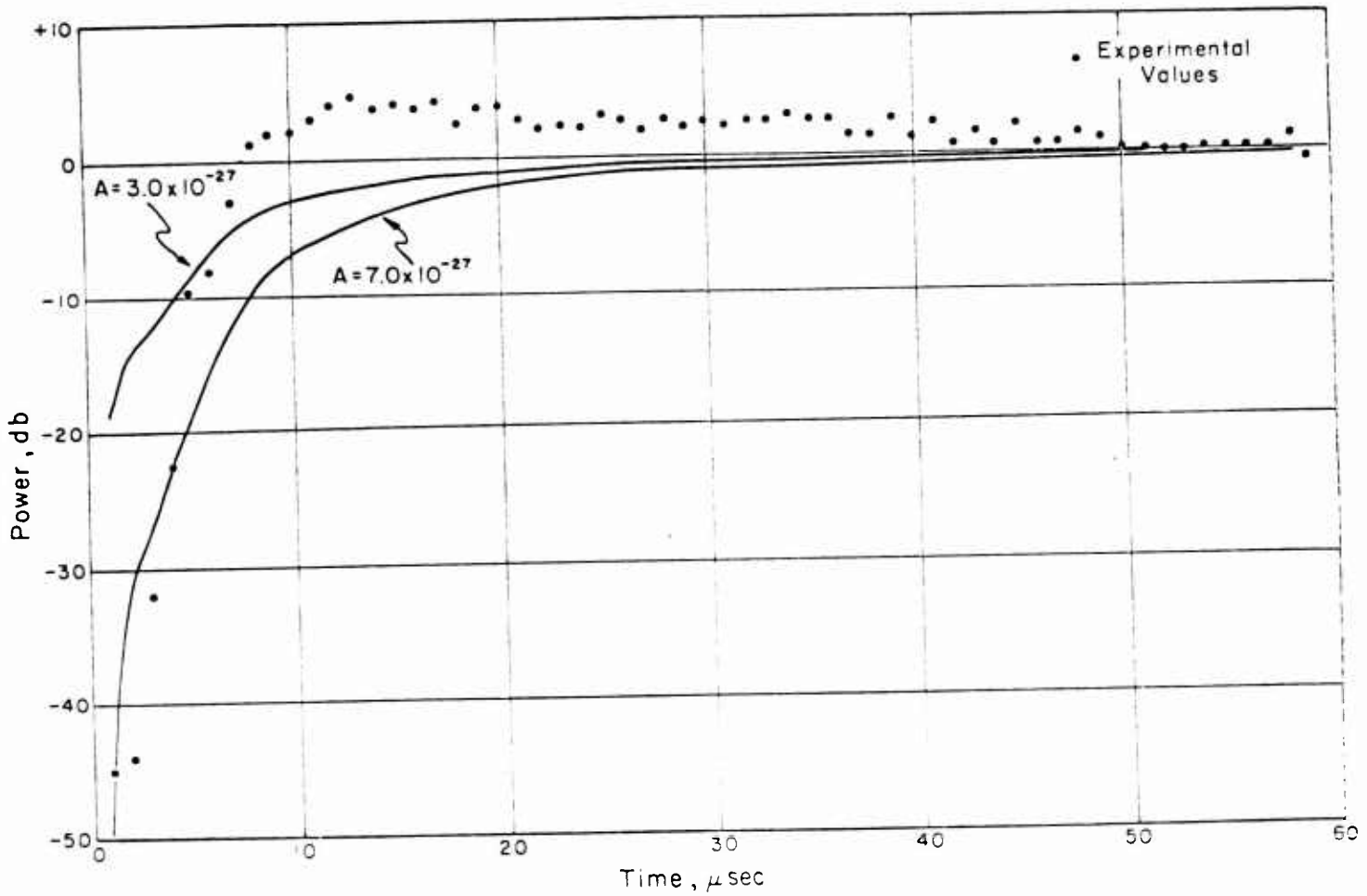

Figure 4.2 Measured and calculated attenuation at Bunker .03, Shot Wilson.

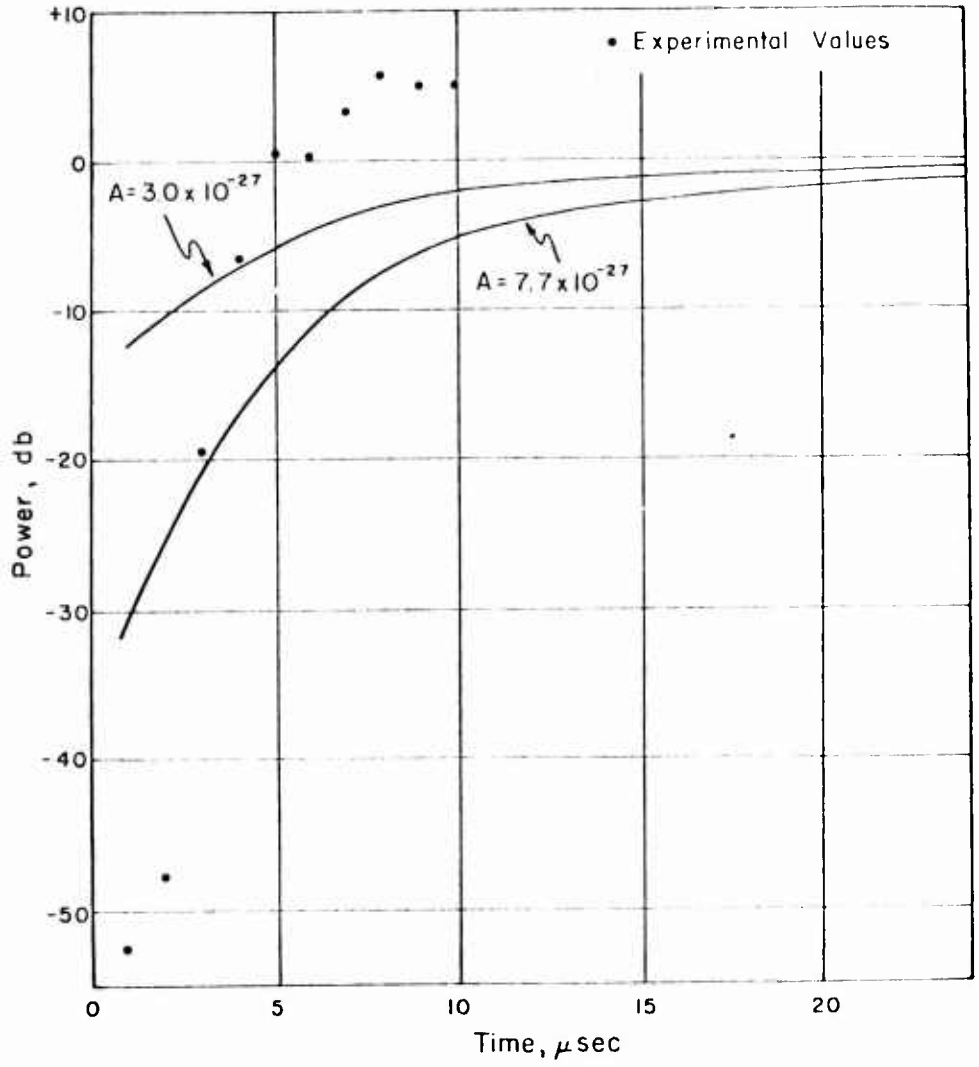

Figure 4.3 Measured and calculated attenuation at Bunker .04, Shot Wilson.

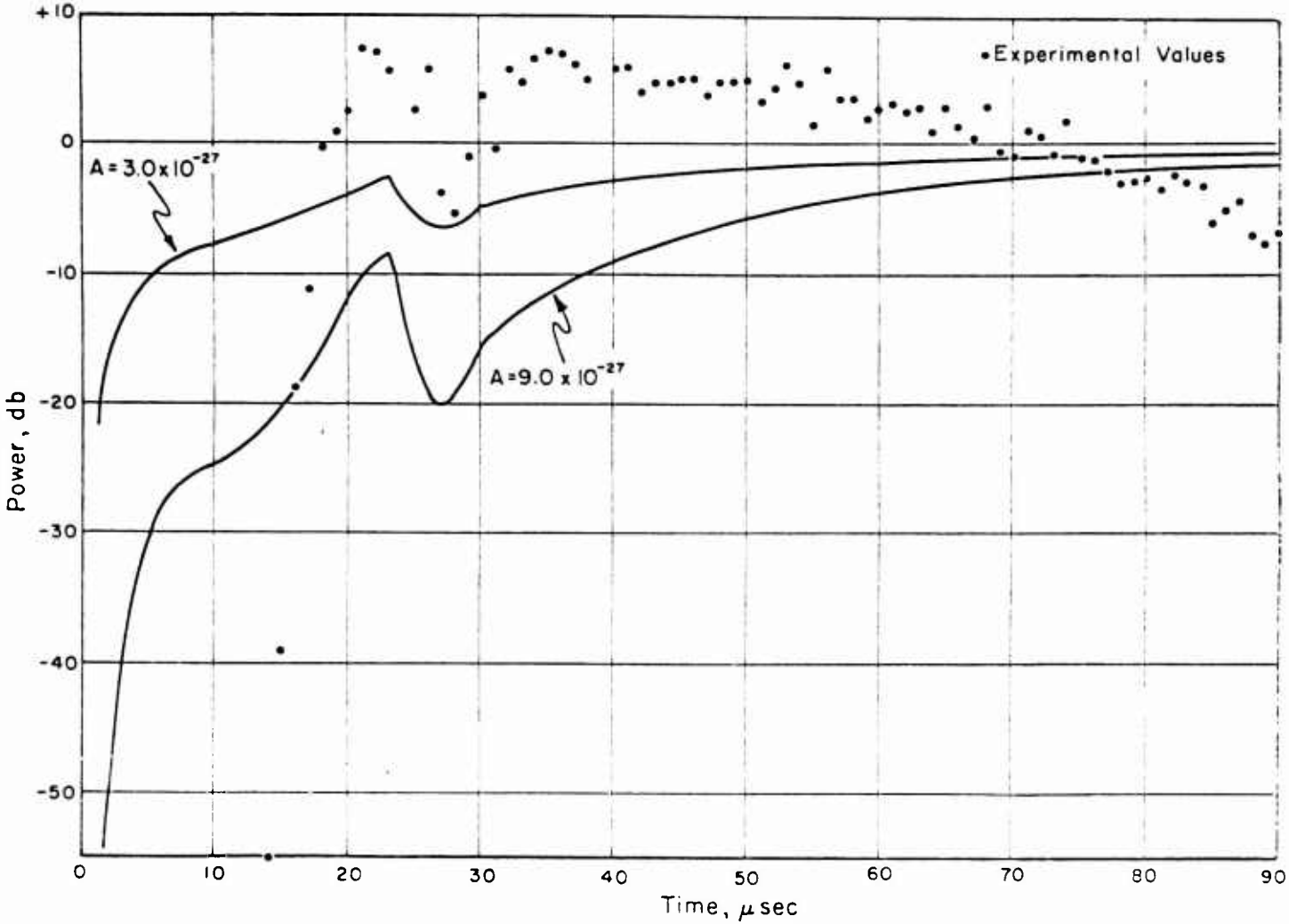

Figure 4.4 Measured and calculated attenuation at Bunker .05, Shot Hood.

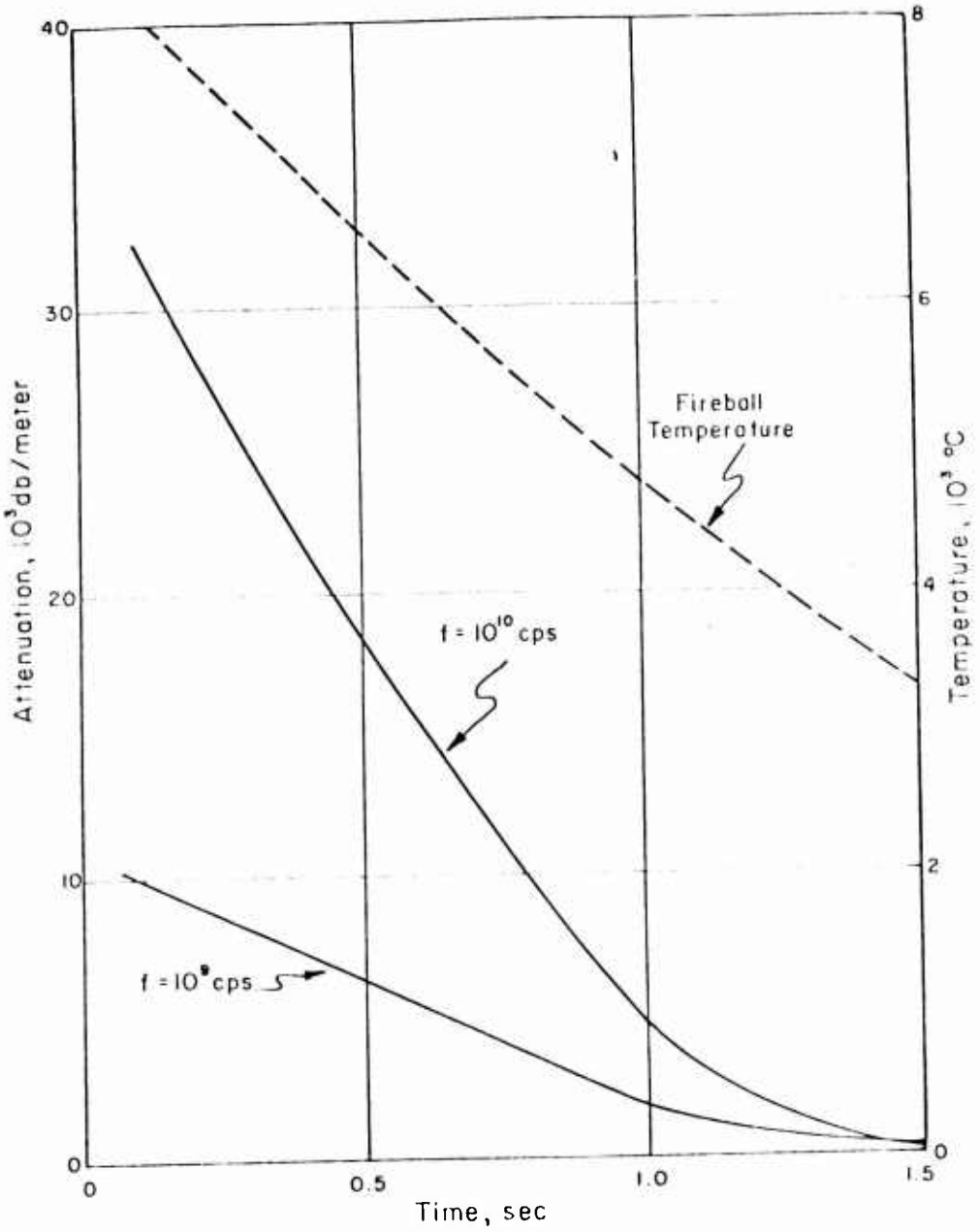

Figure 4.5 Fireball surface temperatures and radio wave attenuation.

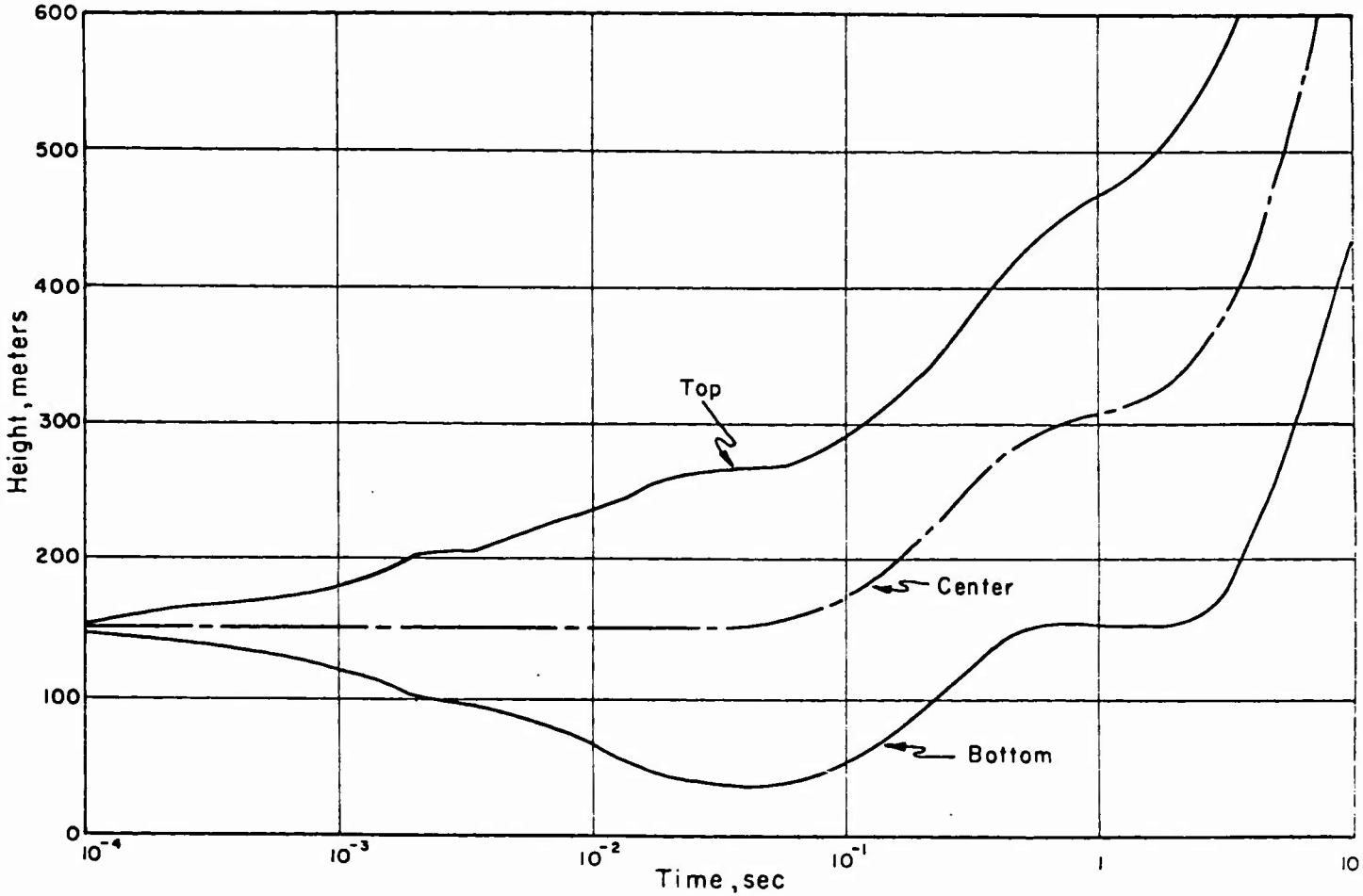

Figure 4.6 Vertical extent of fireball, obtained from EG&G early fireball pictures, Shot Boltzmann.

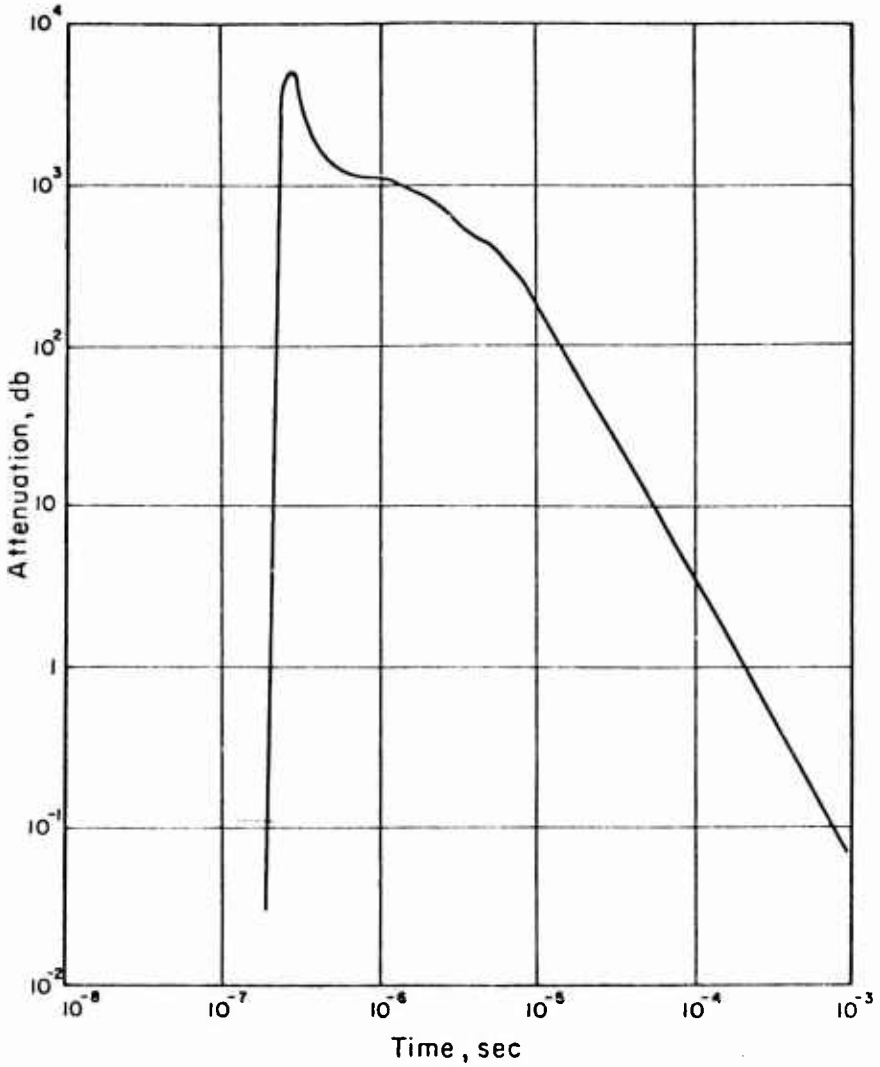

Figure 4.7 Attenuation as calculated for transmission path for early times, Shot Boltzmann.

Chapter 5

CONCLUSIONS AND RECOMMENDATIONS

5.1 CONCLUSIONS

The conclusions given in this chapter are listed separately for Projects 2.7.1 and 2.7.2, although the distinction between the two projects is not clear cut. Project 2.7.1 was primarily aimed at support of high-altitude radiation measurements, which were to be made at Operation Hardtack. Project 2.7.2 was added to provide some basic information concerning radio wave propagation in the vicinity of a nuclear explosion.

5.1.1 Project 2.7.1. In the radial attenuation measurements made during this experiment, it was found that there were large radio wave attenuations (greater than 50 db) for periods of several microseconds. If the electron removal mechanisms at high altitudes are assumed to be similar to those at NTS altitudes, then a simple extrapolation to high altitude indicates that these same conditions will exist for times of the order of seconds. Under these circumstances, it is obvious that it would not be possible to transmit the data directly from the high altitudes involved in the Hardtack measurements, and therefore, it was necessary to incorporate a long time delay system.

Radiation detectors, which had been designed with complete electrical shielding and low-impedance load resistors, performed very satisfactorily. The data obtained from these measurements was consistent and useful in the analysis of the attenuation measurements.

The effectiveness of the EM shielding in the bunkers was satisfactory for most of the purposes of this experiment. There was evidence, however, that the EM field penetrated the shielding in the case of Bunker .03 during Shot Hood. The loss of the data from Bunker .02 for Shot Wilson, when the timing and power cables were not disconnected before the shot, indicated the strong necessity of all of the shielding precautions.

The 4700-Mc high-resolution experiment failed and the reasons for this failure are unknown.

5.1.2 Project 2.7.2. The measurements of attenuation versus time, in general, confirmed the conclusions drawn from measurements made during Operation Redwing (Reference 3). In particular, the data from Shot Wilson could be roughly fitted by the parameters that were used previously. However, an attempt to fit the attenuation data from Shot Hood was unsuccessful; therefore, it must be concluded that there are effects that have not been taken into account.

The two attenuation curves obtained for Shot Wilson were compared, to check the assumed dependence of attenuation on distance. Although this formulation is not unique, the distance dependence agrees with that given by Equation A.20 within about 10 percent.

The measurement made at Shot Hood did not yield much information about the dependence of attenuation on frequency. The three transmitters operated in a very satisfactory manner during the measurement; however, baseline shifts on the recording instruments caused most of the data to be lost. These shifts were traced to voltage fluctuations in the powerlines at the receiving station. Initial-phase attenuation data for Shot Boltzmann seems to indicate that each of the three links on different frequencies recovered at about the same time (≈ 100 μsec). This is just the result to be expected from the Lorentz theory if the radiofrequencies were somewhat less than the effective electron collision frequency.

During Shot Boltzmann, the signal was strongly attenuated during most of the time the fireball was between the transmitter and receiver.. For short periods during this time (0 to ≈ 7

seconds), there were readable signals, probably due to complex reflection, diffraction, and refraction effects. However, from the point of view of radar guidance and control and for data telemetering purposes, the signal would be unreadable.

An upper limit for the reflection coefficient for the surface of the fireball was obtained.

Upper limits for the magnitude of the EM signal in the frequency bands covered by the receivers were obtained.

5.2 RECOMMENDATIONS

In order to be able to transmit data from the vicinity of a high-altitude nuclear explosion, a system that includes a delay of the order of seconds should be used, since the attenuation of telemetry signals under these conditions would be lengthy and severe.

Care must be taken to shield any equipment from the effects of the EM signal during measurements of data at early times. In addition, it is mandatory to make each station self-contained without any leads that pass through this shielding, unless special precautions are taken. In particular, the timing signal and powerlines in the vicinity of a nuclear detonation act as antennas, and severe voltage fluctuations are induced in these lines.

Any future measurements of attenuation versus time and frequency should be carried out at higher altitudes, since not much of an effect can be expected at low altitudes for easily usable frequencies.

Appendix

CALCULATIONS

A.1 ATTENUATION

The electric field of an EM wave in an isotropic, homogeneous conducting medium can be characterized by the following differential equation (Reference 17):

$$\frac{K\mu}{c^2}\frac{\partial^2 \vec{E}(\vec{r},t)}{\partial t^2} + \frac{4\pi\sigma\mu}{c^2}\frac{\partial \vec{E}(\vec{r},t)}{\partial t} = \nabla^2 \vec{E}(\vec{r},t) \tag{A.1}$$

where K, μ, σ, and c are the dielectric constant, the magnetic permeability, the complex conductivity, and the velocity of light, respectively, expressed in gaussian units. Assuming a plane wave solution of the form

$$\vec{E}(\vec{r},t) = \vec{E}_0 e^{i\omega(t - (p/c)\vec{K}\cdot\vec{r})} \tag{A.2}$$

where $\vec{K}$ is a unit vector in the direction of propagation and p is the propagation constant, and substituting into Equation A.1 yields,

$$-\frac{K\mu}{c^2}\omega^2 \vec{E}(\vec{r},t) + \frac{4\pi\sigma\mu}{c^2} i\omega \vec{E}(\vec{r},t) = -\frac{\omega^2 p^2}{c^2}\vec{E}(\vec{r},t)$$

Solving this result for p^2 yields,

$$p^2 = \mu\left(K - i\frac{4\pi\sigma}{\omega}\right) \tag{A.3}$$

If the complex conductivity is written explicitly as

$$\sigma = \sigma_r - i\sigma_i$$

Equation A.3 can then be written as

$$p^2 = \mu\left[\left(K - \frac{4\pi\sigma_i}{\omega}\right) - i\left(\frac{4\pi\sigma_r}{\omega}\right)\right] \tag{A.4}$$

The propagation constant p is normally written in terms of the refractive index n and the extinction coefficient k in the following manner,

$$p = n - ik$$

or

$$p^2 = (n^2 - k^2) - i(2nk) \tag{A.5}$$

Equating the real and imaginary parts of Equations A.4 and A.5,

$$n^2 - k^2 = \mu\left(K - \frac{4\pi\sigma_i}{\omega}\right)$$

and

$$2nk = \mu \frac{4\pi\sigma_r}{\omega}$$

Solving these equations for k, the extinction coefficient,

$$k = \left[\frac{\mu\xi}{2} \left\{ -1 + \left(1 + \left[\frac{4\pi\sigma_r}{\omega\xi} \right]^2 \right)^{1/2} \right\} \right]^{1/2} \tag{A.6}$$

where $\xi = (K - 4\pi\sigma_i/\omega)$, the modified dielectric constant.

The complex conductivity σ is defined by the following equation for the current density:

$$\vec{I}(\vec{r},t) = \sigma \vec{E}(\vec{r},t) \tag{A.7}$$

Free electrons, which can be characterized by a single collision frequency ν, under the action of an EM field satisfy the following equation (Reference 18):

$$m \frac{\partial^2 \vec{R}(\vec{r},t)}{\partial t^2} + \nu m \frac{\partial \vec{R}(\vec{r},t)}{\partial t} = e \vec{E}(\vec{r},t) \tag{A.8}$$

where m is the mass of the electron, e is the electronic charge, and $\vec{R}$ is the position vector of the free electron. Letting

$$\vec{R}(\vec{r},t) = \vec{R}_0 e^{i\omega(t - (p/c)\vec{K}\cdot\vec{r})}$$

and $\vec{E}(\vec{r},t)$ be a plane wave as defined in Equation A.2, and substituting into Equation A.8,

$$\vec{R}(\vec{r},t) = -\frac{e}{m} \vec{E}(\vec{r},t) \frac{(1 + i\nu/\omega)}{\omega^2 + \nu^2}$$

Now since

$$\vec{I}(\vec{r},t) = N_e e \frac{\partial \vec{R}(\vec{r},t)}{\partial t}$$

where N_e is the free electron density,

$$\vec{I}(\vec{r},t) = \frac{N_e e^2}{m} \frac{(\nu - i\omega)}{(\omega^2 + \nu^2)} \vec{E}(\vec{r},t) \tag{A.9}$$

When Equation A.9 is substituted into A.7, the well-known Lorentz formula (Reference 18) is obtained for the conductivity

$$\sigma = \frac{\omega_p^2}{4\pi} \left[\frac{\nu}{\omega^2 + \nu^2} - i \frac{\omega}{\omega^2 + \nu^2} \right] \tag{A.10}$$

where ω_p^2, the plasma frequency, is defined as $4\pi N_e e^2/m$. From the equation defining the quantities σ_r and σ_i, the following relationships can be obtained:

$$\sigma_r = \frac{\omega_p^2}{4\pi} \frac{\nu}{\omega^2 + \nu^2}$$

and

$$\sigma_i = \frac{\omega_p^2}{4\pi} \frac{\omega}{\omega^2 + \nu^2}$$

The next step is to estimate the magnitude of the term $(4\pi\sigma_r/\omega\xi)^2$ in Equation A.6. As typical values let $\nu = 4 \times 10^{11}$, $\omega = 6 \times 10^{15}$ and $N_e = 10^{11}$ which gives

$$\left(\frac{4\pi\sigma_r}{\omega\xi}\right)^2 \approx 1.7 \times 10^{-4}$$

Thus, it is seen that the inner square root in Equation A.6 can be expanded, keeping only two terms in the expansion. After this operation is carried out, the result is

$$k \approx \frac{1}{2}\left(\frac{\mu}{\xi}\right)^{1/2}\left[\frac{4\pi\sigma_r}{\omega}\right]$$

In the cases of interest here, $(\mu/\xi)^{1/2}$ is very nearly unity; hence,

$$k \approx 2\pi\frac{\sigma_r}{\omega} \tag{A.11}$$

If for σ_r the Lorentz value is used from Equation A.10, the resulting value for k is

$$k = \frac{1}{2}\frac{\nu}{\omega}\frac{\omega_p^2}{\omega^2+\nu^2} \tag{A.12}$$

which checks with Equation A.14 of Reference 3.

When the free electrons have an arbitrary distribution of velocities f(v), in contrast with the case when they can be described by a single collision frequency, Reference 19 indicates that the complex conductivity is given by

$$\sigma = \frac{\omega_p^2}{3}\left[\int_0^\infty \frac{\partial}{\partial v}\left(\frac{\nu v^3}{\omega^2+\nu^2}\right) f(v)\,dv - i\omega\int_0^\infty \frac{\partial}{\partial v}\left(\frac{v^3}{\omega^2+\nu^2}\right) f(v)\,dv\right]$$

in which f(v) is normalized such that $4\pi\int_0^\infty f(v)\,v^2\,dv = 1$. If the real part σ_r of this expression is inserted into Equation A.11, the extinction coefficient is obtained:

$$k = K N_e \tag{A.13}$$

where

$$K = \frac{1}{2}\frac{4\pi e^2}{m}\cdot\frac{1}{\omega^2}\frac{4\pi}{3}\int_0^\infty \frac{\partial}{\partial v}\left(\frac{x v^3}{1+x^2}\right) f(v)\,dv \tag{A.14}$$

and $x \equiv \nu/\omega$ is the "normalized" collision frequency, in general, a function of electron velocity. As can be seen from Equation A.14, the extinction coefficient depends in a relatively complicated manner on the collision frequency ν, in contrast with the simple dependence of Equation A.12.

It is easily seen, if x is independent of v, that Equation A.13 leads back to Equation A.12 as it should when a single value of ν is appropriate.

By considering propagation along the z axis only and taking the ratio of the Poynting vectors (proportional to the $|\vec{E}(\vec{r},t)|^2$ of Equation A.2) at Points 0 and z we obtain

$$\frac{|\vec{P}(z)|}{|\vec{P}(0)|} = e^{-2(\omega/c)kz}$$

Expressing this result in terms of the number of decibels of attenuation Ω of the wave, which has traveled a distance z,

$$\Omega = -10\log_{10} e^{-2(\omega/c)kz} = -8.686\,(\omega/c)kz \tag{A.15}$$

If k is a function of distance and time, as it is in the present case, Equation A.14 must be replaced by

$$\Omega = -8.686\,(\omega/c)\int_{z_T}^{z_R} k(z,t)\,dz \tag{A.16}$$

where z_T and z_R designate the positions of the transmitter and receiver respectively. If the extinction coefficient k as given by Equation A.13 is used, then the total attenuation is given by

$$\Omega = -8.686\ (\omega/c)\ K \int_{z_T}^{z_R} N_e(z,t)\ dz \tag{A.17}$$

If, further, $N_e(z,t) \approx Q_e(z)\, Q_e(t)\, \tau$, as was deduced in Equation 1.6, then the resulting expression for attenuation becomes

$$\Omega = -8.686\ (\omega/c)\ K\, \tau\, Q_e(t) \int_{z_T}^{z_R} Q_e(z)\ dz \tag{A.18}$$

If now the transmission path is radial, with the transmitter near the ground zero, then an appropriate $Q_e(z)$ is given by

$$Q_e(R) = \frac{e^{-(R - R_T)/L}}{(R/R_T)^2}\ (1 + \text{B.U.F.})$$

where B.U.F. (buildup factor) takes into account multiple scattering of gamma rays and L is the gamma ray mean free path. Inserting this expression into Equation A.18 yields for the attenuation along a radial path

$$\Omega_R = -8.686\ (\omega/c)\ K\, \tau\, Q_e(t)\, e^{R_T/L}\ (R_T)^2 \cdot \int_{R_T}^{R_r} \frac{e^{-R/L}}{R^2}\ (1 + \text{B.U.F.})\ dR \tag{A.19}$$

where $Q_e(t)$ is now the electron production rate at the position of the transmitter.

A.2 RADIAL ATTENUATION INTEGRAL

If the approximation B.U.F. = $(0.5/E^{1/4})\ (R/L)$ (Reference 2) is adopted, then the integral of Equation A.19 may be written

$$I = \int_{R_T}^{R_r} \frac{e^{-R/L}}{R^2} \left[1 + \left(\frac{0.5}{E^{1/4}}\right) \frac{R}{L}\right] dR \tag{A.20}$$

Where: R_T = transmitter position

R_r = receiver position

L = the mean free path of a gamma ray

E = the energy of the gamma rays in units of $m_e c^2$

If $0.5/E^{1/4} = B$, and $x = R/L$, Equation A.20 reduces to

$$I = \frac{1}{L} \int_{x_T}^{x_R} \frac{e^{-x}}{x^2}\ [1 + B\,x]\ dx \tag{A.21}$$

In the cases of interest for this report, the upper limit of this integral can be replaced by ∞, since the value of this integral from x_R to ∞ is much less than the value from x_T to x_R. Rewriting Equation A.21 in the following form

$$I = \frac{1}{L} \left\{ \int_{x_T}^{\infty} \frac{e^{-x}}{x^2}\ dx + B \int_{x_0}^{\infty} \frac{e^{-x}}{x}\ dx \right\}$$

and carrying out an integration by parts on the first integral in the brackets, then

$$I = \frac{1}{L} \left[\frac{e^{-x_T}}{x_T} - (1 - B) \int_{x_T}^{\infty} \frac{e^{-x}}{x}\ dx \right] \tag{A.22}$$

The integral that remains in Equation A.20 is a standard integral (Reference 20). Using a gamma ray energy of 1 Mev, the values of $L \cdot I(x_T)$ are shown in Figure A.1.

A.3 DIFFRACTION AND REFLECTION

In order that calculation of the fireball diffraction pattern be made tractable, the line-of-sight path was considered to be obscured by a sphere, taken to be a perfect absorber, having the same diameter as the visible fireball. Simplifying further, if the opaque sphere is replaced by a disk, it is seen that this problem is essentially the same as the physical optics problem of diffraction by a "black" disk (Reference 21).

The rigorous solution to this problem requires the solution of an EM boundary value problem. However, it is well known (References 22 through 25) that the rigorous solution may be closely approximated by the Fresnel-Kirchhoff diffraction formula (Reference 26). This approximation is subject to the conditions that the wavelength be much less than the smallest dimension of the diffracting region, and that its dimensions, in turn, be much less than the distances from the transmitter and receiver to the diffracting object. These conditions can be seen to be satisfied (the longest wavelength used was ≈ 2 meters) for the times greater than about 100 μsec, by examining the fireball diameter versus time dependence given in Figure 4.6.

The Fresnel-Kirchhoff diffraction integral for the x component of the electric field, $E_x(R)$, at the position of the receiver, as given by Reference 25, is

$$E_x(R) = -\frac{S_x}{4\pi} ik \iint \frac{e^{ik(r+s)}}{r^2 s^2} [s\,\vec{n}\cdot\vec{r} + r\,\vec{n}\cdot\vec{s}]\, dA \qquad (A.23)$$

in which S_x is the electric field source strength of a point source, polarized in the x direction and located at the position of the transmitter and $k = (2\pi/\lambda)$, where λ is the wavelength of the microwave field. From Figure A.2 it can be seen that $\vec{r}$ is the vector distance from the transmitter to the surface element dA, $\vec{s}$ is the vector distance from dA to the receiver, and $\vec{n}$ is a unit normal to the surface element dA.

In the present application it is not unreasonable to take the antennas to be a point source, since the transmitting antennas produce nearly spherical phase fronts, and the solid angle subtended by the fireball is small compared to the solid angle subtended by the antennas at the half-power points.

To obtain the diffraction field resulting from an opaque disk, the integral should be taken over the entire x-y plane in which the opaque disk is situated with the value of the integral over the disk itself taken to be zero, as is usual, in application of the Fresnel-Kirchhoff formula. This is equivalent to excluding the disk from the region of integration. If E_x^D is the diffraction field resulting from Equation A.23 for the disk excluded from the integration surface, E_x^{un} the field which results from integrating over the entire unobscured x-y plane, and E_x^A the field obtained by integrating over only the region occupied by the disk, (which gives just the field due to an open aperture of the same extent), it is easily seen that

$$E_x^D = E_x^{un} - E_x^A \qquad (A.24)$$

Hence, the computation of E_x^D now involves only an integration over the aperture A along with the use of Equation A.24. Equation A.24 is just a statement of Babinet's principle. E_x^{un} is well known and is just the electric field at a distance $(l_t + l_R)$ resulting from a point source polarized in the x direction,

$$S_x \frac{e^{ik(l_t + l_R)}}{l_t + l_R}$$

To take into account that portion of the total signal that has been reflected from the desert floor (treated as a plane), the fireball diffraction pattern has been calculated at the position of an image receiver, using reflection coefficients between 0 and 1.

The evaluation of the integral of Equation A.23 was done numerically using an LGP-30 computer. Since the contributions from the plane of integration in Figure A.2 do not depend on the azimuthal angle ϕ, except where the absorbing disk is located, the plane was divided into angular rings of width $\Delta\rho = 1$ meter. The total contribution from each ring was calculated and stored. To complete the integration it was necessary only to sum the fractional part of each ring which constituted the absorbing disk, considered here as an aperture, to obtain E_x^A, and then to apply Babinet's principle given in Equation A.24 to finally obtain E_x^D.

The results of this calculation for 160 and 960 Mc are shown in Figures A.3 and A.4 for a representative set of reflection coefficients.

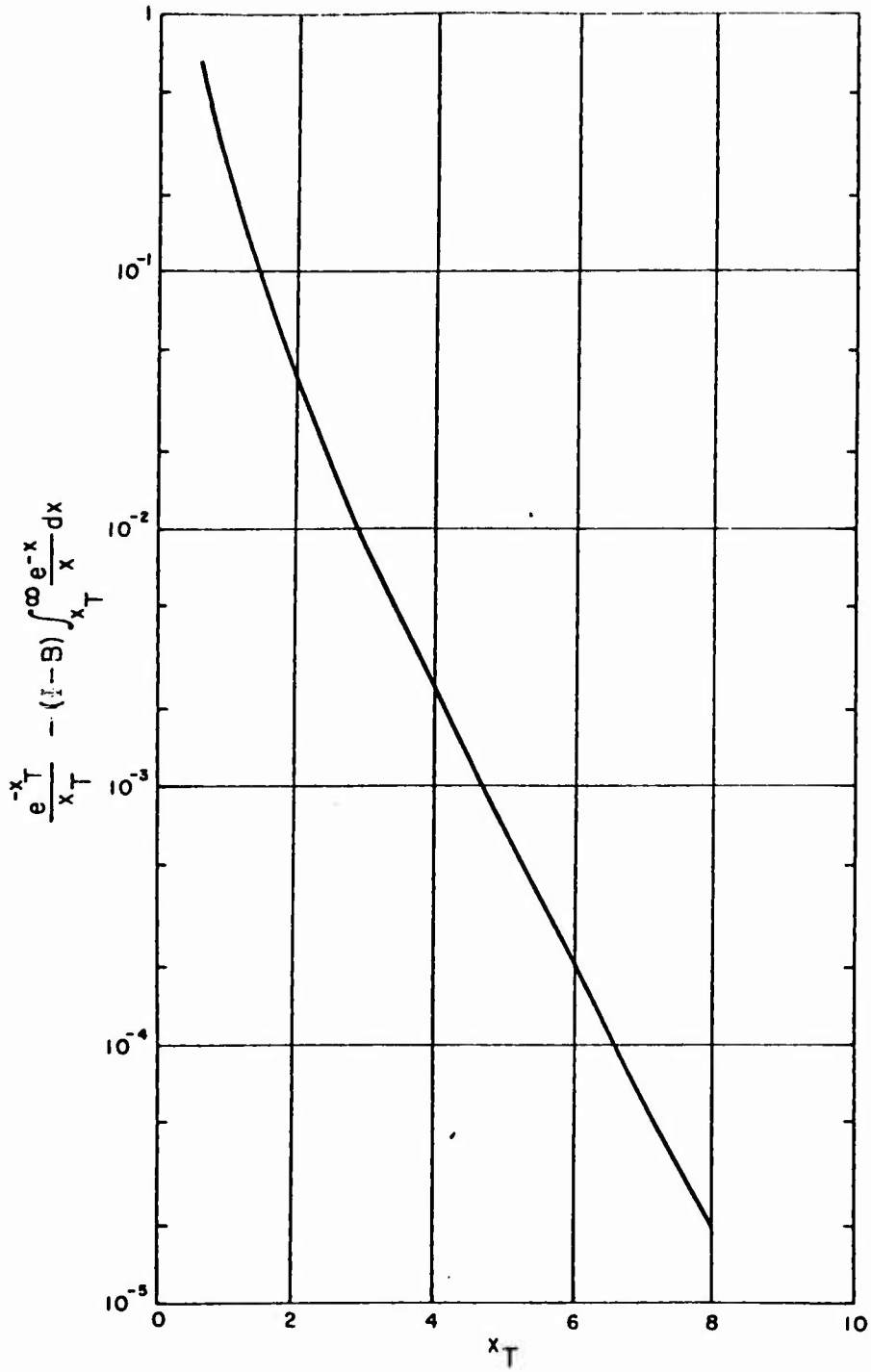

Figure A.1 Results of radial range integral.

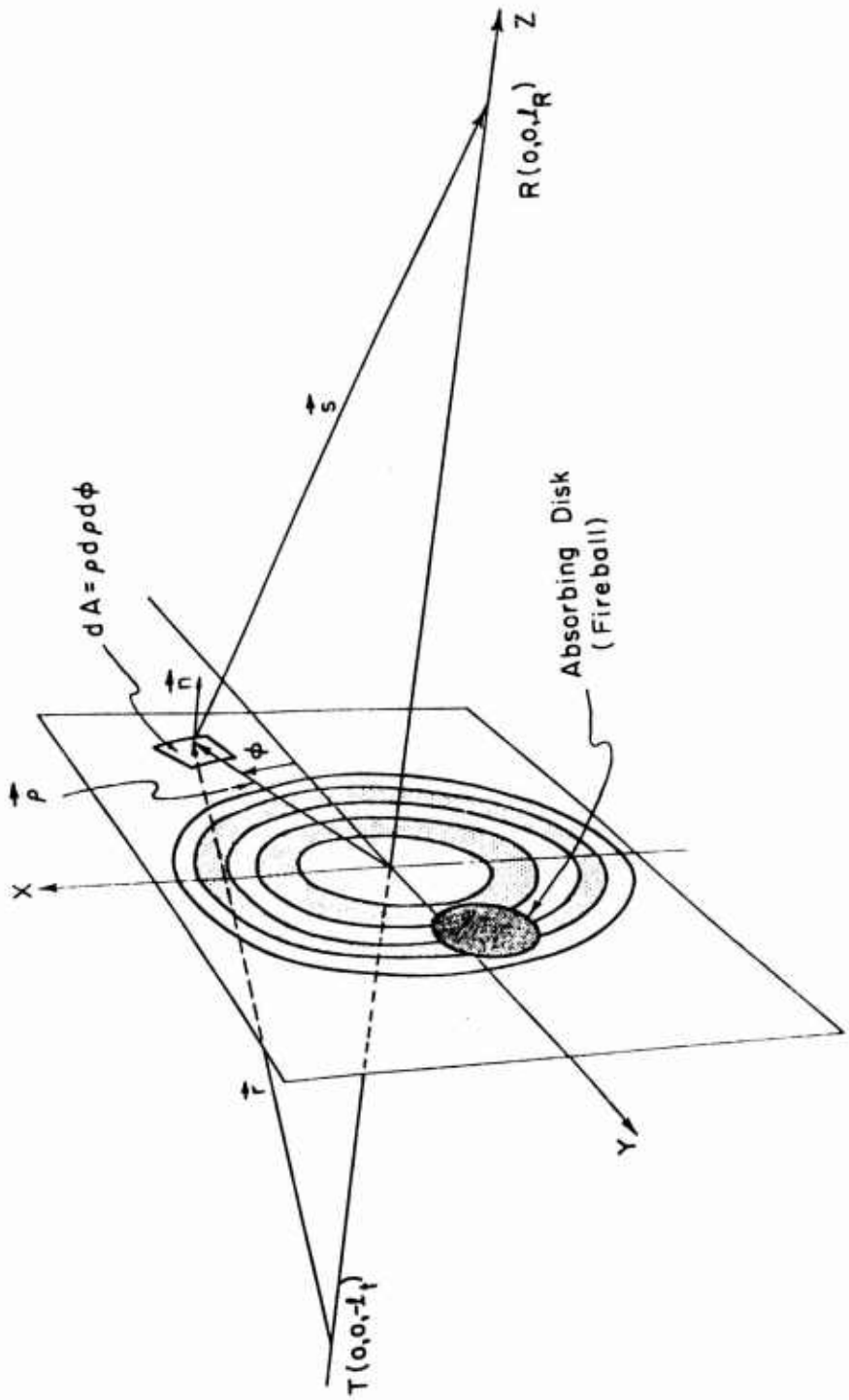

Figure A.2 Diffraction geometry.

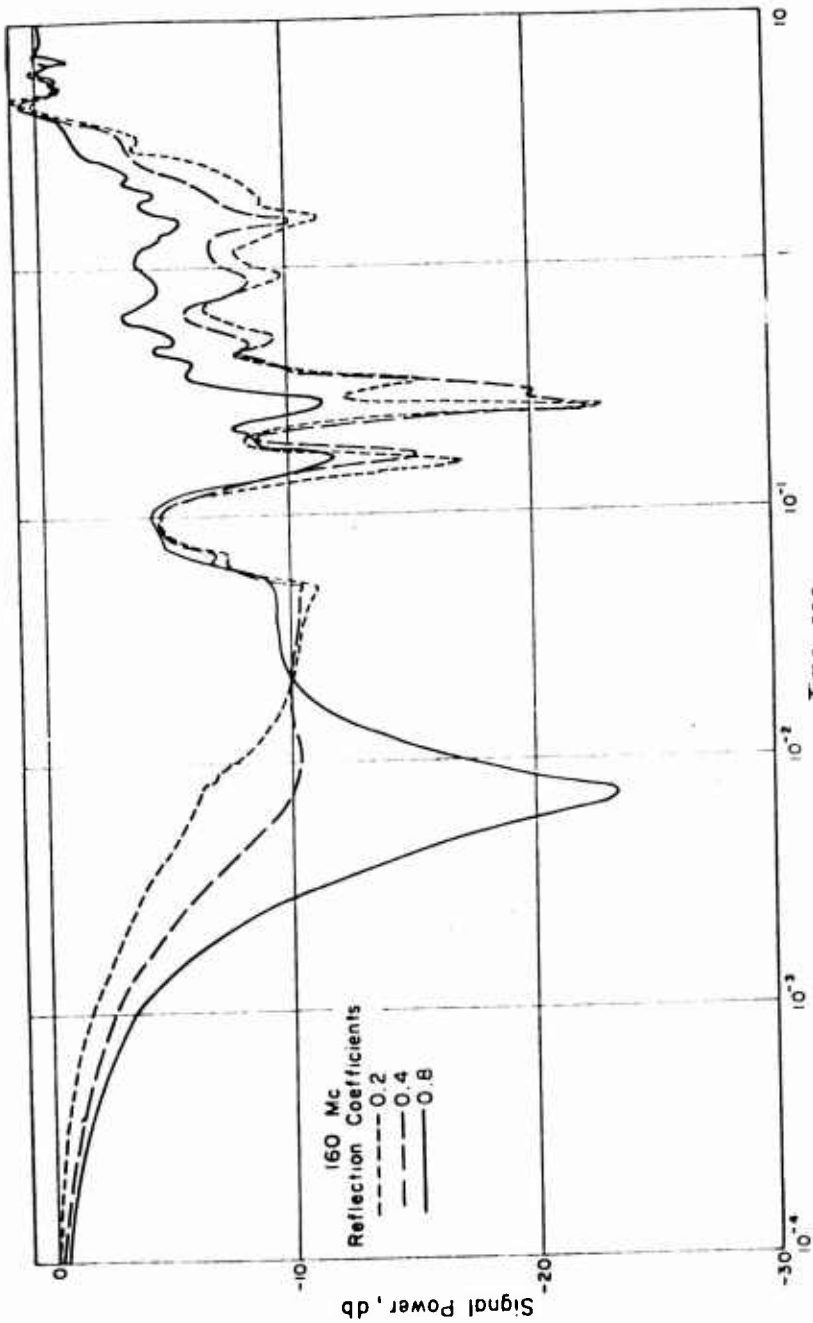

Figure A.3 Results for 160 Mc.

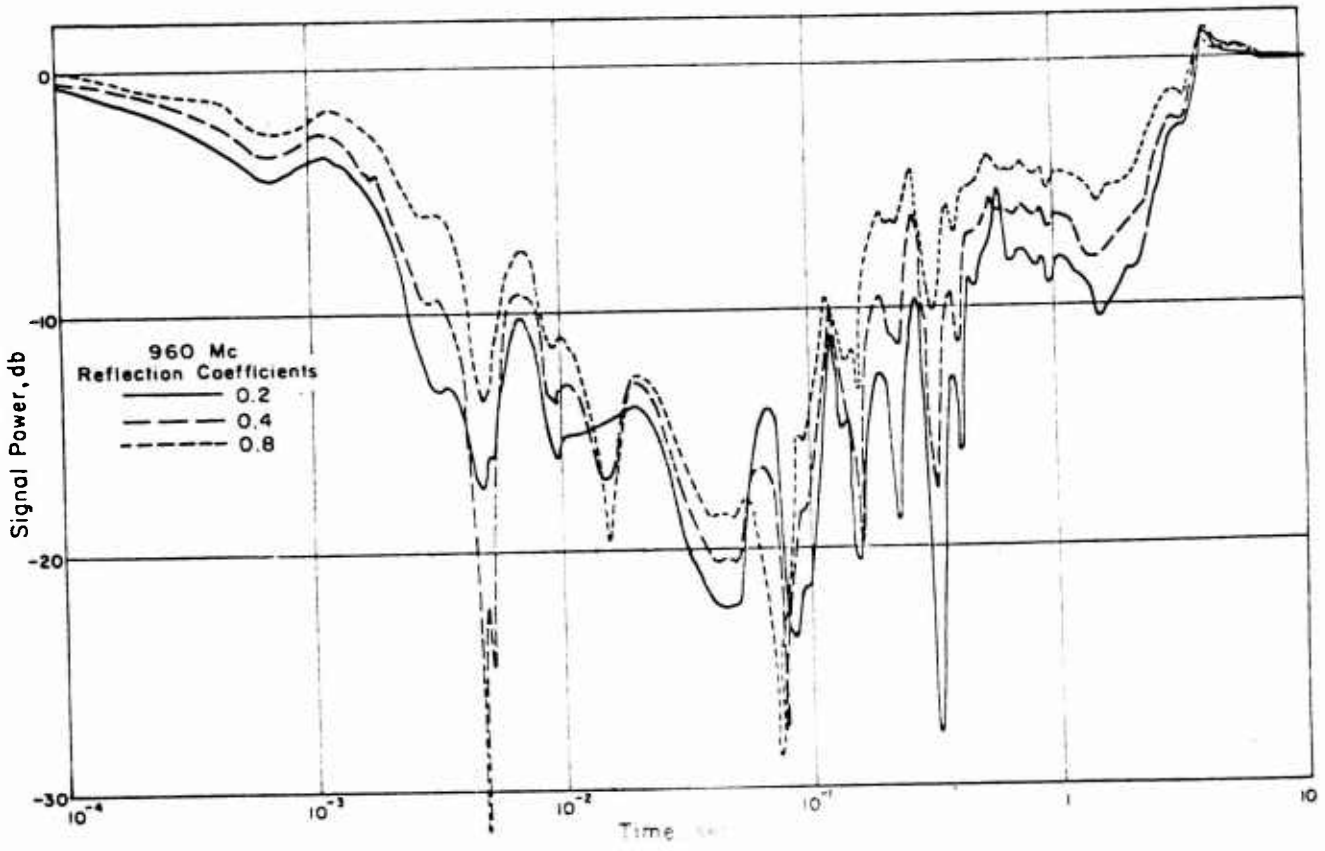

Figure A.4 Results for 960 Mc.

REFERENCES

4. L. M. Chanin; "The Attachment of Slow Electrons in Oxygen"; Research Report 403FD317-R2; Westinghouse Research Laboratories, Pittsburgh, Pennsylvania; Unclassified.

5. L. Loeb; "Basic Processes of Gaseous Electronics"; First Edition, 1955; University of California Press, Berkeley and Los Angeles, California; Unclassified.

6. M. Ishimo; "On the Velocity of Secondary Cathode Rays Emitted by a Gas Under the Action of High-Speed Cathode Rays"; Philosophical Magazine, XXXII, Page 202, 1916; Unclassified.

7. H. D. Hagstrum and J. T. Tate; "Ionization and Dissociation of Diatomic Molecules by Electron Impact"; Physical Review, February 1941, Vol. 59, No. 4, Page 354; Unclassified.

8. D. T. Stewart and E. Gabathuler; "Some Electron Collision Cross Sections for Nitrogen and Oxygen"; Proceedings of the Physical Society of London, 1958, Vol. 72, Page 287; Unclassified.

9. J. D. Craggs, R. Thorburn, and B. A. Tozer; "The Attachment of Slow Electrons in Oxygen"; The Proceedings of the Royal Society of London, Vol. 240, Page 473, 1957; Unclassified.

10. J. B. Fisk; "Theory of the Scattering of Slow Electrons by Diatomic Molecules"; Physical Review, Vol. 49, Page 167, 1936; Unclassified.

12. "The Effects of Nuclear Weapons"; 1957, Page 69; U. S. Government Printing Office; Unclassified.

13. M. P. Bachynsky and others; "Electromagnetic Properties of High-Temperature Air"; Proceedings of the IRE, Vol. 43, No. 3, Page 347, 1960; Unclassified.

14. E. W. Hamlin and others; "X-Band Phase Front Measurements in Arizona During April 1946"; Report No. 6, 1 February 1957; Electrical Engineering Research Laboratory, University of Texas; Unclassified.

15. J. P. Day and L. G. Trolese; "Propagation of Short Radio Waves Over Desert Terrain"; Proceedings of the IRE, Vol. 38, Page 165, 1950; Unclassified.

16. W. R. Young, Jr. and L. Y. Lacy; "Echoes in Transmission at 450 Megacycles from Land-to-Car Radio Units"; Proceedings of the IRE, Vol. 38, Page 255, 1950; Unclassified.

17. M. Abraham and R. Becker; "The Classical Theory of Electricity and Magnetism"; Page 188; Hafner Publishing Company, Inc., New York; Unclassified.

18. H. A. Lorentz; "The Theory of Electrons"; Page 139, 1952; Dover Publications, Inc., New York; Unclassified.

19. H. Margenau; "Conductivity of Plasmas to Microwaves"; Physical Review, Vol 109, No. 6, 1958; Unclassified.

20. E. Jahnke and F. Emde; "Tables of Functions"; Fourth Edition, Page 6, 1945; Dover Publications, Inc., New York; Unclassified.

21. A. Sommerfeld; "Optics"; Page 213, 1954; Academic Press Inc., New York; Unclassified.

22. Ibid, Page 325.

23. J. A. Stratton and L. J. Chu; "Diffraction Theory of Electromagnetic Waves"; Physical Review, Vol. 56, No. 1, Page 99, July 1939; Unclassified.

24. W. Franz; "Zur Formulierung des Huygensschen Prinzips"; Zeitschrift fur Naturforschung, Vol. 34, Page 500, 1948; Unclassified.

25. S. Silver; "Microwave Antenna Theory and Design"; First Edition, 1949; McGraw-Hill Book Company, Inc., New York; Unclassified.

26. M. Born and E. Wolf; "Principles of Optics"; Page 379, 1959; Pergamon Press, New York; Unclassified.